

RECOVERY IN CADMIUM

by

EDMOND CHARLES HAMRE

B.A.Sc., University of British Columbia, 1964

A THESIS SUBMITTED IN PARTIAL FULFILMENT OF
THE REQUIREMENTS FOR THE DEGREE OF
DOCTOR OF PHILOSOPHY

in the Department
of
METALLURGY

We accept this thesis as conforming to the
required standard

THE UNIVERSITY OF BRITISH COLUMBIA

January, 1970

In presenting this thesis in partial fulfilment of the requirements for an advanced degree at the University of British Columbia, I agree that the Library shall make it freely available for reference and study.

I further agree that permission for extensive copying of this thesis for scholarly purposes may be granted by the Head of my Department or by his representatives. It is understood that copying or publication of this thesis for financial gain shall not be allowed without my written permission.

Department of Metallurgy

The University of British Columbia
Vancouver 8, Canada

Date January 12, 1970

ABSTRACT

The recovery of mechanical properties following deformation of single crystal cadmium has been studied. Such recovery has been observed above $0.26 T_M$ (-120°C).

Crystals covering a range of orientation were deformed in tension at -196°C and recovered at elevated temperatures. Transmission electron microscopy to relate tensile and recovery behaviour to dislocation structures was found to be impossible.

It was observed that work hardening during the initial portion of the easy glide region is completely recoverable. At higher strains in easy glide, a portion of the work hardening was not recoverable. It is believed that in this latter section, dislocations are generated on the second order pyramidal system $\{11\bar{2}2\} \langle 11\bar{2}3 \rangle$. These dislocations will combine with basal dislocations to form stable obstacles in the lattice which will be responsible for the non-recoverable work hardening.

The end of easy glide was found to occur at $\chi = 20^\circ$, independent of recovery or initial orientation. This phenomenon is associated with flow on the second order pyramidal system which will produce a much higher density of obstacles at this point, resulting in a higher work hardening rate.

Recovery in stage II was observed to increase the amount of strain attainable. It was also observed that while recovery up to intermediate

strains in stage II affected only basal dislocations, both basal and pyramidal dislocations appear to be recovered at high strains. Pyramidal dislocations may recover by the processes observed by Price.

The rate controlling mechanism for yield and flow of cadmium single crystals is thought to be one of the non-conservative motion of jogs.

An attempt was made to calculate an activation energy for the recovery process, but the data did not yield any meaningful numbers. This may be a result of the definition of recovery adopted for this work.

ACKNOWLEDGEMENT

The author wishes to thank his research director, Dr. E. Teghtsoonian, for his helpful advice and encouragement. He also wishes to thank fellow graduate students for many stimulating discussions.

Financial assistance in the form of a National Research Council Studentship, National Research Council operating grant A-2452 and a hard-working wife is gratefully acknowledged.

TABLE OF CONTENTS

	PAGE
1. INTRODUCTION	1
2. EXPERIMENTAL PROCEDURE	4
2.1 Sample preparation	4
2.2 Tensile testing	5
2.3 Electron microscopy	5
2.4 Recovery tests	7
3. RESULTS	8
3.1 Resolved shear stress - shear strain plots	8
3.2 Recovery results	12
3.2.1 Method (1)	14
3.2.2 Method (2)	20
3.2.3 Method (3)	22
3.3 Strain rate change tests	28
3.3.1 Activation volume	29
3.3.2 $\Delta\tau$ versus τ	32
3.4 Work hardening parameters	38
3.4.1 Stage I	38
3.4.1.1 Critical resolved shear stress	39
3.4.1.2 Work hardening rate	39
3.4.1.3 Length of easy glide	44
3.4.1.4 Recovery effects	49
3.4.2 Stage II	49
3.4.2.1 Orientation effects	49
3.4.2.2 Recovery effects	49
3.4.3 Stage III	50

	PAGE
4. DISCUSSION	54
4.1 Recovery results	54
4.1.1 Activation energy	54
4.1.2 Comparison of recovery methods (1), (2), (3)	59
4.2 Work hardening parameters	66
4.2.1 Easy glide parameters	66
4.2.2 Theories of stage II	69
4.2.2.1 Condensation of vacancies	70
4.2.2.2 Non-active basal dislocations	70
4.2.2.3 Twinning	70
4.2.2.4 Second order pyramidal slip	71
4.2.3 Present model	73
4.3 Strain rate change tests	78
4.3.1 Stage I	80
4.3.1.1 Activation volume behaviour	80
4.3.1.2 Cottrell-Stokes behaviour	84
4.3.2 Stage II	86
4.4 Flow stress following recovery	88
4.5 Work hardening in stage II	89
5. SUMMARY AND CONCLUSIONS	93
6. APPENDIX	95
6.1 Electron microscopy techniques	95
6.1.1 Cutting a thin section	95
6.1.2 Thinning	96
6.1.3 Examination of thinned specimens	97
REFERENCES	98

LIST OF FIGURES

	PAGE
<u>Fig 1.</u> Orientation range of single crystals	6
<u>Fig 2.</u> Typical resolved shear stress - shear strain curve at -196°C	9
<u>Fig 3.</u> Typical resolved shear stress - shear strain curve at 20°C	10
<u>Fig 4.</u> Typical tensile kinks formed at 20°C	11
<u>Fig 5.</u> Definition of recovery	13
<u>Fig 6.</u> The variation of method (1) recovery at 30°C with strain	15
<u>Fig 7.</u> The variation of method (1) recovery at -20°C with strain	16
<u>Fig 8.</u> The variation of method (1) recovery at -70°C with strain	17
<u>Fig 9.</u> The variation of method (1) recovery at -100°C with strain	18
<u>Fig 10.</u> The variation of method (1) recovery with time at $\gamma = 0.25$	19
<u>Fig 11.</u> The variation of saturation recovery with strain	21
<u>Fig 12.</u> The variation of method (2) recovery at 20°C with strain	23
<u>Fig 13.</u> The variation of method (2) recovery at -30°C with strain	24
<u>Fig 14.</u> The variation of method (2) recovery at -70°C with strain	25
<u>Fig 15.</u> The variation of method (2) recovery at -90°C and -110°C with strain	26
<u>Fig 16.</u> The effect of temperature on easy glide deformation	27
<u>Fig 17.</u> The determination of load change with strain rate change	29
<u>Fig 18.</u> Comparison of activation volume data obtained from strain rate up-change and down-change	30
<u>Fig 19.</u> The strain dependence of activation volume	31
<u>Fig 20.</u> The effect of saturation recovery on activation volume in easy glide	33
<u>Fig 21.</u> The effect of saturation recovery on activation volume in stage II	34
<u>Fig 22.</u> The variation of $\Delta\tau$ with τ	35
<u>Fig 23.</u> The variation of $\Delta\tau - \tau$ with saturation recovery in easy glide	36

<u>Fig 24.</u>	The variation of $\Delta\tau - \tau$ with saturation recovery in stage II	37
<u>Fig 25.</u>	Orientation dependence of the critical resolved shear stress	40
<u>Fig 26.</u>	Temperature dependence of the critical resolved shear stress	41
<u>Fig 27.</u>	Orientation dependence of stage I work hardening rate	42
<u>Fig 28.</u>	Orientation dependence of the length of easy glide (schematic).	43
<u>Fig 29</u>	Temperature dependence of stage I work hardening rate	45
<u>Fig 30.</u>	The effect of orientation on the length of stage I (specific example)	47
<u>Fig 31.</u>	Twins formed in the stage I - stage II transition (x 200)	48
<u>Fig 32.</u>	The effect of saturation recovery on the length of stage II	51
<u>Fig 33.</u>	Relative shapes of crystals deformed at 20°C and -196°C	52
<u>Fig 34.</u>	The variation of $\log (1-R)$ with time,	56
<u>Fig 35.</u>	The variation of \log (slope) with reciprocal absolute temp.	58
<u>Fig 36.</u>	Comparison of saturation recovery with deformation at -196°C and 20°C	60
<u>Fig 37.</u>	Schematic diagram of recovery to a similar stress level with deformation at different temperatures	63
<u>Fig 38.</u>	Typical method (2) recovery at -30°C and -70°C	65
<u>Fig 39.</u>	Comparison of present work to that of Bocek and Kaska regarding the temperature dependence of the critical resolved shear stress	67
<u>Fig 40.</u>	Comparison of shear stress on second order pyramidal plane with that on basal plane	74
<u>Fig 41.</u>	The variation of saturation recovery with orientation	76
<u>Fig 42.</u>	The variation of flow stress following saturation recovery in stage II	90

LIST OF TABLES

	PAGE
Table I. The effect of initial orientation and recovery on the length of stage I	46

1. INTRODUCTION

Recovery may be defined generally as the reversion towards an initial state by a meta-stable structure when sufficient energy is present. For the purposes of this study, this definition may be stated more specifically. In this case, recovery occurs when the flow stress of a cadmium single crystal decreases towards the initial yield stress when thermal energy is added to the system. This decrease in flow stress is probably caused by a decrease in dislocation density as a result of egress of dislocations from the system. When recovery occurs concurrently with deformation, it is termed dynamic recovery, whereas if it takes place under static conditions it is termed static recovery.

Dynamic recovery is an important phenomenon in that in many instances it is responsible for at least part of the temperature sensitivity of some work hardening parameters. This recovery takes place at intermediate temperatures - high enough so that dislocations may rearrange themselves, but not so high as to promote recrystallization. Dynamic recovery probably accounts for most of the difference in the work hardening rate of cadmium between liquid nitrogen and room temperatures. The suppression of both static and dynamic recovery by the thoria dispersion is thought to be responsible for the high strength at high temperatures in T.D. nickel.

Most studies of recovery per se have not dealt with the change of mechanical properties, but rather have been concerned with the behaviour of point defects which have been introduced to the crystal lattice either by deformation or radiation.⁴³ This type of recovery usually takes place at temperatures below that where the mechanical properties are significantly affected, and the principal method for measuring such recovery is the change in electrical resistivity.⁴⁴

One study which looked at the change in flow stress in conjunction with electrical measurements was that of Sharp, Mitchell and Christian.¹ They found an annealing peak in Cd at $T_H = .25$ which they associated with single vacancy migration. $T_H = .25$ is the same temperature at which dynamic recovery becomes apparent. These results are comparable to those of a similar study by Peiffer and Stevenson.²

Electron microscope studies on evaporated platelets of zinc by Kroupa and Price³ associated dynamic recovery with conservative climb of prismatic dislocation loops. In this mechanism, the area inside the loop is conserved, and the loop climbs by the transfer of vacancies around it by pipe diffusion. Hirsch and Lally⁴ found that dynamic recovery in thin foils of Mg was due to cross-slip and subsequent annihilation of screw dislocations. Risebrough⁵ thinks that this mechanism would not be operative in Cd due to the lack of a suitable cross-slip system.

Studies which looked specifically at the change in mechanical properties due to recovery were performed by Rath et al⁶ and by Lücke et al⁷. The former was concerned with the thermal activation characteristics of recovery in aluminum single crystals, and the latter looked at the effect of recovery on various work hardening parameters in zinc. Neither of these studies concluded anything about the dislocation arrangements or the effect of recovery on dislocations.

Other studies which were concerned with the activation parameters related to load decay after strain (Oelschlägel⁸ on zinc; Lukáč⁹ on cadmium; Feltham¹⁰ on Mg) did not draw any conclusions with respect to dislocation motion.

It was the aim of this study to investigate the recovery of mechanical properties in single crystal cadmium with specific reference to the dislocation behaviour during recovery. This work covers the range

of temperature from the first observance of recovery up to temperatures at which strained single crystals would recrystallize.

In the course of this work, the overall work hardening behaviour of cadmium single crystals has been studied so that the effects of recovery may be better understood.

Cadmium was chosen as the material to be used in this work primarily because of its crystal structure. In the past, most dislocation theories have been concerned with the simplest crystal structure, namely face-centered cubic, and as a result relatively little is known of the dislocation mechanisms in hexagonal close-packed metals. A second reason for choosing cadmium is the ease with which single crystals may be produced in quantity. Other hexagonal metals such as zirconium and titanium do not possess this quality. Finally, cadmium was chosen because of the ductility it exhibits at temperatures below the recovery range. Zinc, which is similar to cadmium in most other respects has a tendency to cleave at low temperatures.

Other characteristic properties of cadmium such as its strength, largest of all c/a ratios, medium stacking fault energy, and anisotropy were not significant factors.

Single crystals were used instead of polycrystalline material to exclude the complicating grain boundary constraints. With single crystals it is possible to calculate the shear stress on any particular plane at any time.

2. EXPERIMENTAL

2.1 Sample preparation

The material used for this study was 99.999% Cd as supplied by Cominco Ltd., Trail, B.C. This material was received in the form of one-half inch bars, and was extruded to 0.2 inch rods for subsequent growth into single crystals.

Single crystals were grown using a modified Bridgman in evacuated 5 mm. inside diameter pyrex tubes which had previously been coated on the inside surface with Aquadag. The Aquadag, which is a suspension of colloidal graphite in water, prevented the partial wetting of the pyrex by molten cadmium. If such wetting did take place, the surface of the resultant single crystal was marked by many craters not unlike bubbles. The tubes were lowered at a rate of 6 cm/hr. through a furnace with a thermal gradient of 25°C/cm.

Randomly oriented crystals were produced by this method, while crystals oriented for long easy glide, which were required for most recovery tests, were produced with a standard seeding technique once a suitable orientation had been obtained.

The pyrex tubes were removed from the crystal by dissolution in concentrated HF, following which the crystals were etched in concentrated HCl. This etch revealed any grain boundaries which may have been present, and also removed any Aquadag which may have adhered to the specimen surface. Crystals were chemically polished in a fresh solution of:

320 gm. CrO_3

40 gm. Na_2SO_4

1000 ml. H_2O

to remove approximately 0.002 inches from the surface.

The orientation of each specimen was determined to an accuracy of $\pm 1^\circ$ using the back reflection Laue technique. The orientation range of crystals used in this study is shown in Fig. 1. The majority of samples had an orientation of $40^\circ \leq \chi_0 \leq 46^\circ$ where χ_0 is the initial angle between the basal (0001) plane and the tensile axis.

2.2 Tensile testing

Tensile deformation of the crystals was carried out on a floor model Instron (Model TTM) at initial strain rates varying from $1.3 \times 10^{-2} \text{sec}^{-1}$ to $1.3 \times 10^{-5} \text{sec}^{-1}$, with the majority of tests being done at $1.3 \times 10^{-3} \text{sec}^{-1}$.

Crystals 10 cm. long were soldered into aluminum grips for testing. Since there was no reduced gauge section on the specimens, the length between the grips constituted the gauge length. This length was 6 to 8 cm., and with a diameter of 0.5 cm., the length to diameter ration always exceeded 10 to 1.

Test temperatures were maintained by immersing the specimen into an appropriate liquid held at the required temperature. The baths used and their respective temperature ranges were:

liquid nitrogen	-196°C
petroleum and ether	-140 to -70°C
ethanol	-70 to 0°C
water	0 to 100°C

2.3 Electron microscopy

An attempt to correlate mechanical properties and recovery behaviour to dislocation distribution was made by means of transmission electron microscopy. Unfortunately, experimental difficulties and the opacity of cadmium to electrons rendered this investigation fruitless.

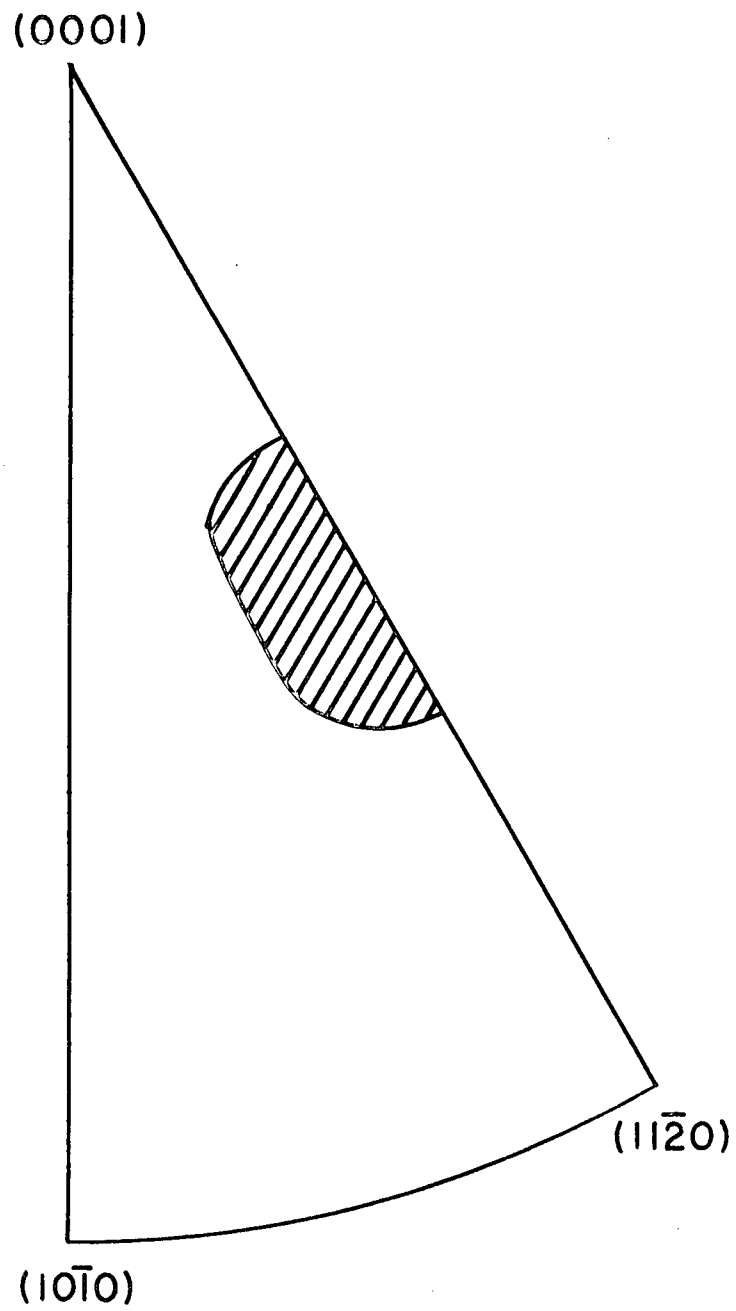


Fig 1. Orientation range of single crystals.

An account of the techniques employed and the problems encountered is given in Appendix 1.

2.4 Recovery tests

Recovery tests were carried out on cadmium single crystals in three different ways:

- 1) Crystal was deformed at -196°C to a predetermined strain, the load was removed from the specimen, and the temperature was raised to allow recovery for a fixed time. The temperature was lowered to -196°C , and deformation resumed for an arbitrary strain increment. Referred to in the following text as either method (1) or type (1) recovery.
- 2) Crystal was deformed to some predetermined strain, the load was removed, and the crystal allowed to recover for some fixed time, then deformation was resumed for a suitable strain increment, all at a constant temperature. Referred to in the following text as method (2) or type (2) recovery.
- 3) Crystal was deformed to a predetermined strain, the Instron crosshead was stopped, and the load allowed to decay during recovery for a fixed time, then deformation was resumed for an arbitrary strain increment, all at a constant temperature. Referred to in the following text as method (3) recovery.

3. RESULTS

3.1 Resolved shear stress - shear strain plots

Load-elongation data were transformed to resolved shear stress-resolved shear strain plots using the following relationships¹¹:

$$\tau = \frac{P}{A} \sin\chi_0 \left[\left(\frac{l_1}{l_0} \right)^2 - \sin\lambda_0 \right]^{\frac{1}{2}} \frac{l_0}{l_1} \quad (1)$$

$$\gamma = \frac{1}{\sin\chi_0} \left\{ \left[\left(\frac{l_1}{l_0} \right)^2 - \sin\lambda_0 \right]^{\frac{1}{2}} - \cos\lambda_0 \right\} \quad (2) *$$

Calculation and plotting of the results was performed on a IBM 7044 and later on a IBM 360/67 computer.

A typical curve for a crystal deformed at -196°C is shown in Fig 2. The critical resolved shear stress has been determined by extrapolating the linear easy glide back to zero strain. For comparison between various tests, the length of easy glide (γ_I) was defined as the strain at the intersection of the extrapolated linear stage I and stage II sections. In general, fracture occurred in the stage II region of the curve at -196°C , and as a consequence a third stage to the work hardening curve with a lower work hardening rate was not observed. Twinning generally occurred during the transition from stage I to stage II, as evidenced by load drops on the load-elongation plots, and by metallographic examination.

At 20°C , the curve still showed essentially two stages of work hardening, with the work hardening rate higher in the second stage

* It is realized that equations (1) and (2) are valid only for slip on a single slip system. While this is probably not true for cadmium following easy glide, the calculations have been extended to failure to allow comparison of present results to other work.

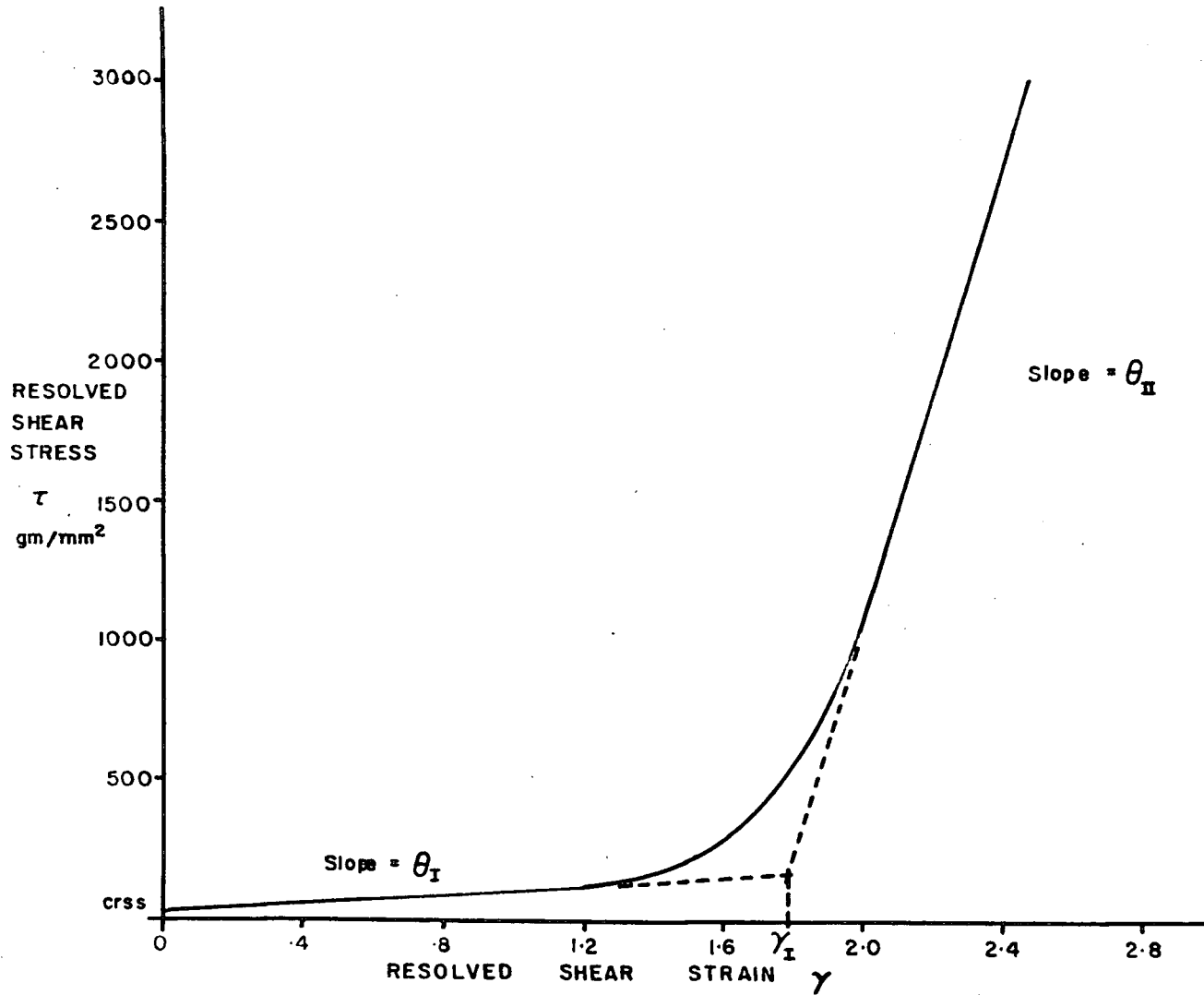


Fig 2. Typical resolved shear stress - shear strain curve at -196°C .

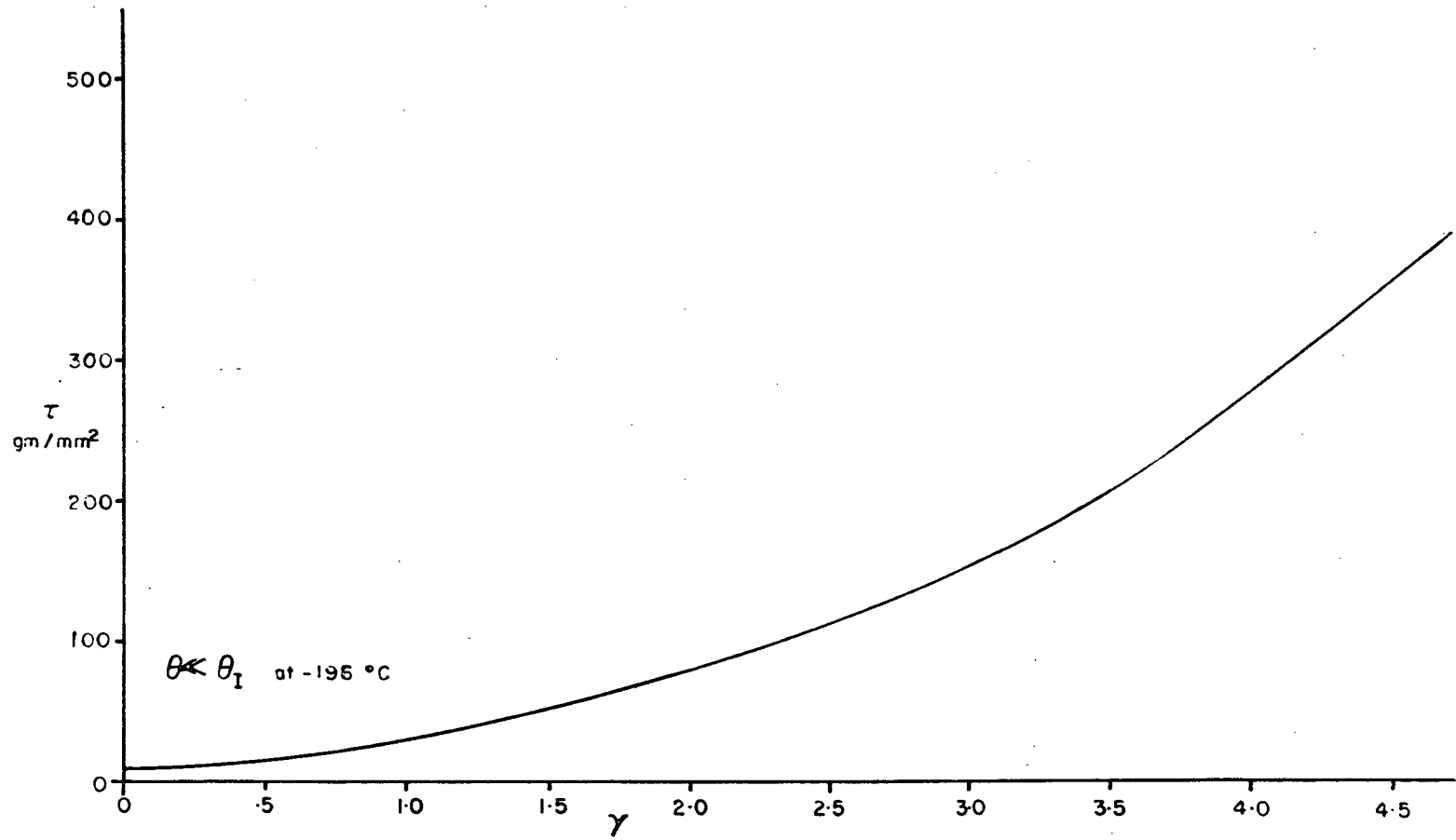


Fig 3. Typical resolved shear stress - shear strain curve at 20°C .

than in the first as shown in Fig. 3. These work hardening rates are substantially lower than those obtained at -196°C . Fig. 3 also shows that the work hardening curve is not as linear as it is at -196°C . During the initial deformation at 20°C , the crystals developed many tensile kinks (10 to 20 in an initial 8 cm. length) as shown in Fig. 4. At -196°C the deformation was more homogeneous, with fewer less sharply defined kinks formed. Twinning was also a feature at 20°C . In this case, the twinning was not operative until very high strains ($\sim 400\%$ shear strain).

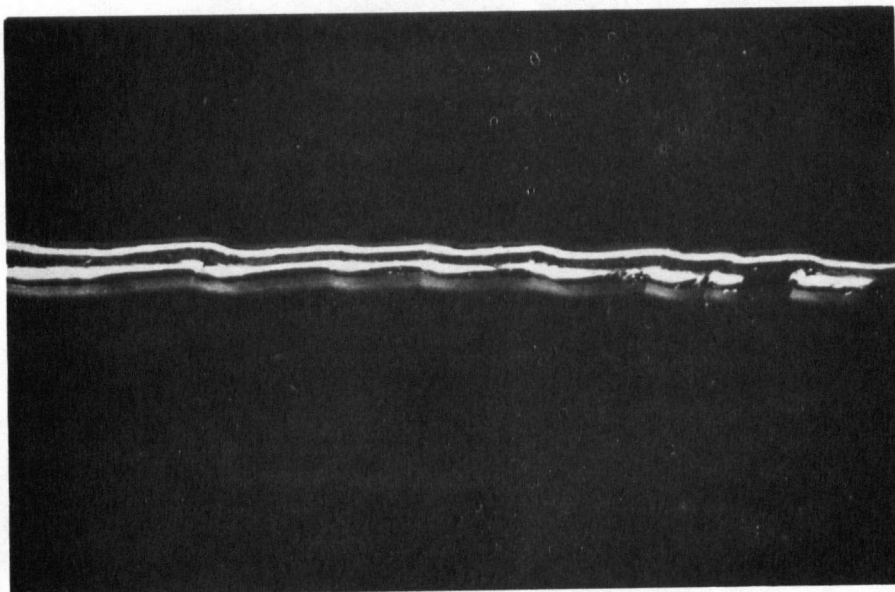


Fig 4. Typical tensile kinks formed at 20°C .

3.2 Recovery results

Risebrough⁵ has found that dynamic recovery in cadmium does not take place at temperatures less than -120°C . This has been confirmed in the present study, where it was found that for an anneal of 60 min. at -140°C , no recovery was detectable, whereas 15 min. recovery at -110°C showed significant recovery. Thus recovery must begin in the range $-140^{\circ} < T < -110^{\circ}\text{C}$. Accordingly, most attention has been focussed on results from method (1), in which all deformation is at -196°C , and recovery takes place in an unloaded specimen at elevated temperatures. Under these circumstances, recovery takes place only during the anneal cycles and not during deformation. Both methods (2) and (3) involve recovery during deformation.

One problem involved with any study of recovery is the definition of recovery itself. For this study, recovery has been defined as that fraction of the work hardening which is removed by a given anneal. In terms of flow stress parameters, this is:

$$R = \frac{\tau_{i-1} - \tau_i}{\tau_{i-1} - \text{crss}} = \frac{\text{softening due to anneal}}{\text{work hardening}}$$

and is described graphically in Fig. 5. This definition allows for a range of recovery from zero for no change in flow stress to 100%, for a recovery which results in a flow stress equal to the initial critical resolved shear stress. Recovery, as defined, is independent of strain or absolute flow stress values. This definition is also consistent with that used by other workers^{6,7}.

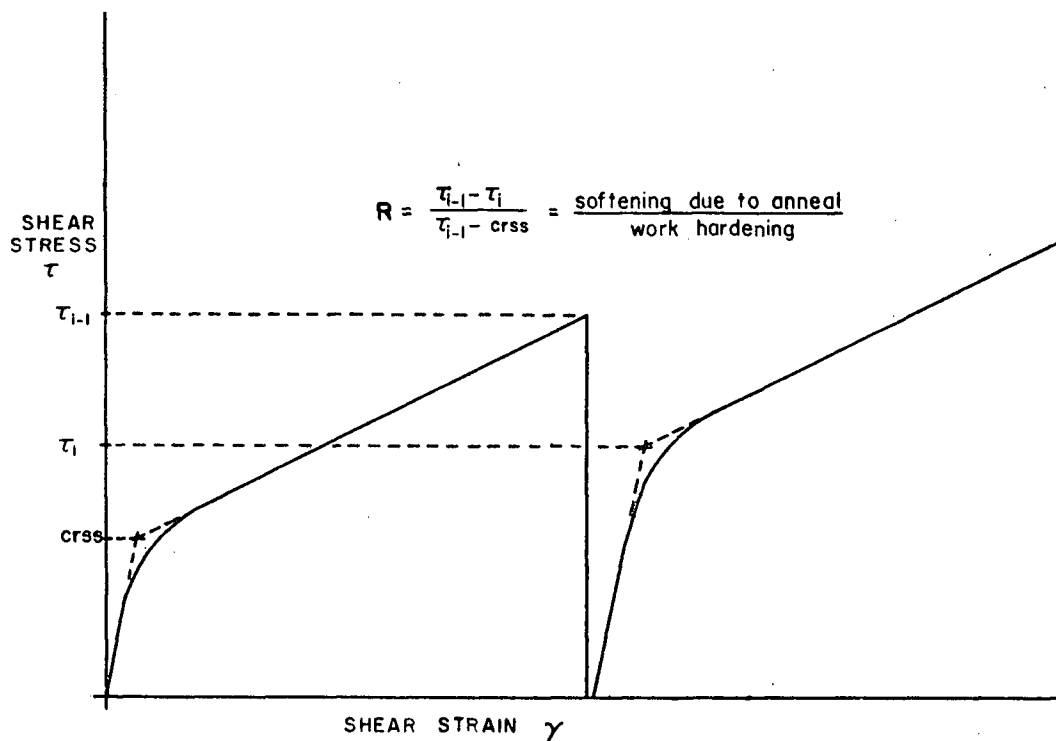


Fig 5. Definition of recovery.

A second method of measuring recovery which may be applicable, but which has not been used in this study would be to compare the flow stress under test conditions to that at -196°C . In this way both static and dynamic recovery would be measured and accounted for in tests in which both occurred. It would be difficult to interpret such data since there are variables involved such as stress and strain which are difficult to standardize. Consequently, this approach has not been applied to the data.

3.2.1 Method (1)

The results obtained for method (1) recovery are shown in Figs. 6 through 9, which are plots of recovery (R) vs. strain (γ). Comparing these plots, it is readily seen that recovery increases with increasing temperature and time. R, however, also varies with strain, and this must be taken into account when comparing recovery under various conditions.

With all deformation at -196°C , the resolved shear stress - shear strain curves were similar. If recovery is a similar function of strain at all times and temperatures investigated, the recovery values may be compared at any arbitrary value of strain. The same value of strain should provide comparison of recovery at a constant structure and so provide a constant activation entropy. Such a comparison at an arbitrary strain of $\gamma = 0.25$ is shown in Fig. 10. Some of the points on this plot have been determined by extrapolation of the individual graphs (Figs. 6-9), but this should not introduce any significant errors since comparison at the end of stage I showed that while the values of recovery were reduced, the overall effect of time and temperature was the same. (i.e. the slope of the plot of recovery vs. time was the same at most temperatures). At -100°C , the values were obtained by maintaining the difference between the two curves which is present at γ_I ($\gamma = 1.8$), and extrapolating the 40 min. curve to $\gamma = 0.25$. This operation in effect neglects the initial value at 90 min., but it was felt that the difference at γ_I is a more reliable value than the single point which was neglected. A second case in which the behaviour of recovery with time was not the same at $\gamma = .25$ and $\gamma = \gamma_I$ was with the $+30^{\circ}\text{C}$ set of data. In this case, it was found that recovery was essentially independent of time at the end of stage I as shown in Fig. 6. A possible reason for this anomaly will

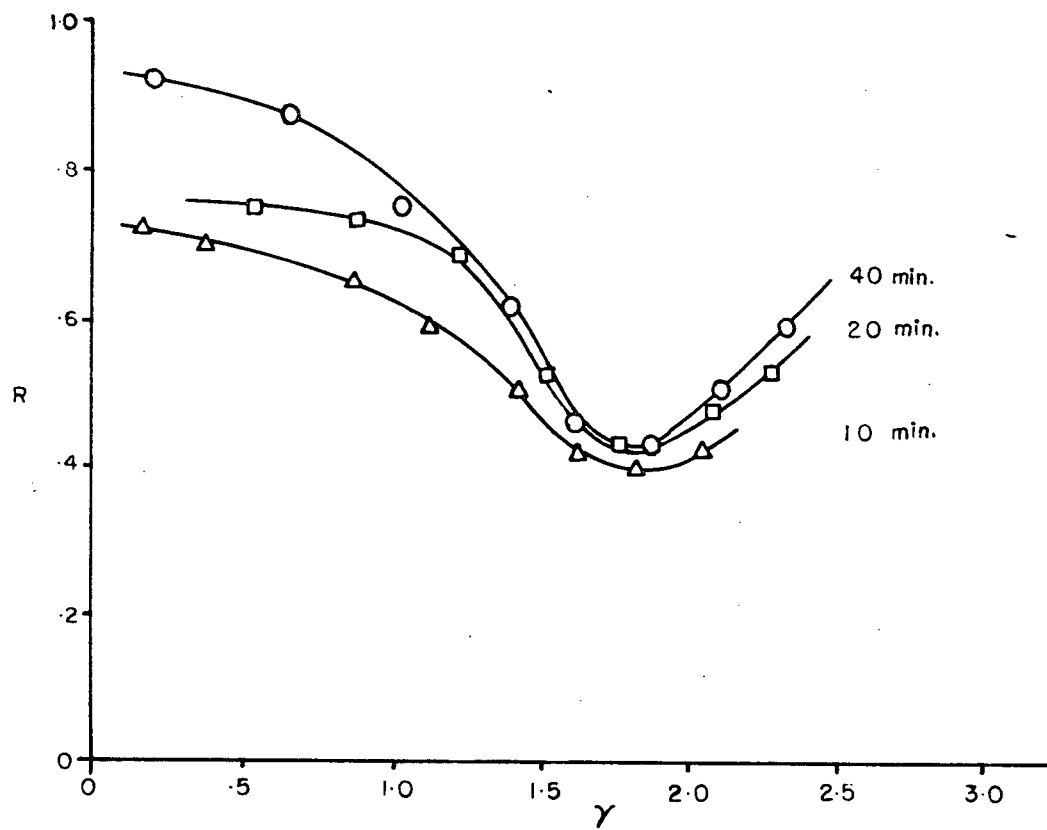


Fig 6. The variation of method (1) recovery at 30°C with strain.

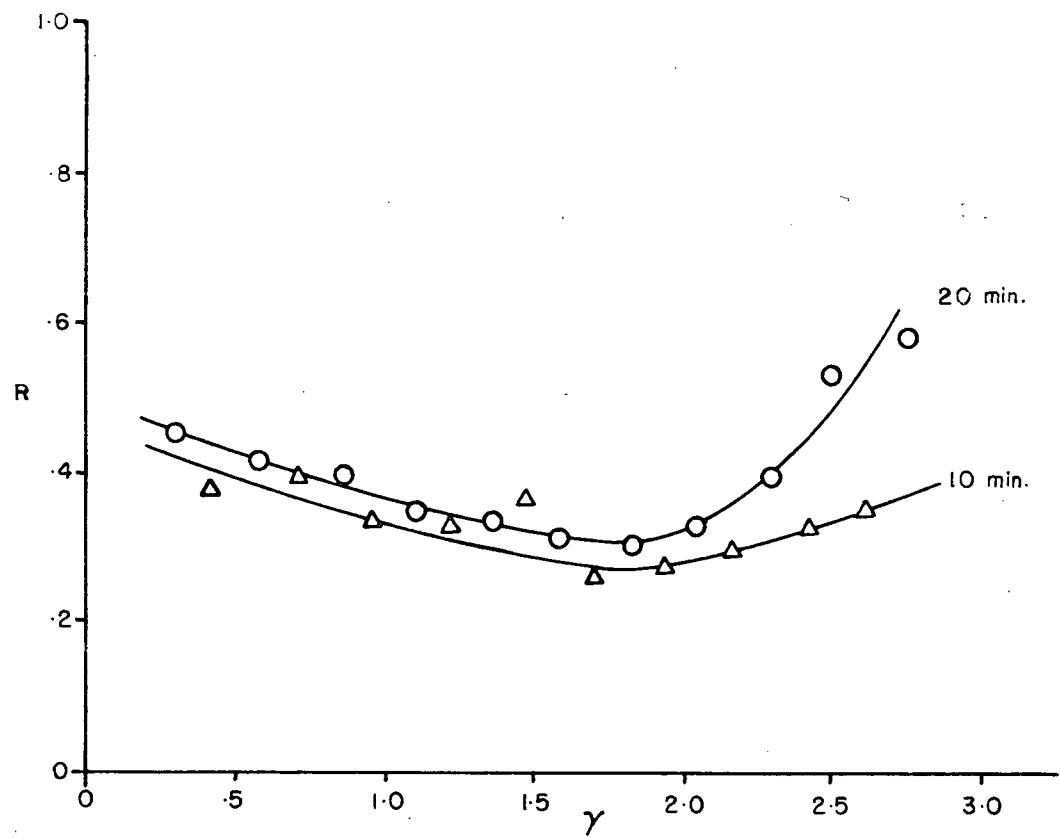


Fig 7. The variation of method (1) recovery at -20°C with strain.

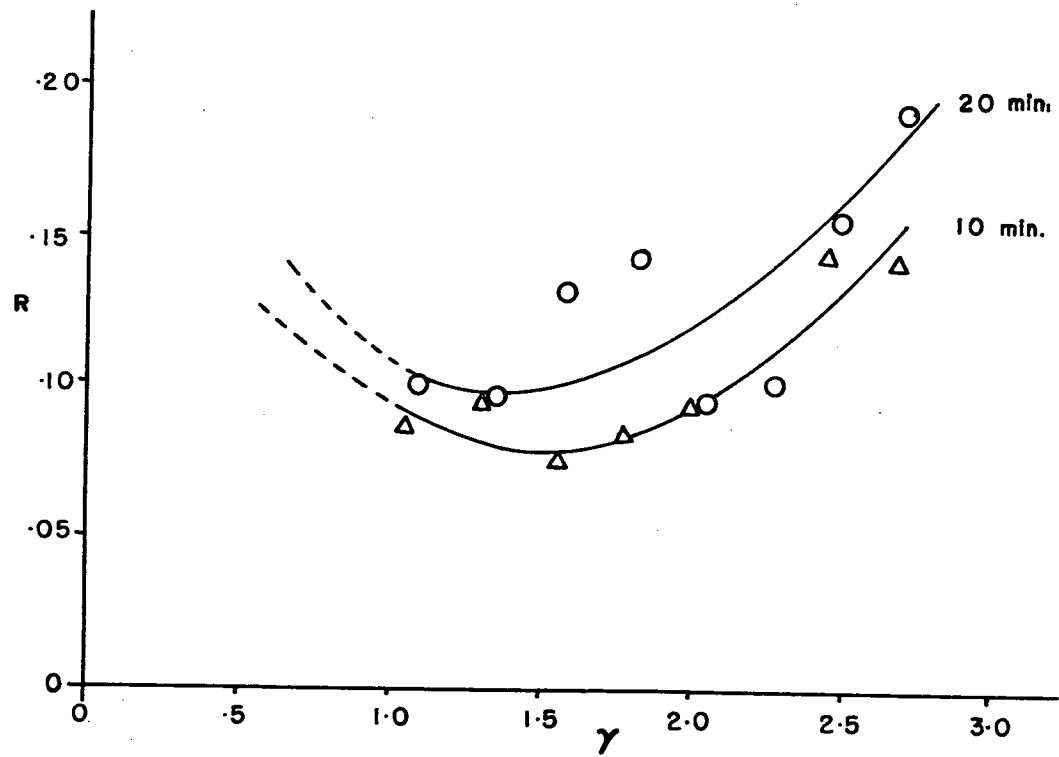


Fig 8. The variation of method (1) recovery at -70°C with strain.

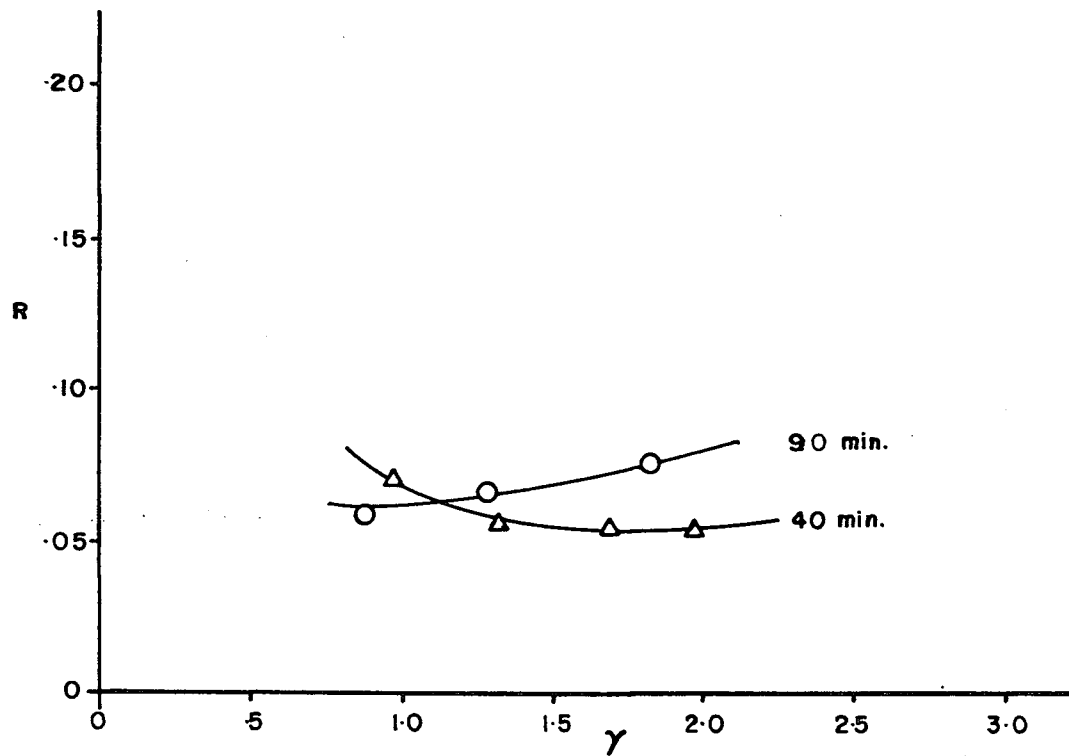


Fig 9. The variation of method (1) recovery at -100°C with strain.

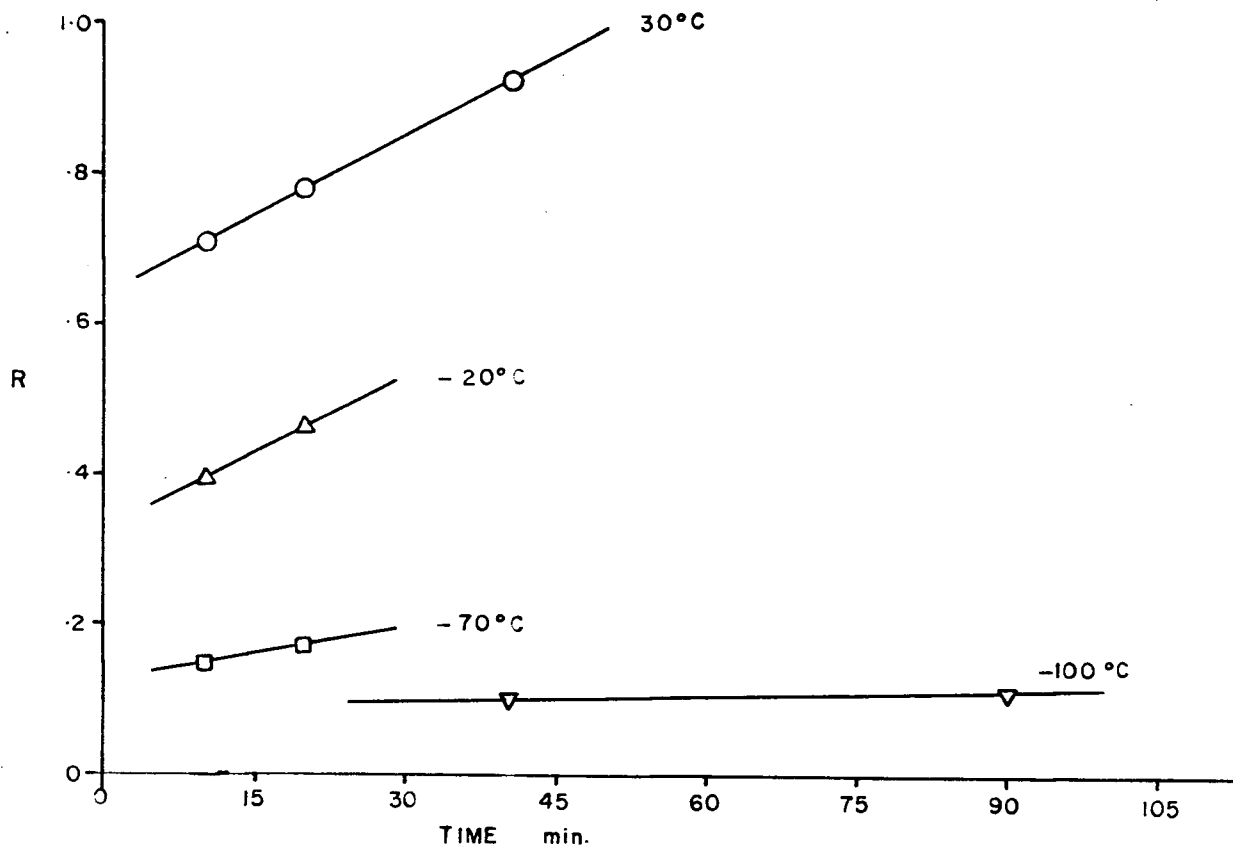


Fig 10. The variation of method (1) recovery with time at $\gamma = 0.25$.

be discussed later with respect to saturation recovery.

Fig. 11 shows the results of type (1) recovery at various strains in the high temperature range 50°C to 100°C. These points are from a variety of experimental annealing conditions, yet form no systematic variation with either time or temperature. Although Fig. 11 shows only a few different annealing conditions, within each listed condition there may have been a variation of as much as $\pm 10^\circ\text{C}$ in temperature and/or $\begin{matrix} +30 \\ -0 \end{matrix}$ min. in time and there was still no systematic variation in recovery. It is believed that each individual point represents the maximum recovery attainable for its particular crystal at the strain shown. Individual points were not, however, tested to determine whether or not maximum recovery had been reached, but since all recovery values are not significantly higher than those obtained in 40 min. at 30°C (Fig. 6), it is felt that the conditions employed were more than adequate to achieve the maximum recovery attainable. It was found that higher temperatures ($\geq 100^\circ\text{C}$) initiated recrystallization.

While it is apparent that there is some scatter in the data, this scatter does occur in a reasonably narrow band. The curve in Fig. 11 represents the upper limit of recovery, and because it does depict the maximum recovery attained, it is termed the "saturation recovery". This curve shows that recovery is essentially complete at low strains, but at strains in excess of 75%, it decreases markedly. The overall shape of this curve is very similar to those of Fig. 6, and may also show a minimum at γ_I .

3.2.2 Method (2)

Results of method (2) recovery are shown in Figs. 12 to 15. As was the case for method (1), the amount of recovery is a function of

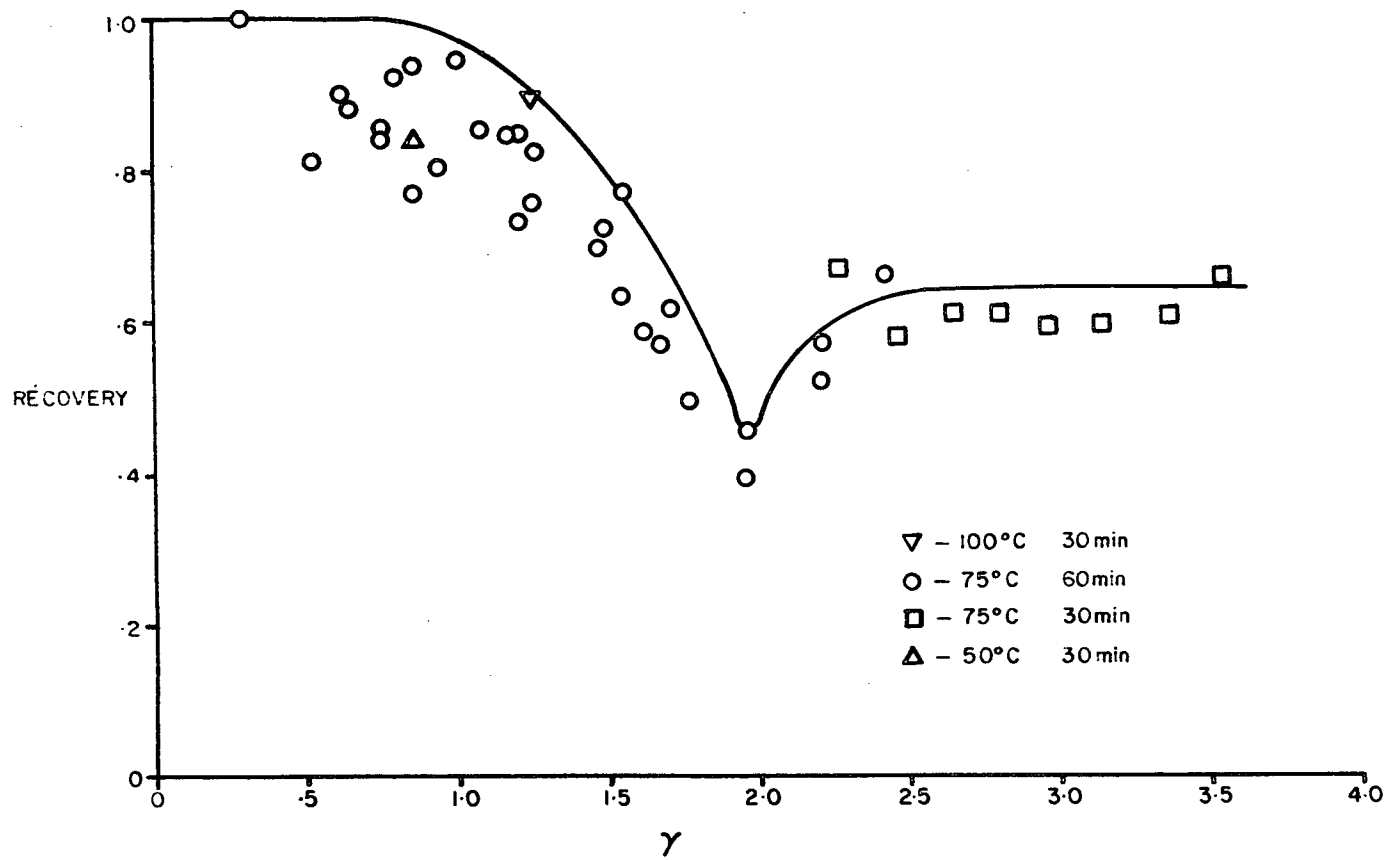


Fig 11. The variation of saturation recovery with strain.

annealing time, temperature and strain. The general shape of the curves is also similar. The primary differences are in the magnitude of recovery and in the regularity of data. The regularity of data with this method as compared to method (1) may be due to the fact that method (2) tests were much easier to perform experimentally than were those for method (1).

In order to compare the dynamic recovery present in method (2) tests with the static recovery in method (1), a crystal was deformed initially at -196°C , then allowed to completely recover (60 min. at 75°C ; i.e. method (1)) and finally deformed at 20°C . The results of this test are compared to a crystal deformed at 20°C , recovered under the same conditions and at the same strain (i.e. method (2)), and then deformed at 20°C in Fig. 16. It can be seen that the flow curve of the first crystal is identical to that of the second following the recovery anneals. Thus it is concluded that at least up to the strain at which recovery was performed that the static recovery measured in method (1) is equivalent to static and dynamic recovery measured in method (2).

3.2.3 Method (3)

In method (3), where the load was not removed during recovery, the results are very similar to method (2), both in magnitude of recovery and in the general shape of the recovery vs. strain curves. Direct comparison of the curves showed that in most cases, the effect of the applied load on recovery was negligible. Whenever any deviation did occur between the two methods it was such that the recovery was enhanced by the applied load, but always in negligible amounts.

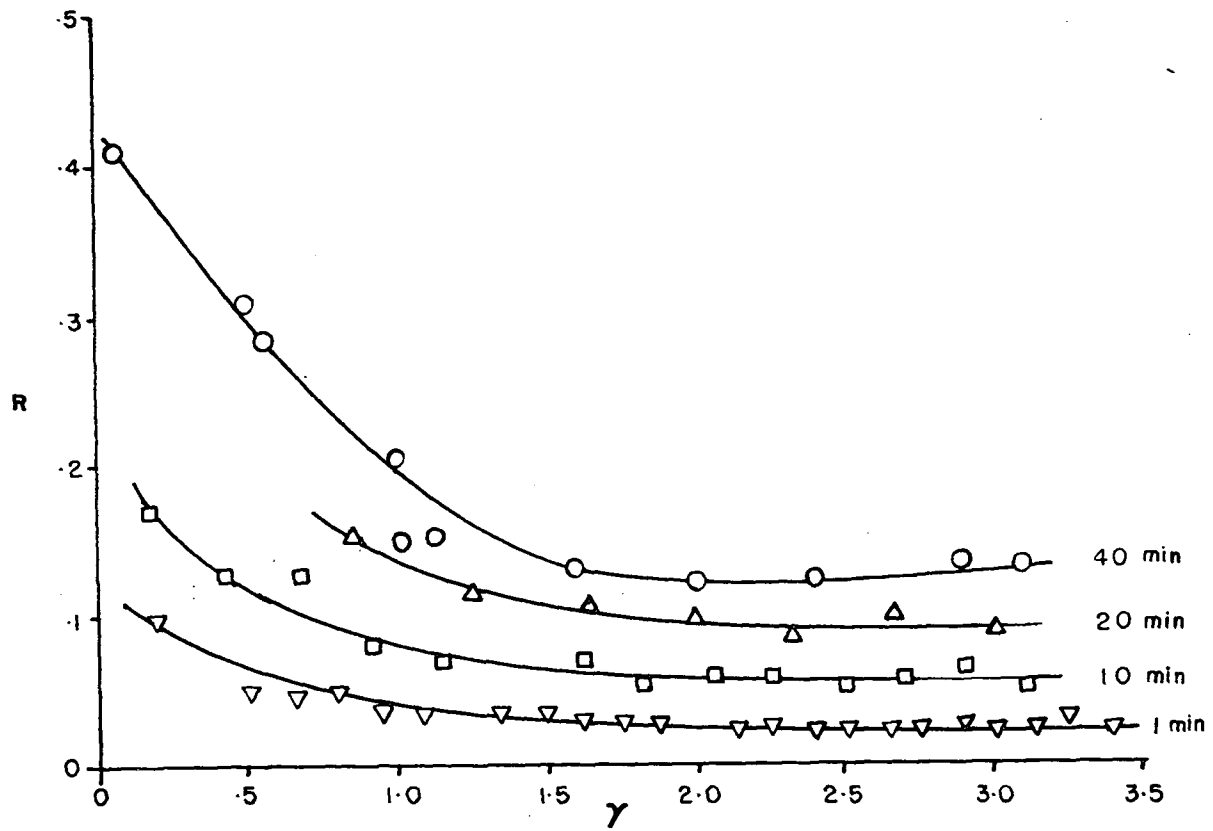


Fig. 12. The variation of method (2) recovery at 20°C with strain.

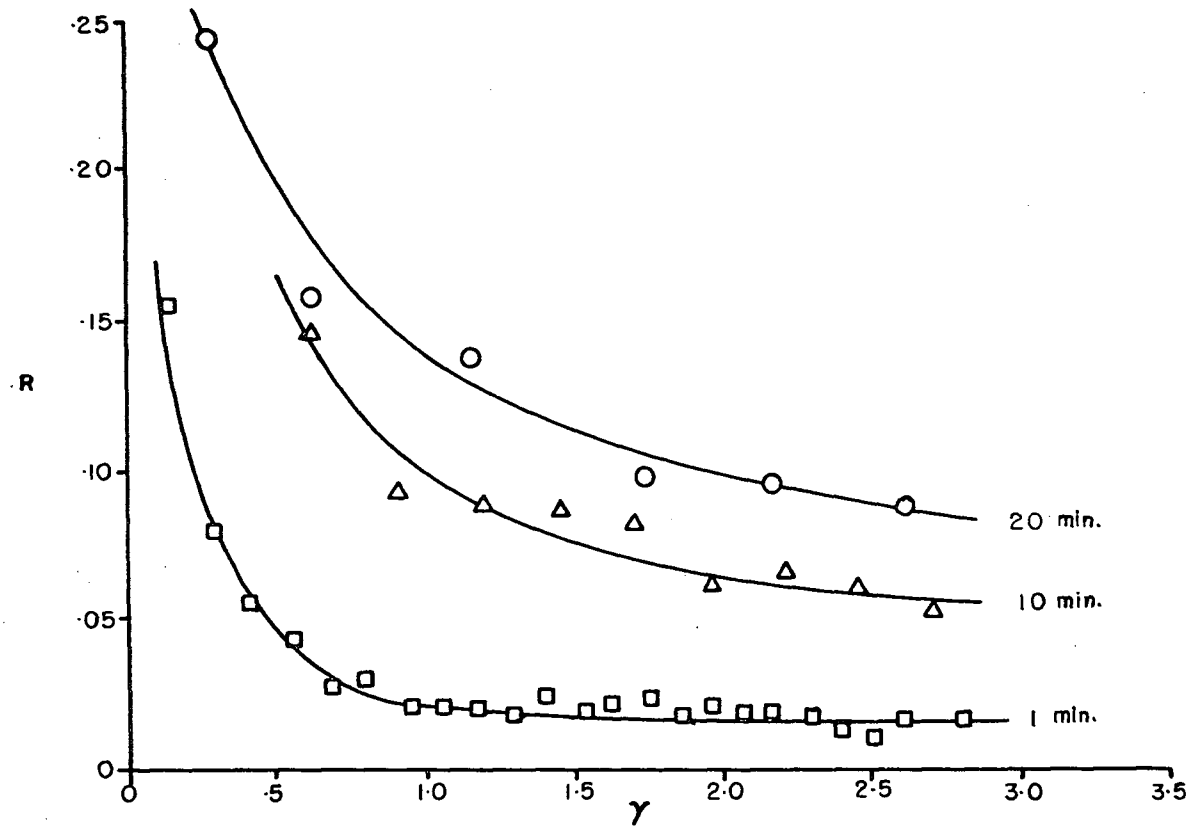


Fig 13. The variation of method (2) recovery at -30°C with strain.

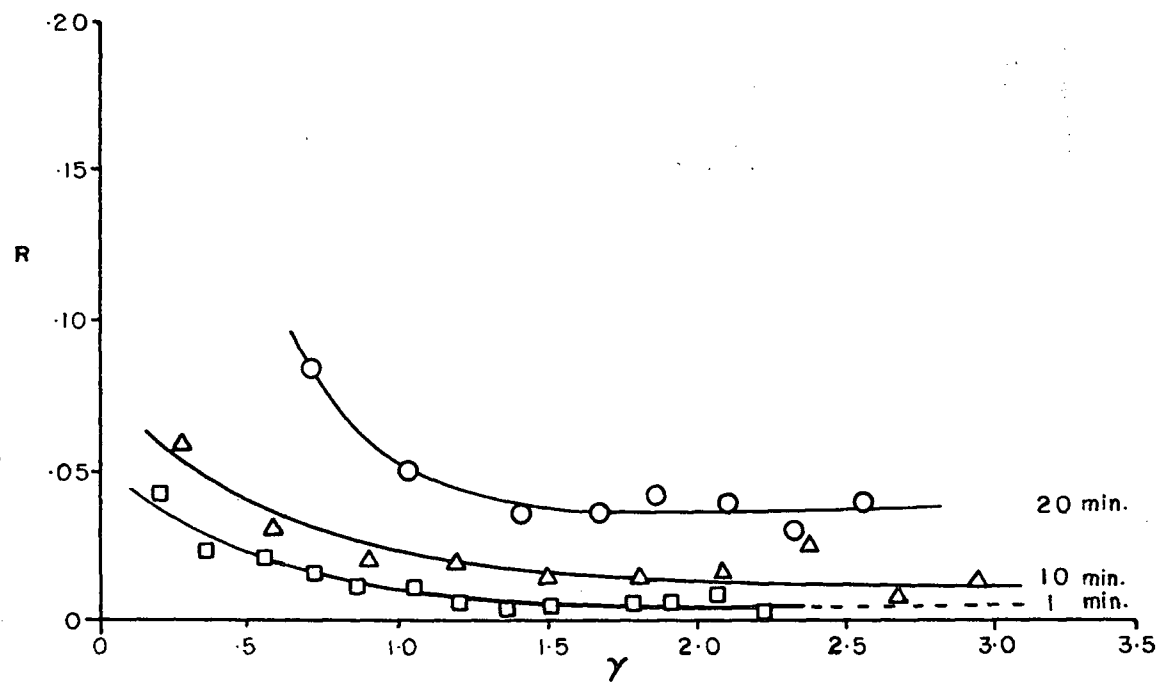


Fig 14. The variation of method (2) recovery at -70°C with strain.

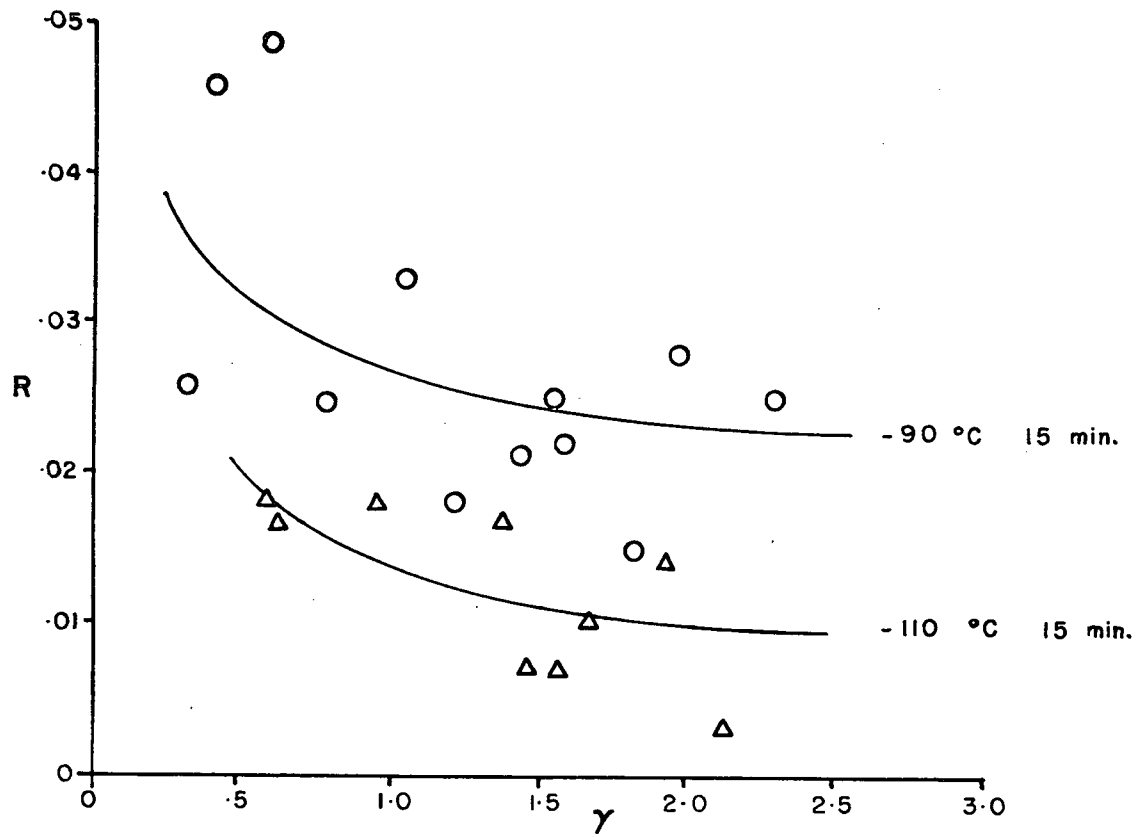


Fig 15. The variation of method (2) recovery at -90°C and -110°C with strain.

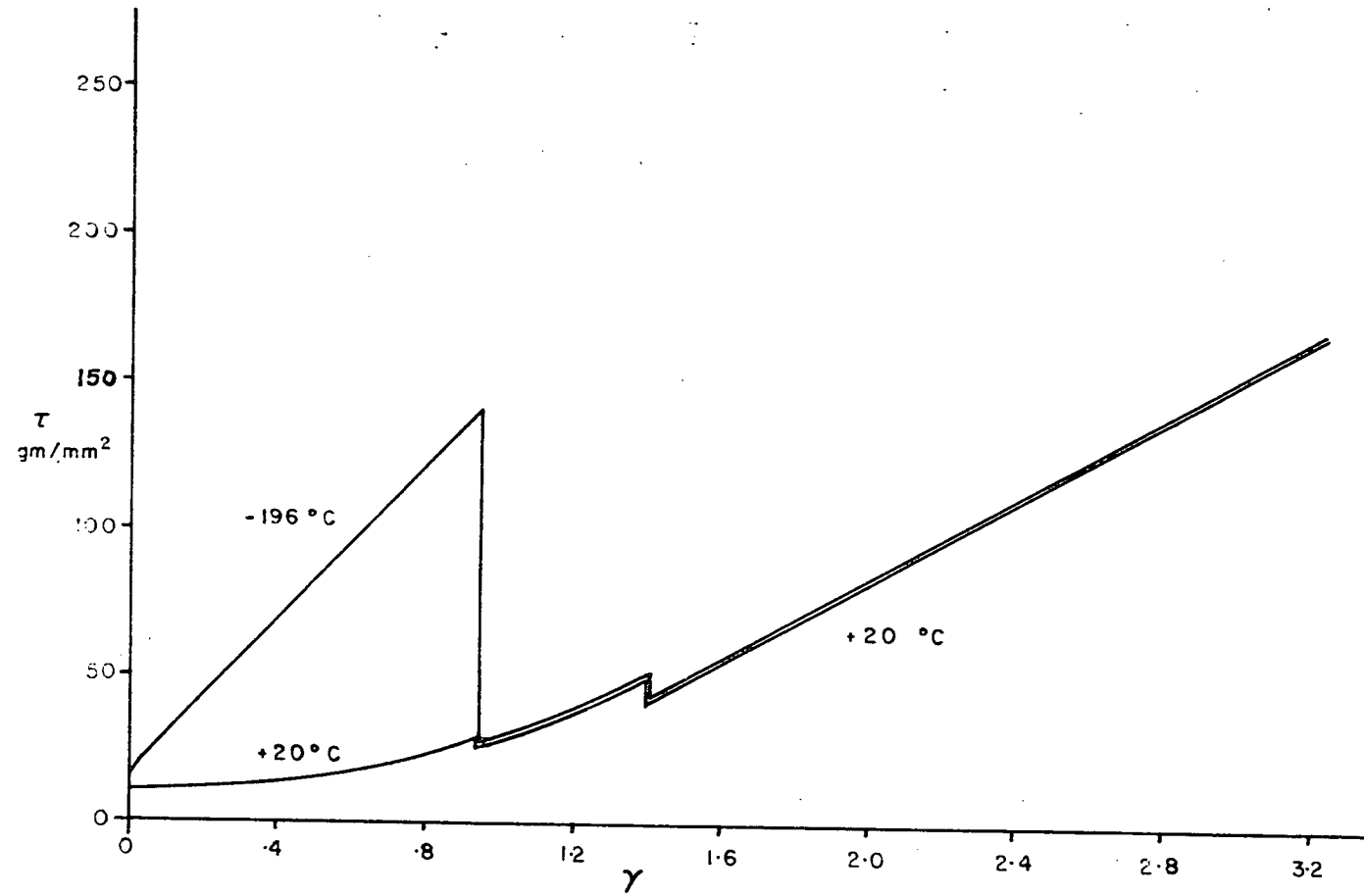


Fig 16. The effect of temperature on easy glide deformation.

3.3 Strain rate change tests

Strain rate change tests were performed on cadmium single crystals at -196°C . These crystals were similar to those used for recovery experiments in that they were oriented to show a long easy glide. The results of such experiments should show the variation in activation volume¹² with strain, and also whether or not this material obeys the Cottrell-Stokes¹³ law, since both of these parameters are calculated from strain rate change data.

In addition to strain rate changes, recovery anneals were performed intermittently during some tests to determine the effects of recovery on both activation volume and Cottrell-Stokes behaviour.

The typical shape of the load-elongation plot during a strain rate change cycle is shown in Fig. 17. Also shown in this plot is the method employed to measure the change in flow stress accompanying a change in strain rate. It was found experimentally that the values measured from an increase in strain rate (ΔP_U) were much more reproducible than those associated with a decrease in strain rate (ΔP_D). This was probably due to the time lag associated with a strain rate decrease on the Instron tensile machine. An example of the difference between these two measurements is shown in Fig. 18. This is a plot of activation volume (which is proportional to ΔP^{-1}) as a function of strain. As a result of the scatter in ΔP_D , only ΔP_U values have been used for the following results.

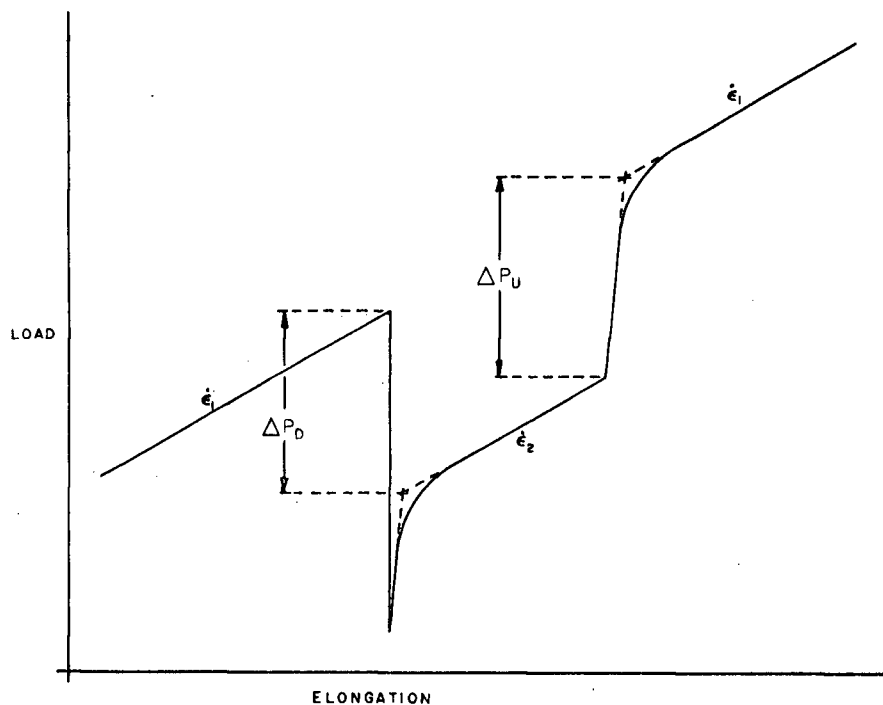


Fig 17. The determination of load change with strain rate change.

3.3.1 Activation volume

The first method of presentation of the strain rate change data is in the form of activation volume. This is defined as:

$$v = kT \frac{\ln \dot{\epsilon}_1 / \dot{\epsilon}_2}{\Delta \tau}$$

Activation volume determination should give some idea as to the rate controlling processes of deformation.

The variation in activation volume with strain is shown in Fig. 19. It is seen that v is a steadily decreasing function of strain throughout the entire range.

The effect of saturation recovery (60 min. at 75°C) on activation

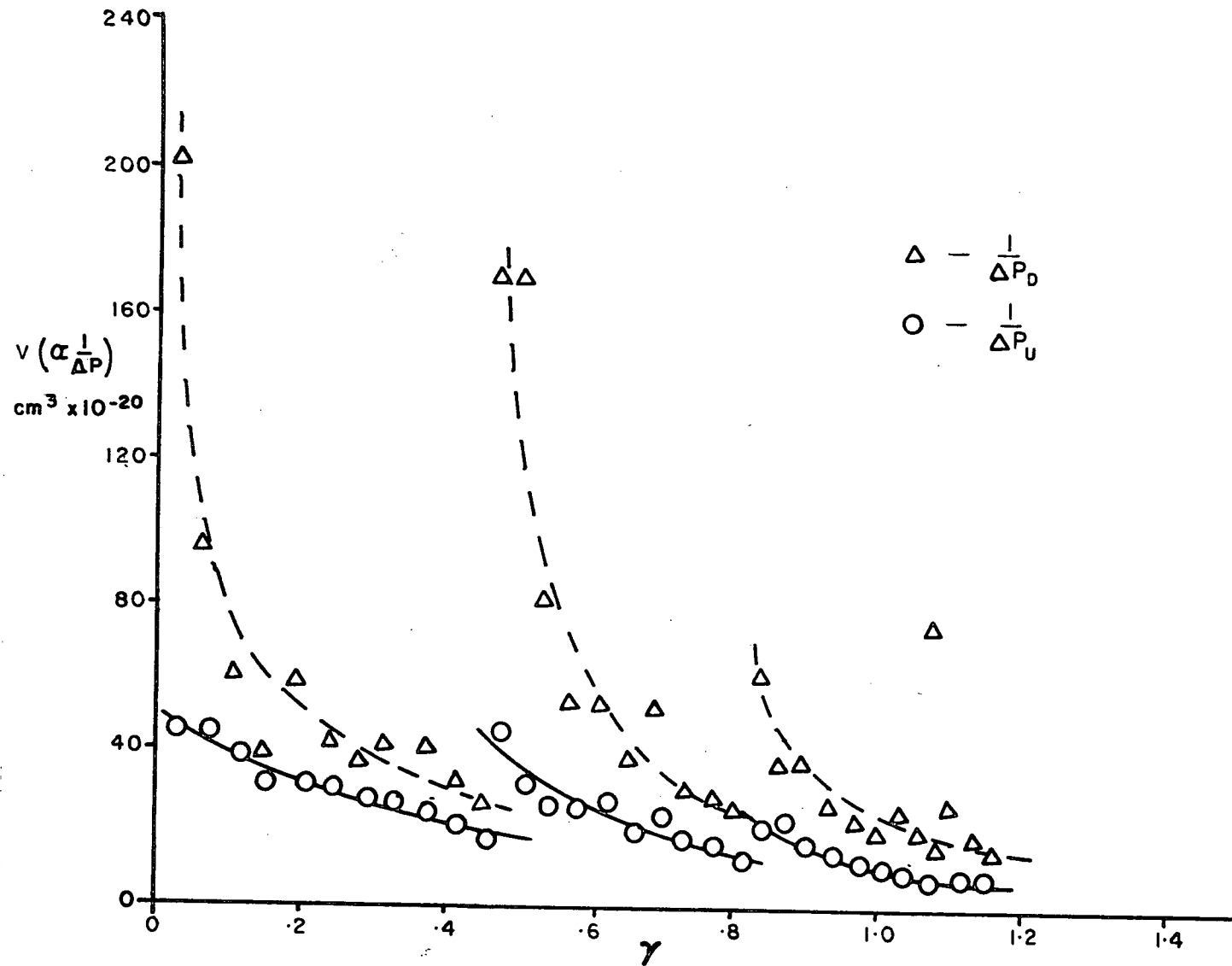


Fig 18. Comparison of activation volume data obtained from strain rate up-change and down-change.

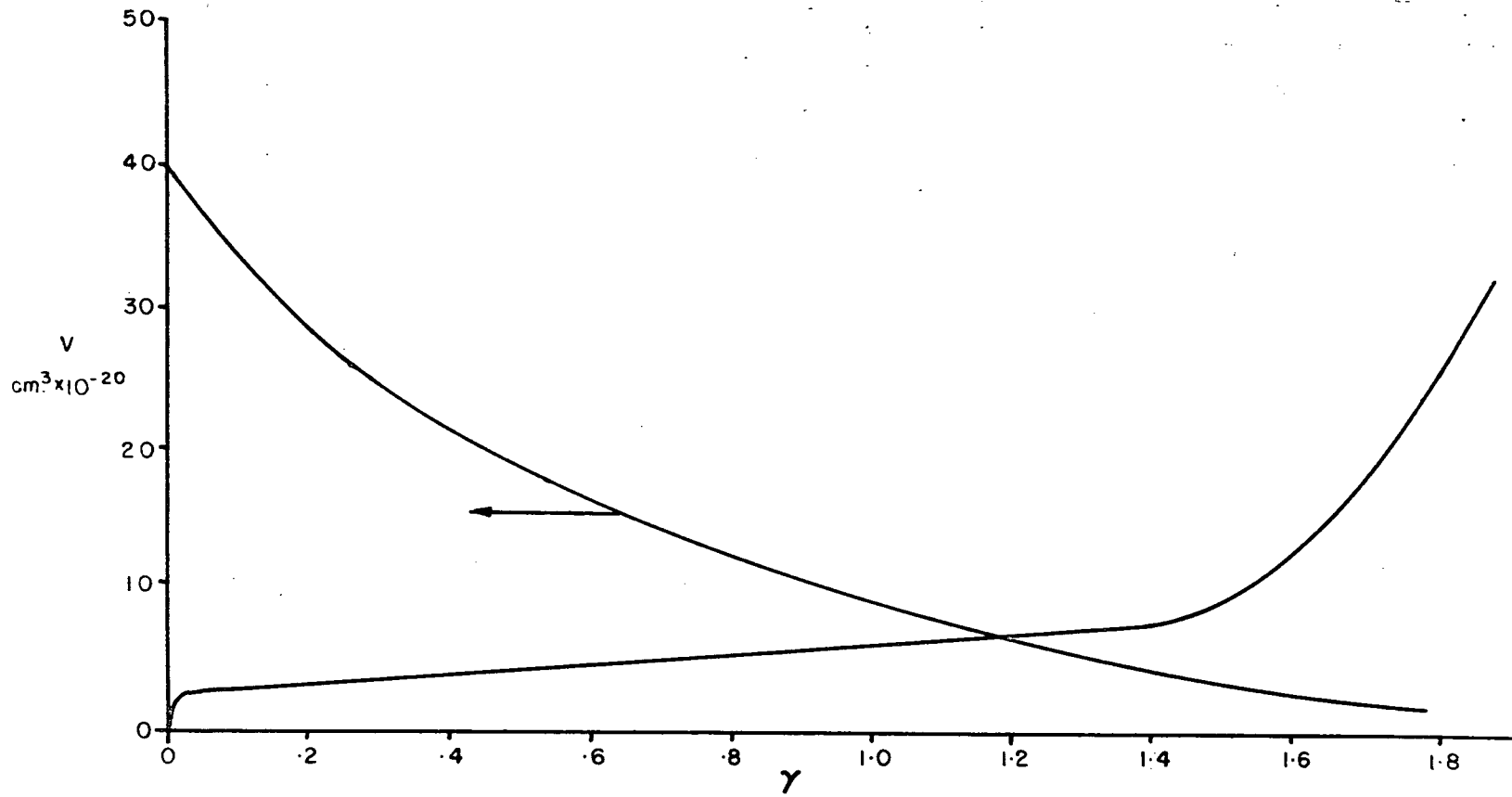


Fig 19. The strain dependence of activation volume. (The relevant portion of the stress-strain curve is shown for comparison.)

volume in easy glide is shown in Fig. 20. It is seen that at low strain, recovery increases the value of activation volume back to the value that was found at yield. At higher strains (>70%) it was found that recovery still increased the value of activation volume considerably, but not to a value as high as that at yield. In stage II, recovery still increased the value of activation volume as shown in Fig. 21. In this range, the change in v with recovery is essentially constant, and not a function of strain.

3.3.2 $\Delta\tau$ versus τ

Another method of presenting the same data is to plot $\Delta\tau$, rather than v which is proportional to $\Delta\tau^{-1}$, versus τ rather than strain. If such a plot is linear, and passes through the origin then the Cottrell-Stokes law is considered to be obeyed. Risebrough⁵ and Davis¹⁶ found that the Cottrell-Stokes law was obeyed in cadmium single crystals at -196°C , during stage II deformation. The obedience or non-obedience of this law is not clearly understood with respect to hexagonal metals; however the plot does provide much useful information.

The plot of $\Delta\tau$ vs. τ for single crystal cadmium is shown in Fig. 22. It is seen that there is a distinct change in this plot at the end of linear easy glide, but the Cottrell-Stokes law is not strictly obeyed in either region.

When saturation recovery anneals are performed in stage I, it is seen in Fig. 23 that the first anneal has no effect on the $\Delta\tau - \tau$ relationship, but after the second anneal there is a slight increase in slope.

Saturation recovery in stage II has a much different effect than it did in stage I as shown in Fig. 24. After the first anneal there is a large shift in the curve to the left. This is because recovery reduces

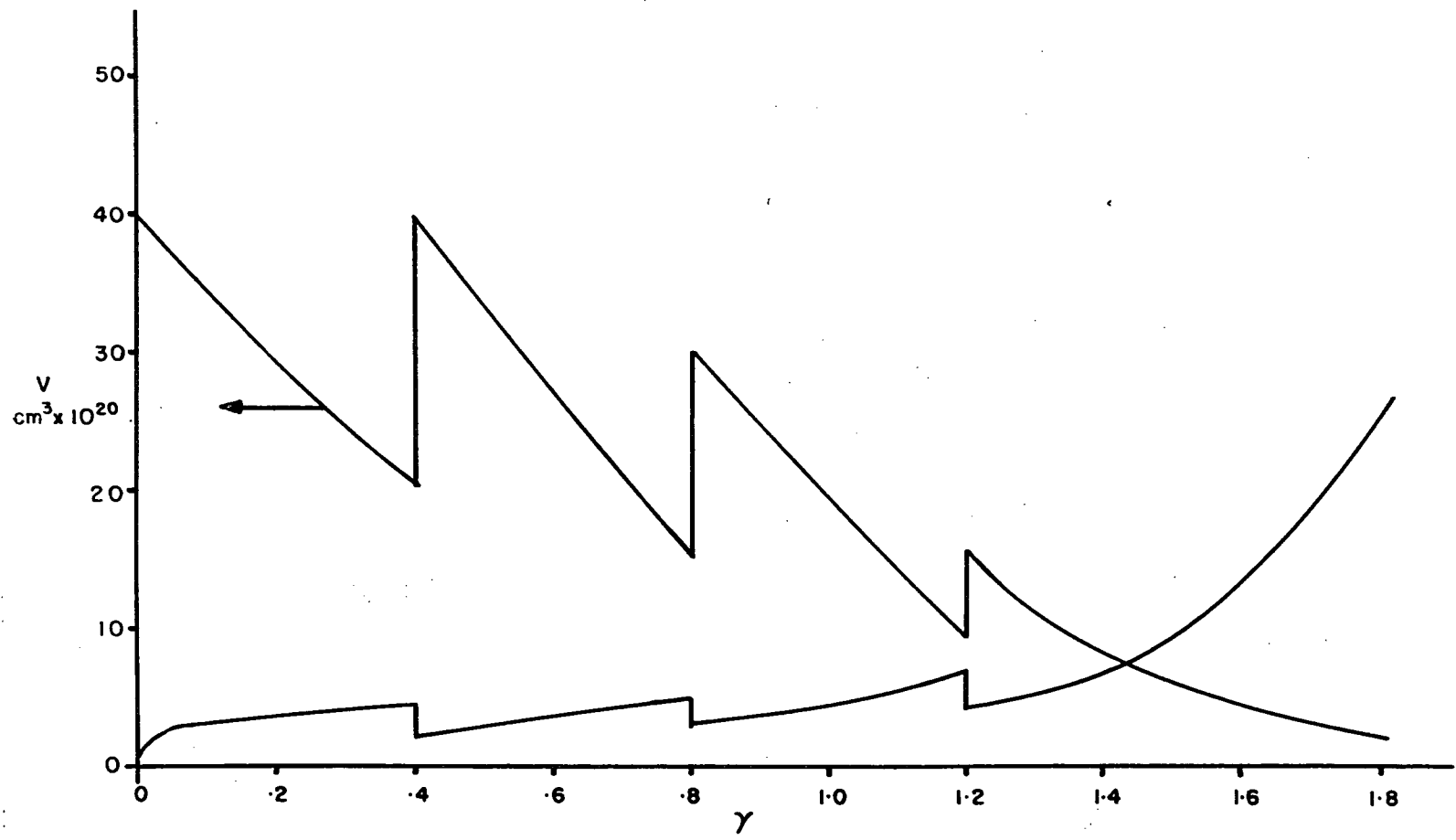


Fig 20. The effect of saturation recovery on activation volume in easy glide.
 (The relevant portion of the stress-strain curve is shown for comparison.)

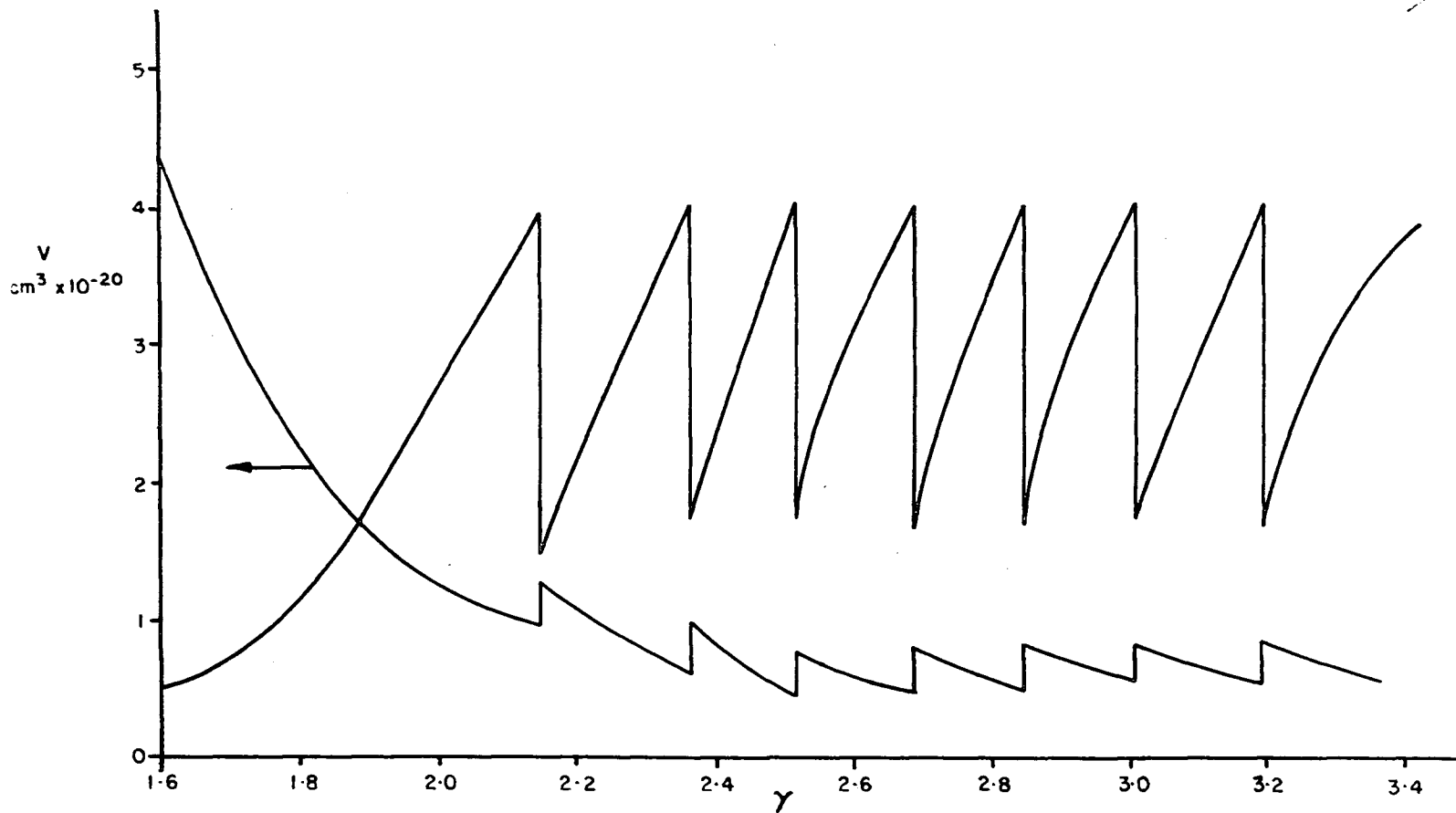


Fig 21. The effect of saturation recovery on activation volume in stage II.
 (The relevant portion of the stress-strain curve is shown for comparison.)

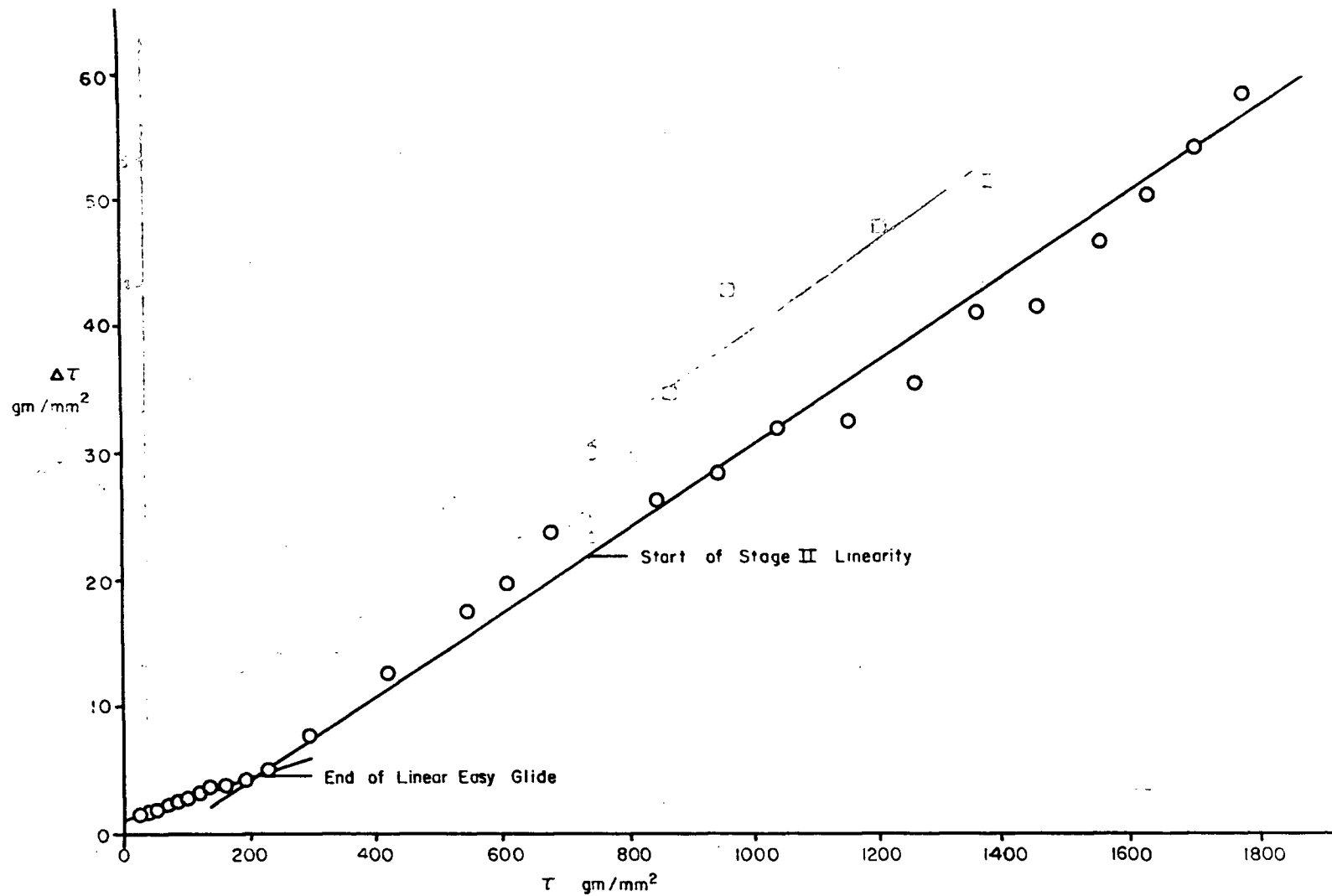


Fig 22. The variation of $\Delta\tau$ with τ .

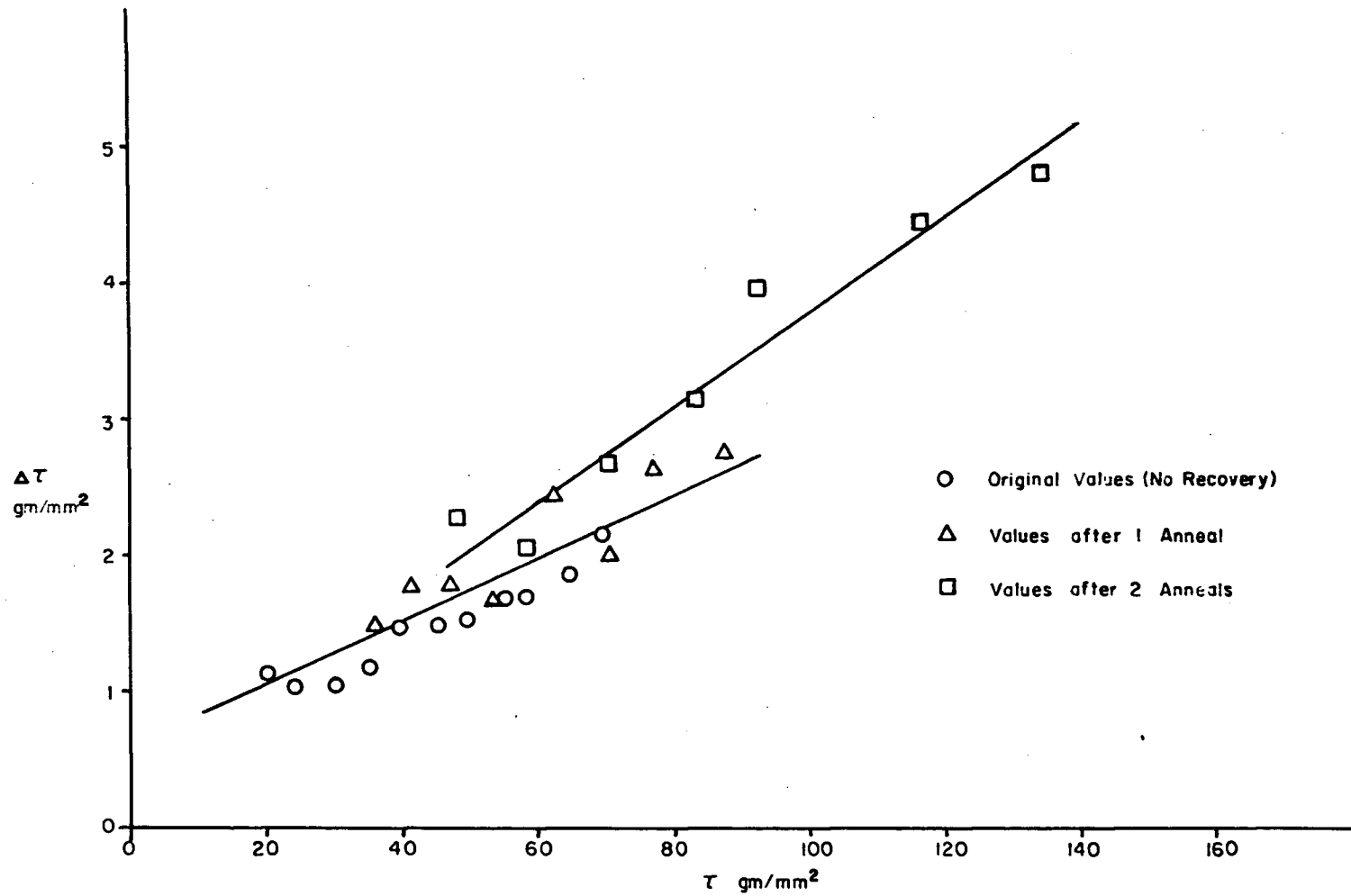


Fig 23. The variation of $\Delta\tau - \tau$ with saturation recovery in easy glide.

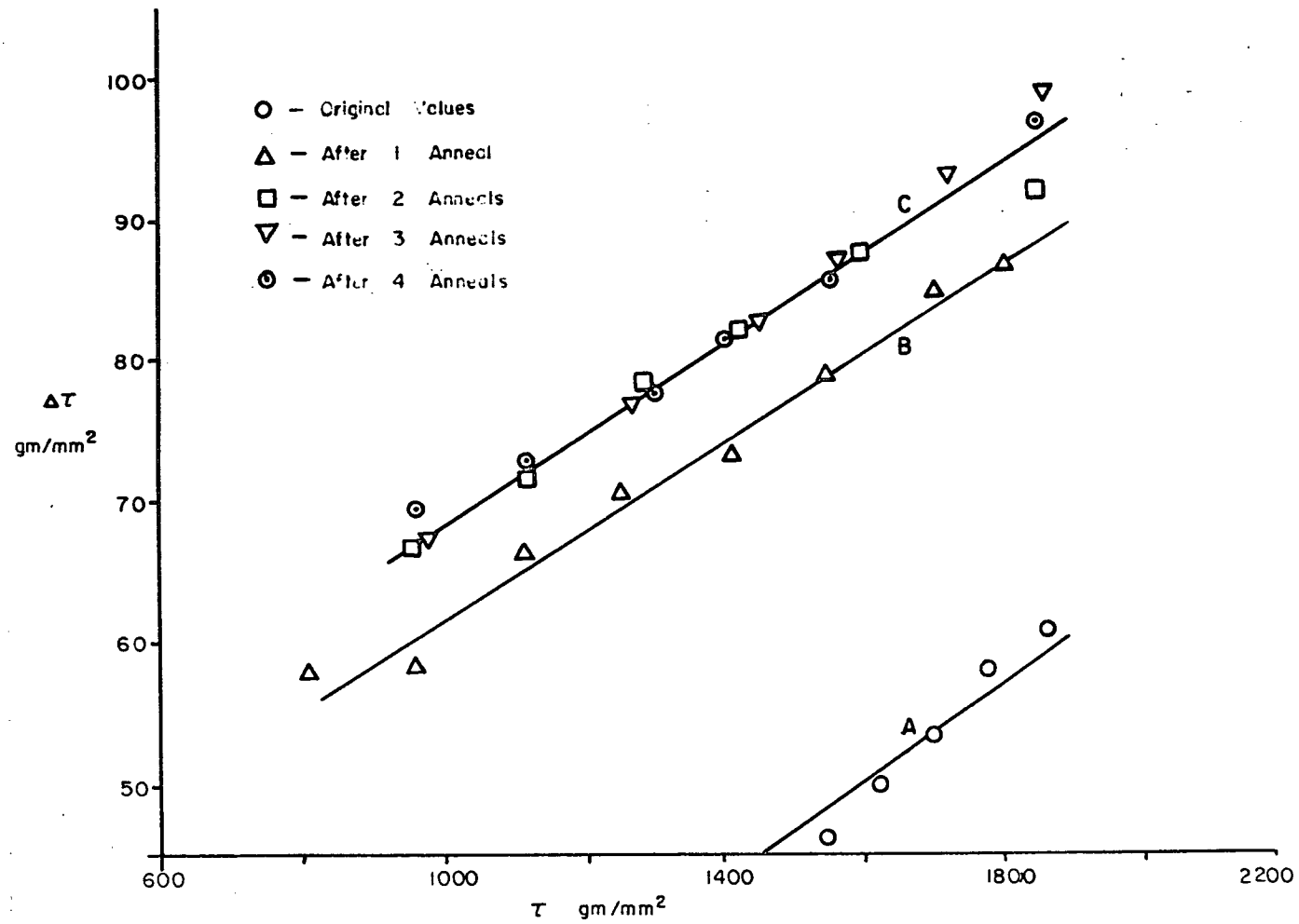


Fig 24. The variation of $\Delta\tau - \tau$ with saturation recovery in stage II.

τ significantly but leaves $\Delta\tau$ essentially unchanged. The slope of the curve following this recovery is the same as it was prior to recovery. A second anneal in stage II caused a further shift to the left since although $\Delta\tau$ did decrease at this point, it did not decrease as much as it had increased from the previous recovery. Again, the slope of the plot was the same. Further recoveries show that both $\Delta\tau$ and τ decrease by the same amount that they increased during strain from the previous recovery. Note that each recovery was performed when the stress on the system reached 2000 gm/mm².

3.4 Work hardening parameters

To determine the effects of crystal orientation on various work hardening parameters, a study was carried out using a wide range of initial orientations. This study should also help to differentiate between effects which are caused by the changing orientation of a crystal during a tensile test and those which are characteristic of recovery. Crystals with initial orientation χ_0 ranging from 25° to 48° were investigated. In all cases λ_0 was very nearly equal to χ_0 .

3.4.1 Stage I

Stage I has been defined as the first linear stage of hardening during the deformation of a cadmium single crystal. The primary work hardening parameters to be considered are the initial flow stress or critical resolved shear stress, the work hardening rate and the amount of linear strain. These factors, and the effects of orientation and recovery on them, are discussed below.

3.4.1.1 Critical resolved shear stress

The critical resolved shear stress at -196°C was found to be $19.4 \text{ gm/mm}^2 \pm 4.5 \text{ gm/mm}^2$, and essentially independent of initial orientation as shown in Fig. 25. This is in agreement with Schmid's shear stress law¹¹ which states that there should be no orientation dependence of this stress.

The variation in critical resolved shear stress with temperature is shown in Fig. 26. The stress values have been corrected for the temperature dependence of the shear modulus by dividing each by the shear modulus at its particular temperature. Values of shear modulus (C_{44}) were obtained from Gerland and Silverman¹⁴. It is seen that at low temperatures, there is no change in crss with temperature, while at higher temperatures there appears to be a slight decrease. There is so much scatter in the data that it is statistically difficult to make any definite statements about this behaviour.

3.4.1.2 Work hardening rate

The work hardening rate in easy glide (θ_I) was found to increase about 50% with χ_0 decreasing from 45° to 25° as shown in Fig. 27.

The effect of recovery on this parameter was to increase θ_I to a value comparable to that for a virgin crystal with initial orientation equal to the orientation which had been achieved by strain to the point of recovery. This is illustrated in Fig. 28 where sample S39A was deformed from an initial orientation of 45° to 35° . Sample M4A had an initial orientation of 35° , and it is seen that following recovery of sample S39A, the work hardening rate of the two crystals is the same.

Fig. 29 shows the variation of θ_I with temperature at an initial strain rate of $1.3 \times 10^{-3} \text{ sec}^{-1}$. Shown for comparison are the results of

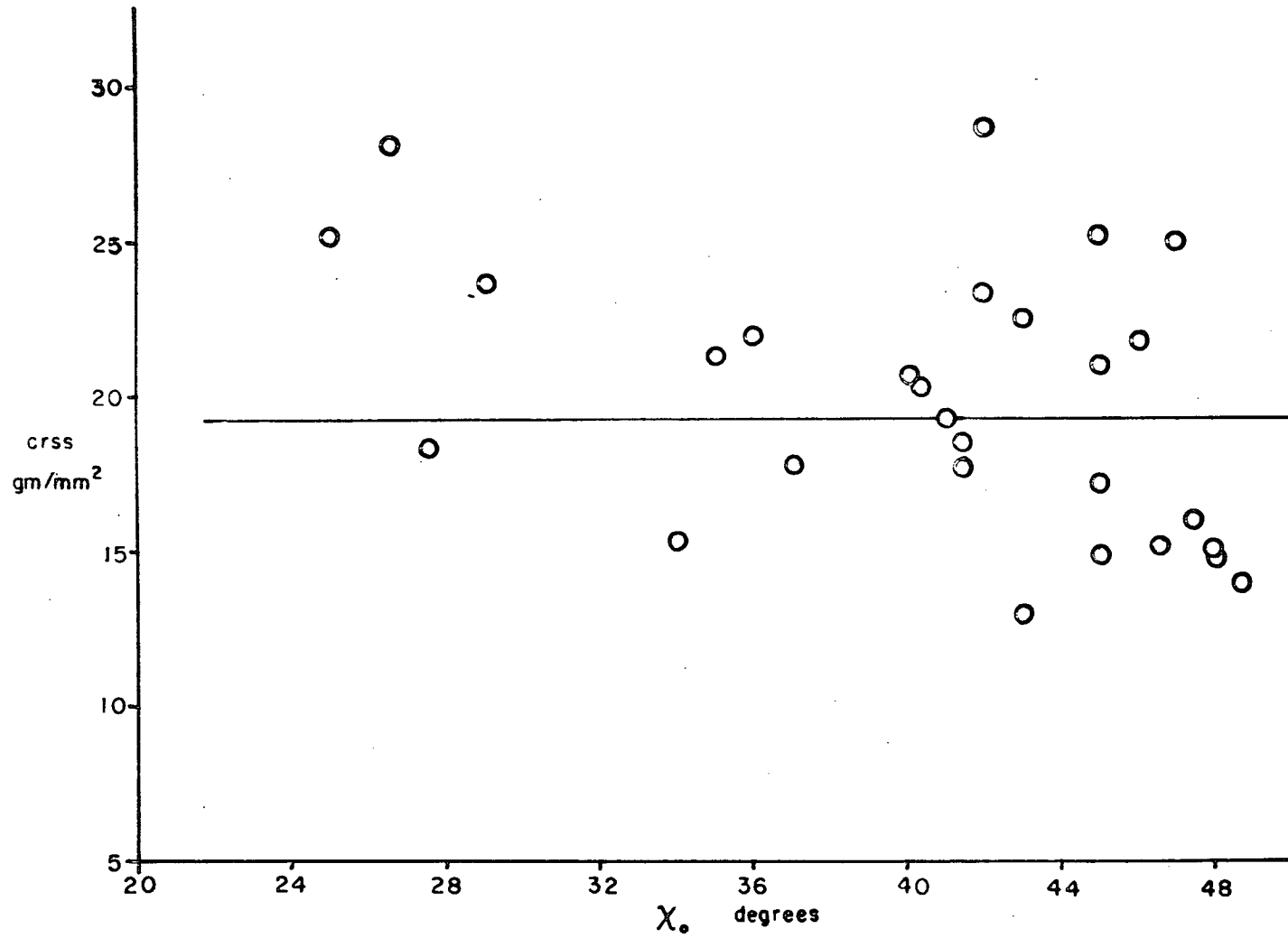


Fig 25. Orientation dependence of the critical resolved shear stress.

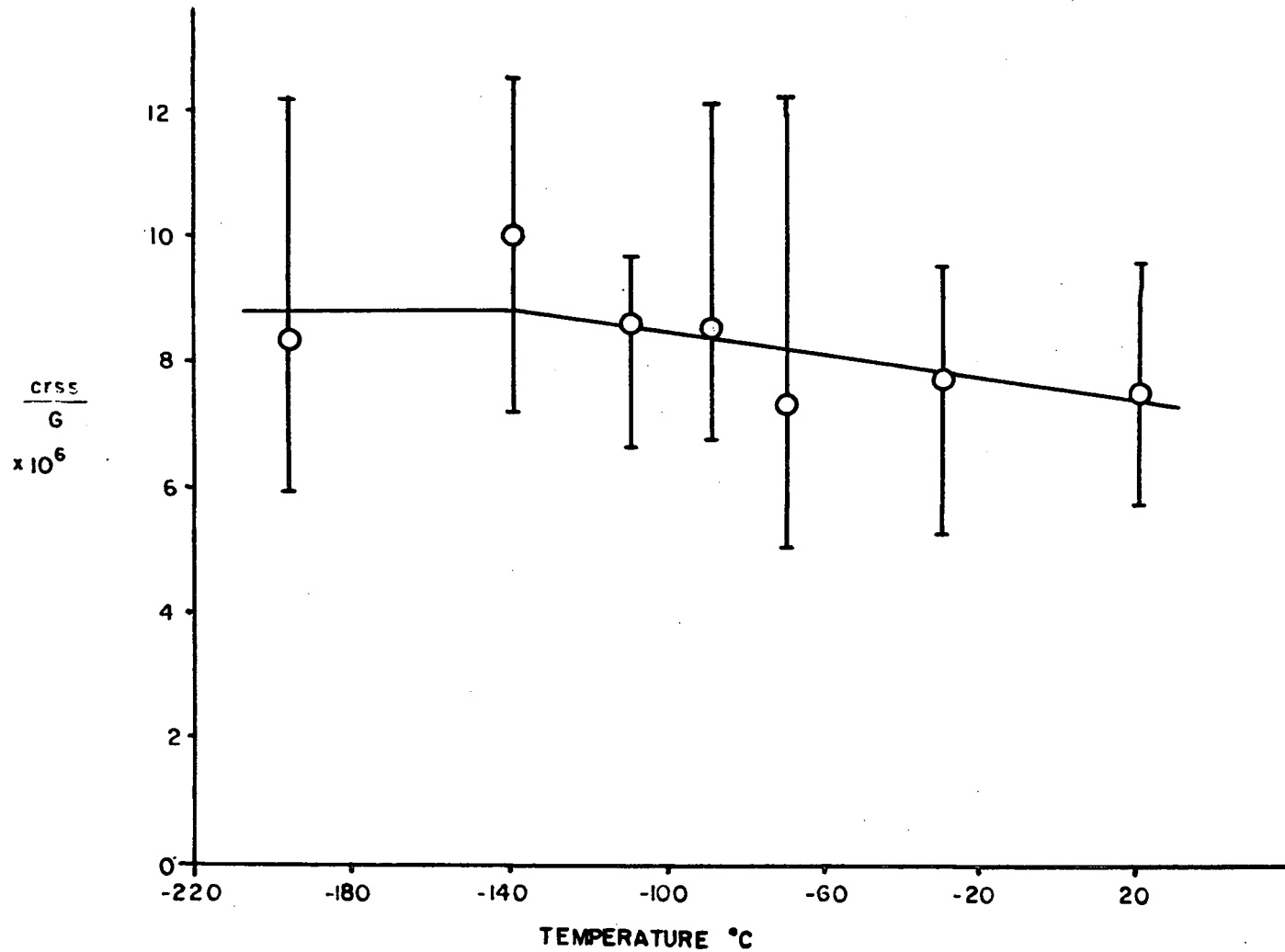


Fig 26. Temperature dependence of the critical resolved shear stress.

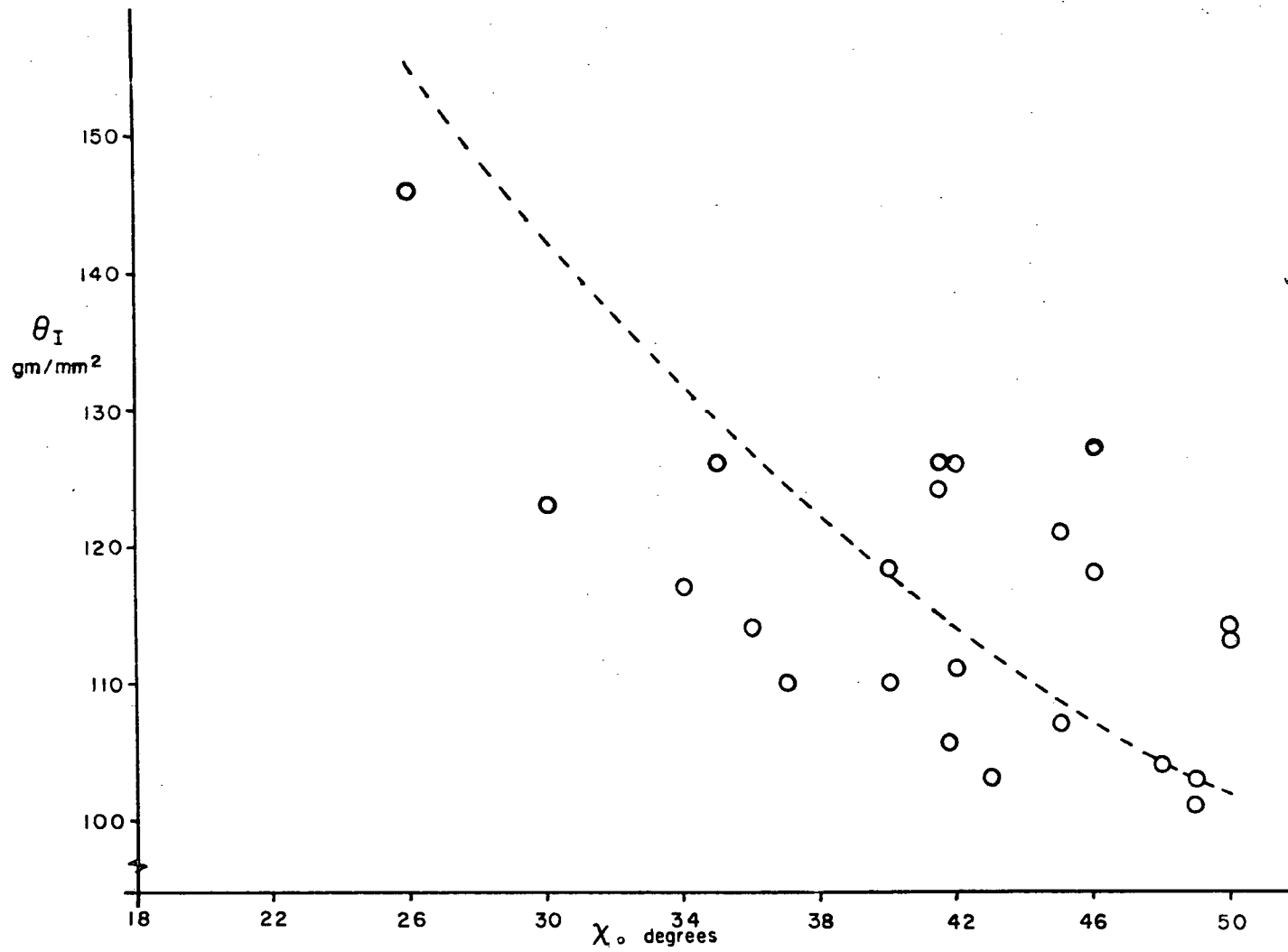


Fig 27. Orientation dependence of stage I work hardening rate.

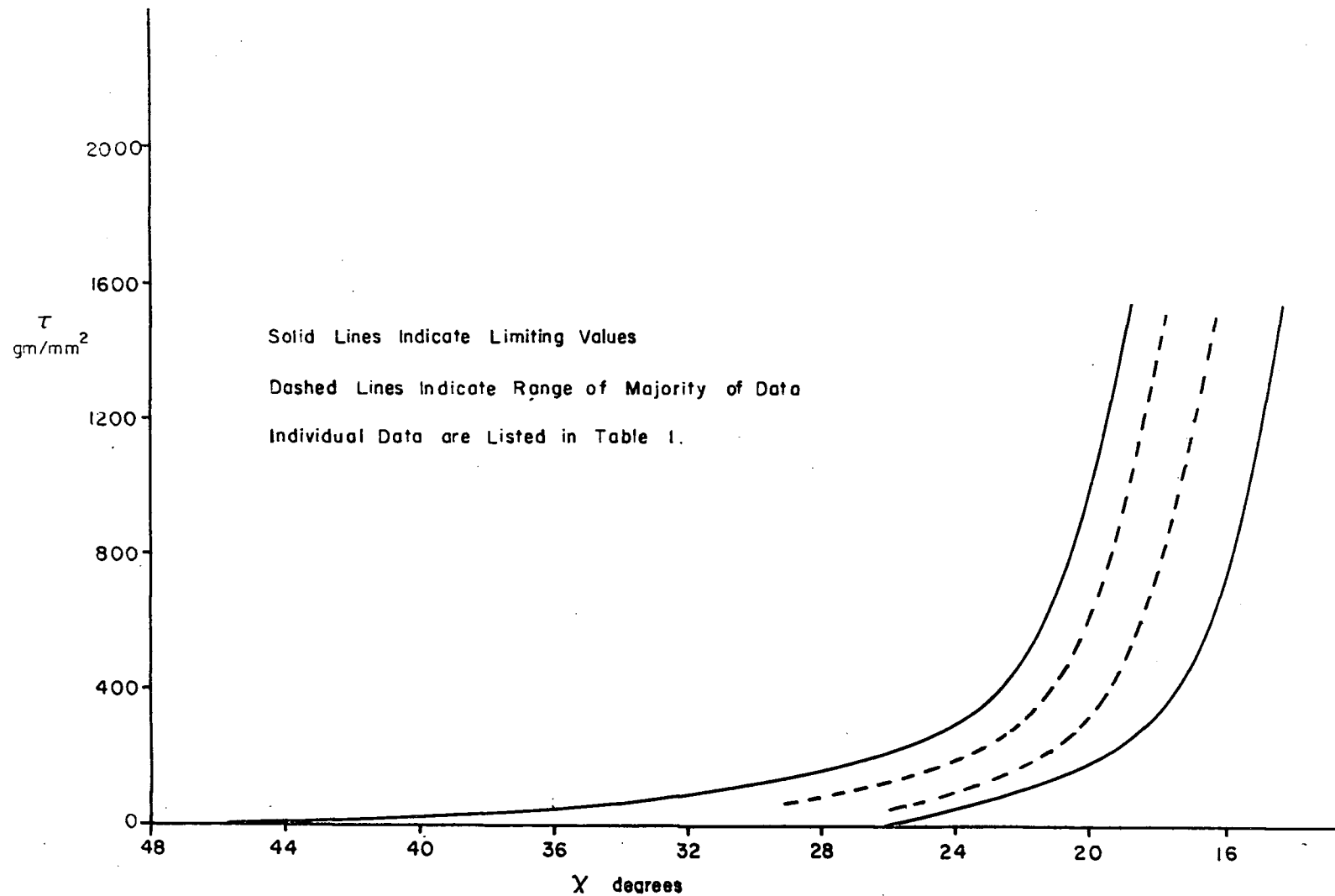


Fig. 28. Orientation dependence of the length of easy glide (schematic).

Risebrough⁵. It is seen that the two sets of data are comparable with the exception of the present point at -110°C . This point is high and may result from the fact that it was obtained very early in the course of this work at which time production, handling and testing procedures had not been fully developed. Consequently, the crystal may have contained undiscovered substructure or other flaws which would have caused it to be discarded at a later date.

The initial work hardening rate at 20°C at a strain rate of $1.3 \times 10^{-5} \text{sec}^{-1}$ was found to be 7.9 gm/mm^2 .

3.4.1.3 Length of easy glide

The data in Table I, which is shown schematically in Fig. 30, shows that the end of easy glide occurs when $\chi = 20.2 \pm 1.2^{\circ}$, irrespective of initial orientation or recovery. This figure is a stress-strain plot on which strain has been converted to orientation by the relation:

$$\sin \chi = \frac{l_0}{l} \sin \chi_0$$

The data in Table I and from Fig. 27 show that recovery has an effect such that a crystal deformed to an orientation χ in stage I and completely recovered has the work hardening rate and new stage I length equal to a virgin crystal of orientation χ .

It was also noted that the end of easy glide at -196°C was marked by twinning in the sample. These twins are shown in Fig. 31. The stress at which twinning occurred was slightly higher than the stress at which the stress-strain curve deviated from linearity. This stress was 300 to 400 gm/mm^2 , and independent of initial orientation. At 20°C , twinning occurred at an equivalent stress of $310 - 380 \text{ gm/mm}^2$. This stress was not reached until very high strains, approximately 3.5 to 4.0.

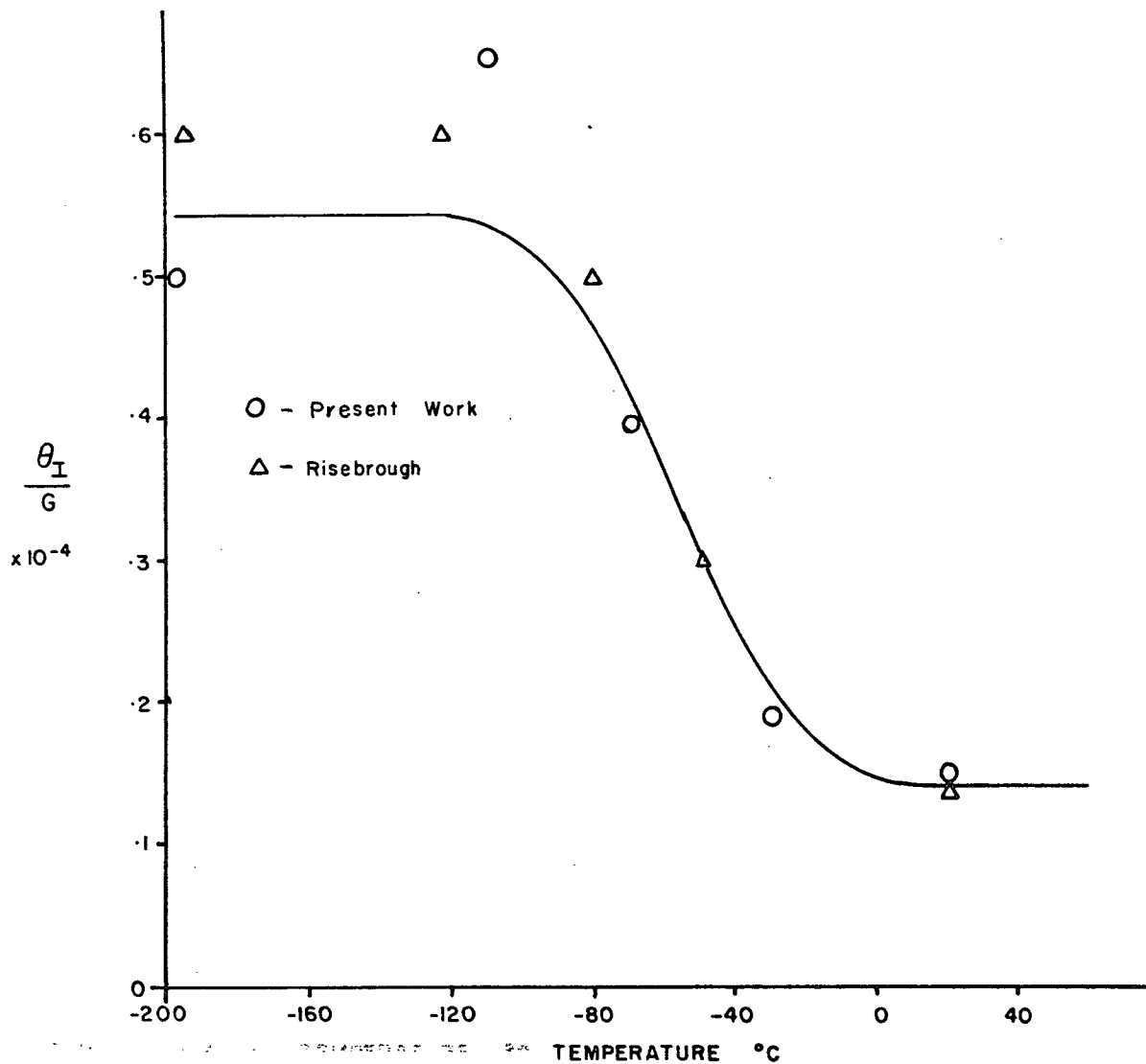


Fig 29. Temperature dependence of stage I work hardening rate.

Table I. The effect of initial orientation and recovery on the length of stage I.

<u>Specimen</u>	<u>χ_0°</u>	<u>χ_{II}°</u>	<u>Recovery in stage I</u>
S39B	48	20.3	20 min. -20°C
S39D	48	20.5	90 min. -100°C
S39C	48	21.5	40 min. -100°C
S41B	47	20.3	30 min. $+50^\circ\text{C}$
S37C	46	19.2	20 min. -70°C
S37B	46	20.5	70 min. -70°C
S36D	46	20.9	10 min. $+30^\circ\text{C}$
S39A	45	20.7	10 min. -20°C
M9B	45	21.0	none
M12C	45	22.5	saturation
L3C	43	23.0	saturation
S37A	42	19.3	20 min. $+30^\circ\text{C}$
M15B	42	19.6	none
M11C	42	19.6	none
L3B	42	20.4	saturation
M8A	41	18.5	none
M12A	40	19.0	saturation
M11B	40	20.5	none
S29B	36	19.7	saturation
M4A	35	19.8	none
M2C	34	20.1	saturation
S42A	29	18.7	none
U1C	27	22.0	none
M6B	26	18.4	none
L2A	25	19.0	none

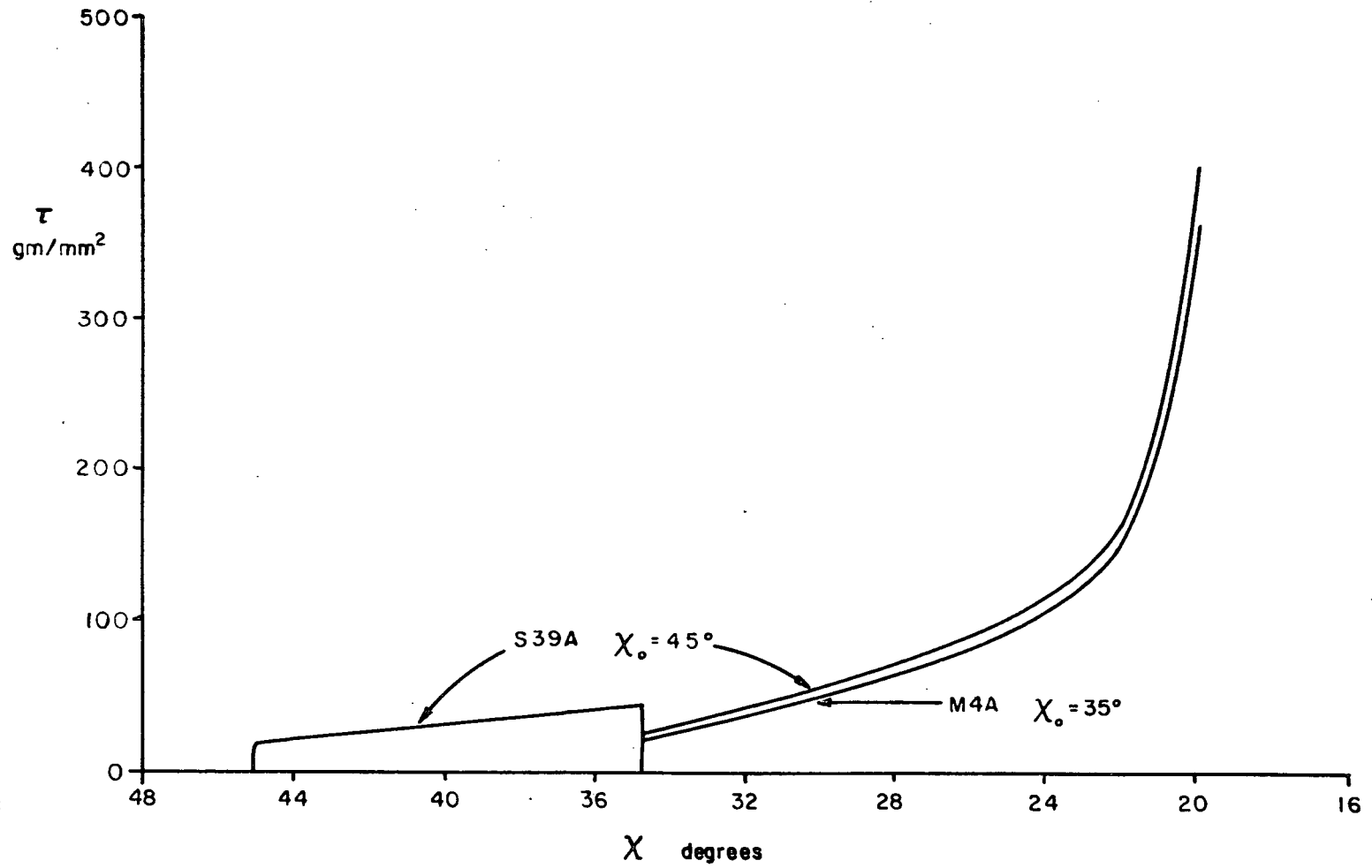


Fig 30. The effect of orientation on the length of stage I (specific example).

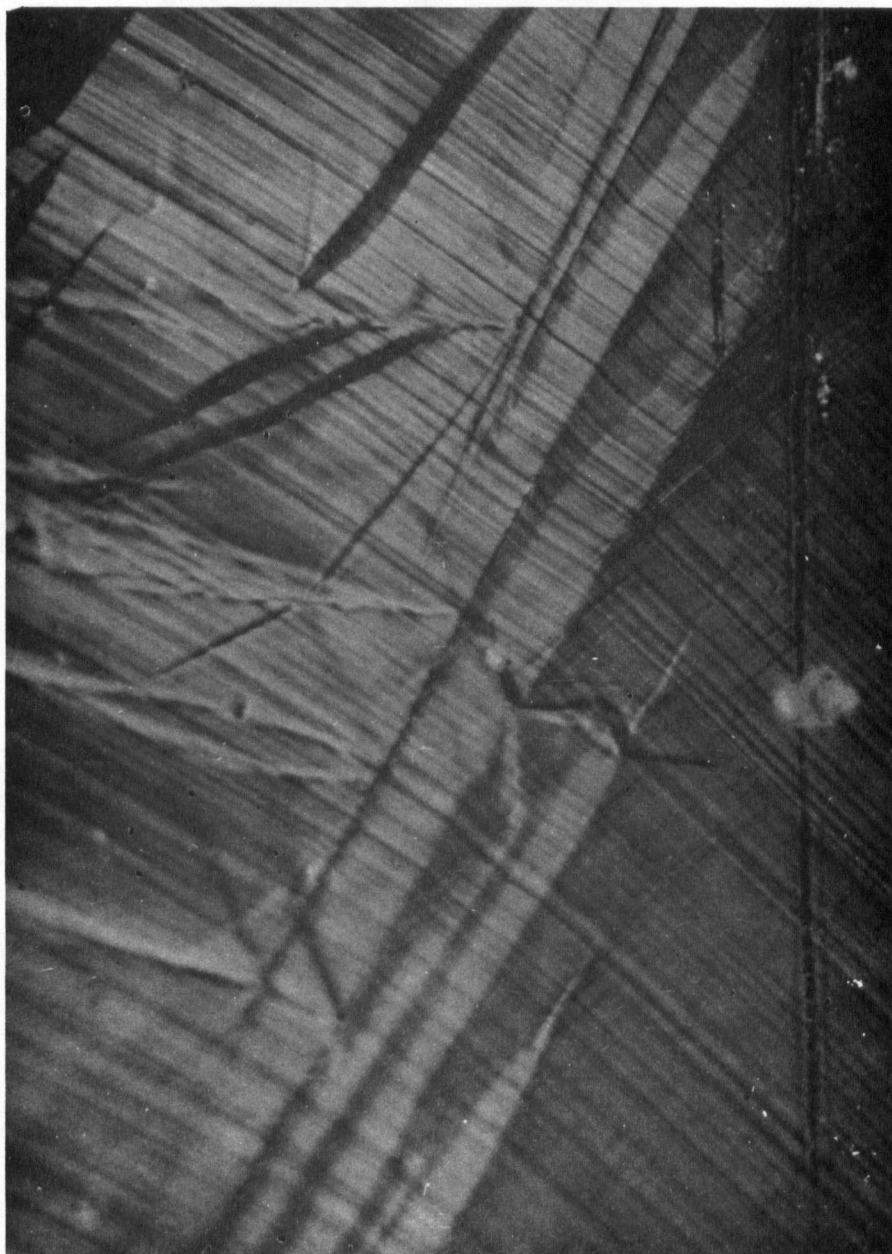


Fig 31. Twins formed in the stage I - stage II transition (x 200).

3.4.1.4 Recovery effects

Summarizing the principal effects of recovery on the various stage I work hardening parameters, it has been found that recovery has no effect on the length of stage I; it increases the work hardening rate. Recovery has no effect on the strain at which twinning occurs.

3.4.2 Stage II

Stage II is the second linear hardening portion of the work hardening curve and is characterized by a work hardening rate significantly higher than stage I. In the ensuing discussion, the transition region from stage I to stage II has been ignored since it was essentially the same in all specimens.

3.4.2.1 Orientation effects

All crystals tested in this study had an initial orientation χ_0 greater than 25° . Consequently, all showed some easy glide before stage II began at an angle of approximately 20° . Therefore there was no variation in orientation with which to compare stage II work hardening parameters. There was no effect of initial orientation in stage I on stage II parameters.

At -196°C , the stress level at the beginning of the transition region from stage I to stage II was found to be 150 to 250 gm/mm^2 for all tests.

The work hardening rate in stage II was approximately 4250 gm/mm^2 .

3.4.2.2 Recovery effects

While there was no noticeable effect on the length of stage I, it was found that recovery had a considerable effect on the length of stage II.

Fig. 32 is a plot of the resolved shear stress - shear strain data from two comparable crystals. Crystal M4A was deformed continuously at -196°C . Crystal M15B was deformed to a stress of 2000 gm/mm^2 at -196°C and then recovered at 75°C for 30 min. These conditions are in excess of the minimum requirements for saturation recovery. Following this recovery, the specimen was again strained at -196°C to a stress of 2000 gm/mm^2 and then recovered. This cycle was continued until the specimen broke.

The total shear strain obtained from the end of easy glide in specimen M4A was 80%. Crystal M15B exhibited 180% shear strain from the end of easy glide. The total strain achieved in this crystal was comparable to the strain achieved during deformation at 20°C . It is not suggested that deformation plus recovery in stage II is equivalent to deformation at 20°C . Fig. 33 shows the final shape of crystal M15B and a crystal deformed at 20°C . It is seen that the two crystals are significantly different. Crystal M15B is considerably more rumped than the other.

The work hardening rate in stage II at -196°C was found to be about 4250 gm/mm^2 . This is the rate shown by crystals M4A and M15B; up to the first anneal as shown in Fig. 32. Following the first anneal, the work hardening rate increased by 1250 gm/mm^2 to 5500 gm/mm^2 .

3.4.3 Stage III

The majority of tests at -196°C exhibited only two stages of hardening, with failure occurring while the specimens were still in stage II. The stress at failure in these specimens was approximately 3500 gm/mm^2 . The crystals with initial orientation less than 30° , a third stage with a

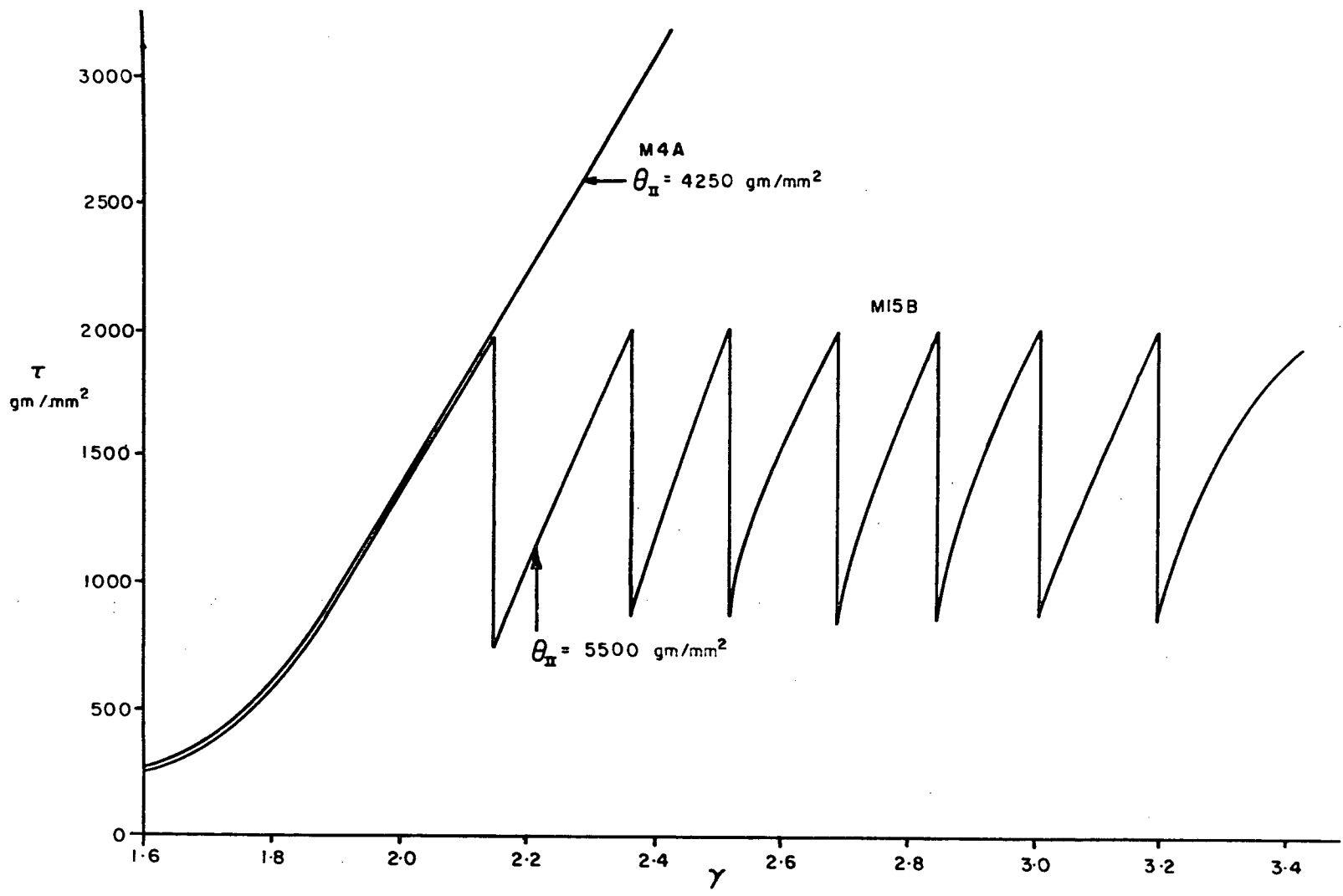
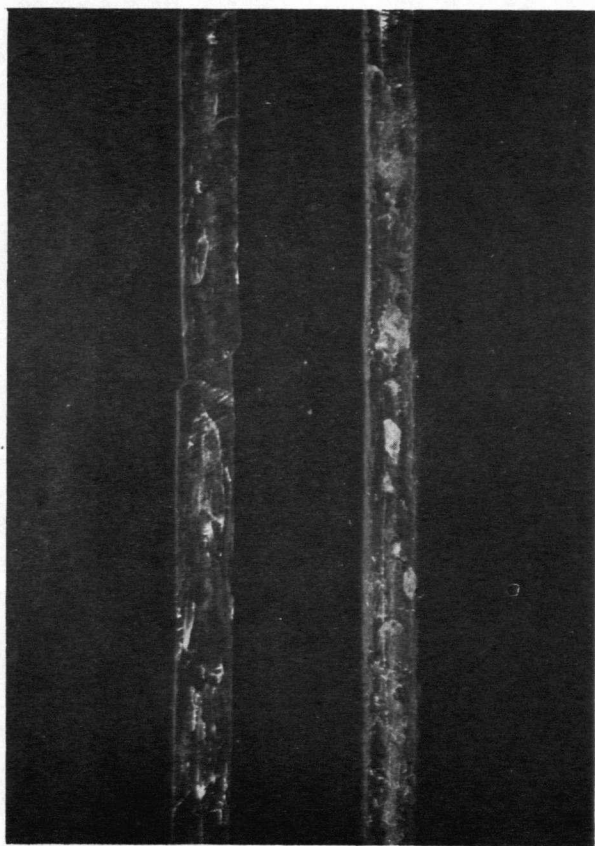
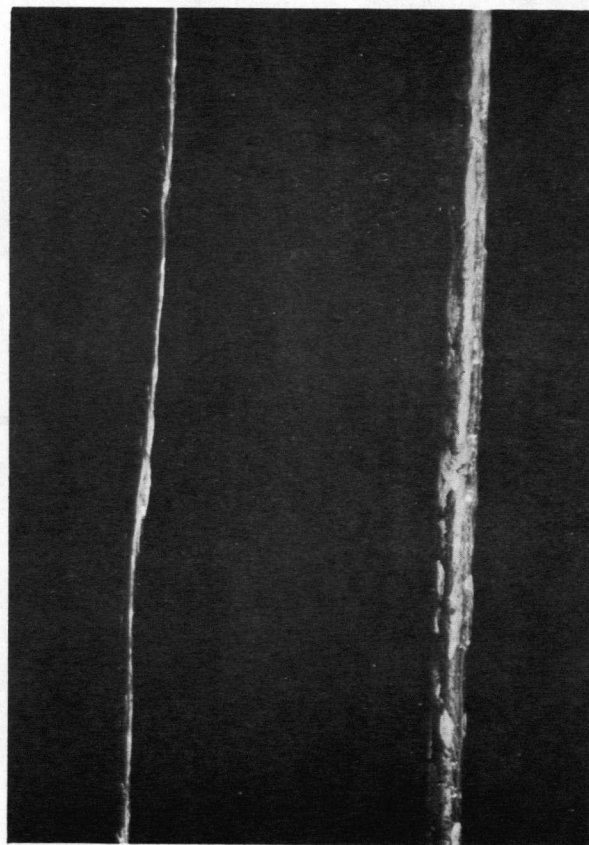


Fig 32. The effect of saturation recovery on the length of stage II.



20°C -196°C

a) Front view



20°C -196°C

b) Side view

Fig 33. Relative shapes of crystals deformed at 20°C and -196°C.

substantially lower non-linear work hardening rate was often observed.

Sample M15B was annealed extensively in stage II. After the first few anneals, the work hardening rate increased, but at higher strains it decreased and deviated from linearity as shown in Fig. 32. This may be due to a third stage of hardening.

4. DISCUSSION

4.1 Recovery results

4.1.1 Activation energy

As a first step in the evaluation of the recovery data, an attempt was made to calculate an activation energy for tests in which all deformation was performed at -196°C , with recovery anneals at higher temperatures (Figs. 5-8). These data were used in preference to those in which deformation was at elevated temperature because they should provide consistent boundary conditions for the anneals. That is, the dislocation configuration should be similar preceding the various anneals, which would not be the case for high temperature deformation since it has been shown that dynamic recovery takes place at temperatures greater than -120°C .

The recovery data were normalized to a common γ_I , the reasons for which will be discussed with respect to the orientation results. Comparing recovery results as a function of time (Fig. 9) it was seen that with the exception of $+30^{\circ}\text{C}$, the difference in recovery with time is not particularly strain sensitive. That is, the shape of the recovery-strain curves was consistent at a given temperature, so that a change in recovery time changes the recovery by a constant amount, irrespective of strain.

With respect to the results at 30°C , Fig. 10 showed that work hardening in crystals was completely recoverable up to about 50% shear strain. At higher strains, some work hardening occurred which was not recoverable. Thus it was not possible to achieve high recovery values close to γ_I . Since it was observed that the majority of recovery took place at short times (Fig. 5), the approach of saturation may explain the similarity in recovery

values for various times at 30°C close to γ_I .

Since saturation recovery may be significant at γ_I at 30°C, the comparison of recovery has been limited to strain less than 50%. The value of strain chosen arbitrarily for this comparison was 25%, and in some cases this required the back extrapolation of recovery curves.

A trial and error technique of curve fitting was employed to try to establish a recovery-time relationship. By this method, it was found that recovery is not a power function of time.

$$\text{i.e. } R \neq At^x$$

Rath et al⁶ found that for aluminum single crystals, recovery was proportional to the logarithm of time. For the present work, there is insufficient data to prove whether or not such a relationship holds. However, if it is assumed that recovery is proportional to log time for cadmium single crystals, the calculation of a meaningful activation energy was found to be impossible from this data. During the calculation, the derivation of the recovery rate constant caused the temperature dependence of recovery to be effectively cancelled so that the resultant activation energy was zero.

Following the analysis of Rath et al⁶ did not produce any meaningful values for activation energy from present results. For values of recovery from $R = 0.1$ to $R = 0.5$, activation energy values ranged from almost zero to 20,000 cal/g. atom, and the Arrhenius plots from which these values were calculated were not linear. This method of analysis is somewhat dubious because it does not use a true rate constant which is independent of time or recovery for calculation of activation energy. Also, this relation predicts that recovery will exceed unity which is impossible by definition. Consequently, the relationship $R \propto \log t$ is rejected for the present work.

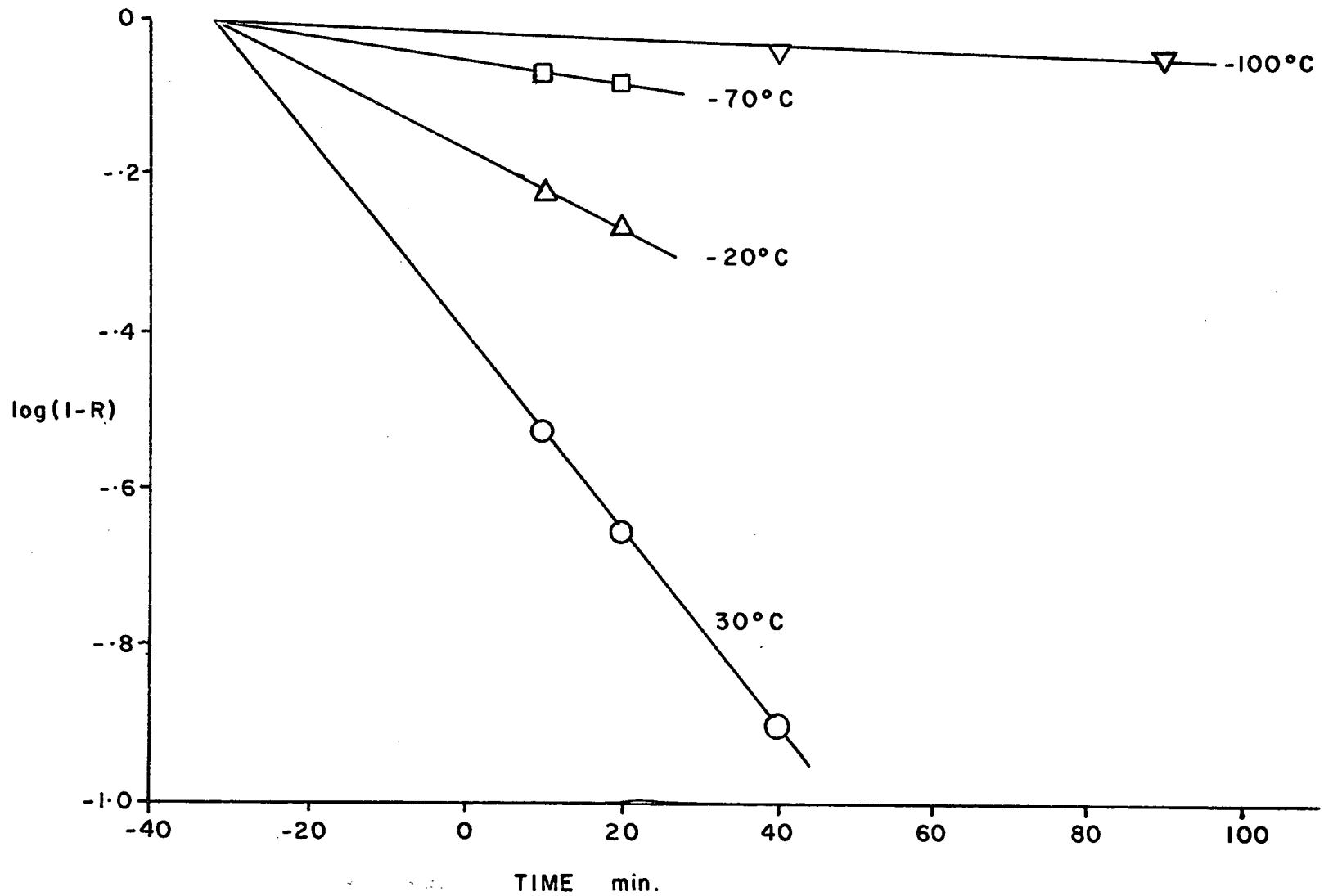


Fig. 34. The variation of $\log(1-R)$ with time.

The relationship between recovery and time which has been adopted for this work is:

$$\log (1-R) = At$$

This rate law is not defensible on the basis of present data, however it is consistent in that recovery may never exceed one, and is a first order rate law.

A plot of the present data is shown in Fig. 34,. It is seen that the plot at each temperature may be made to pass through a common point on the time axis at $\log (1-R) = 0$. The fact that this time is negative is not a serious drawback to this analysis since analogies to physical and chemical systems may be drawn in which such a phenomenon would be expected. For instance, a nucleation and growth system in which the number of nuclei decreases with time would exhibit a similar curve when the growth is extrapolated back to zero.

Since the rate law used in this analysis is first order, the slope of the plots at each temperature represents the rate constant, and as such may be used to calculate the activation energy. This is shown in Fig. 35. The activation energy found from this plot is 2500 cal/g. atom. This value is too small to be meaningful, but if $\log (1-R) = At$ does describe the rate of recovery, then the rate controlling process is first order, and in the solid state this would probably be diffusion. Since the value is so small it is not possible to determine whether this would be bulk diffusion or pipe diffusion. The activation energy for bulk diffusion in single crystal cadmium is about 18,500 cal/b. atom, and that for pipe diffusion is about half of this.

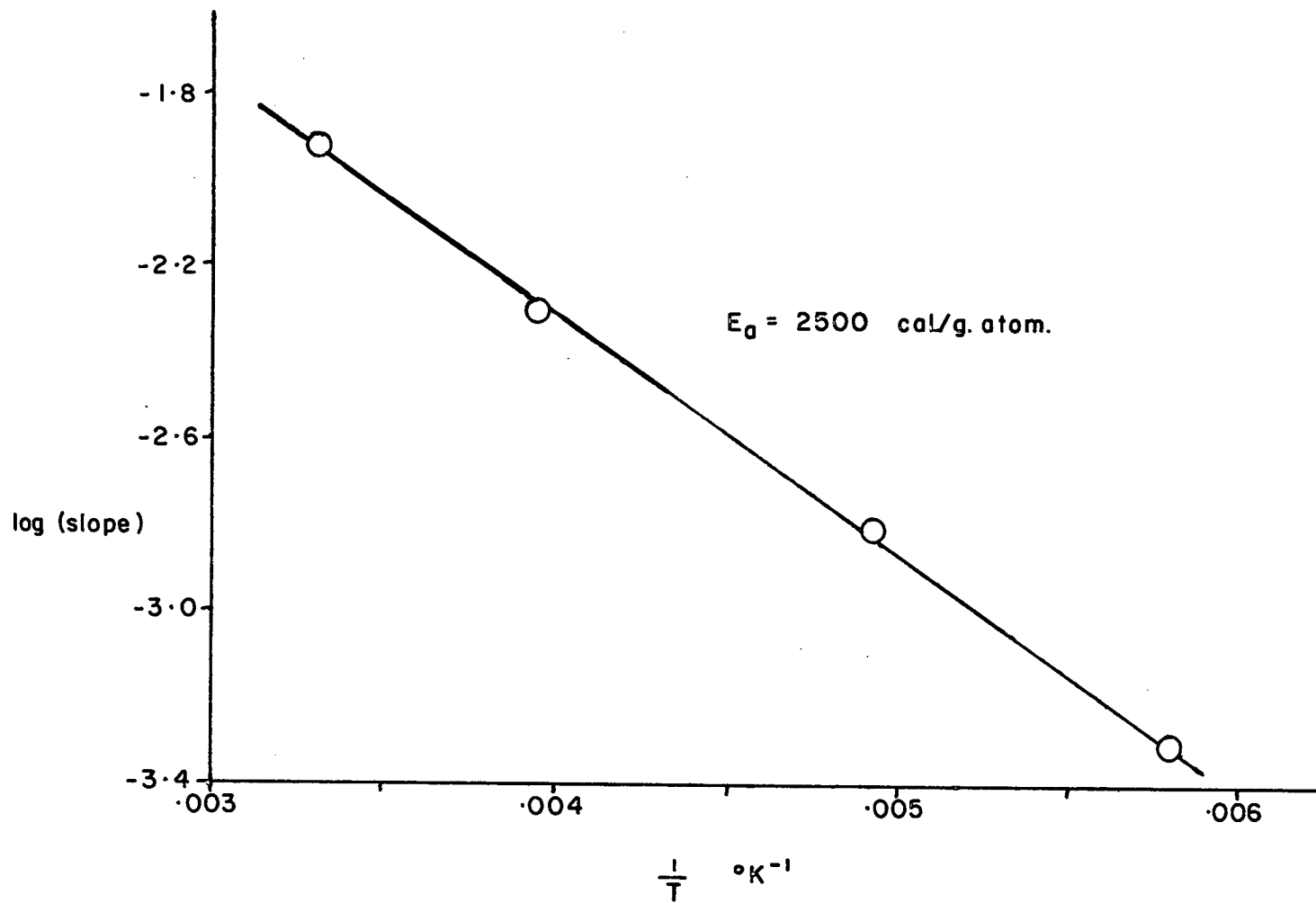


Fig. 35. The variation of log (slope) with reciprocal absolute temperature.

4.1.2 Comparison of recovery methods (1), (2), (3)

In method (1) recovery, all recovery was obtained under static conditions but experimental conditions for types (2) and (3) were such that there was significant dynamic recovery during deformation in addition to the measured static recovery. In order to compare the results of all methods directly, it must first be determined whether or not dynamic and static recoveries are equivalent. The following calculation shows that they are equivalent only at low strains.

Fig. 11 defined a value of saturation recovery which is dependent only on strain. This curve in Fig. 11 is now used to determine the minimum attainable flow stress of a crystal deformed at -196°C . This flow stress is the value which would be obtained from a crystal which was fully recovered after each infinitesimal increment of strain. The results of this calculation are shown in Fig. 36.

In Fig. 36, the solid line labelled "Saturation Recovery" shows the minimum flow stress as calculated from a typical stress-strain curve at -196°C and from Fig. 11. This curve represents that portion of

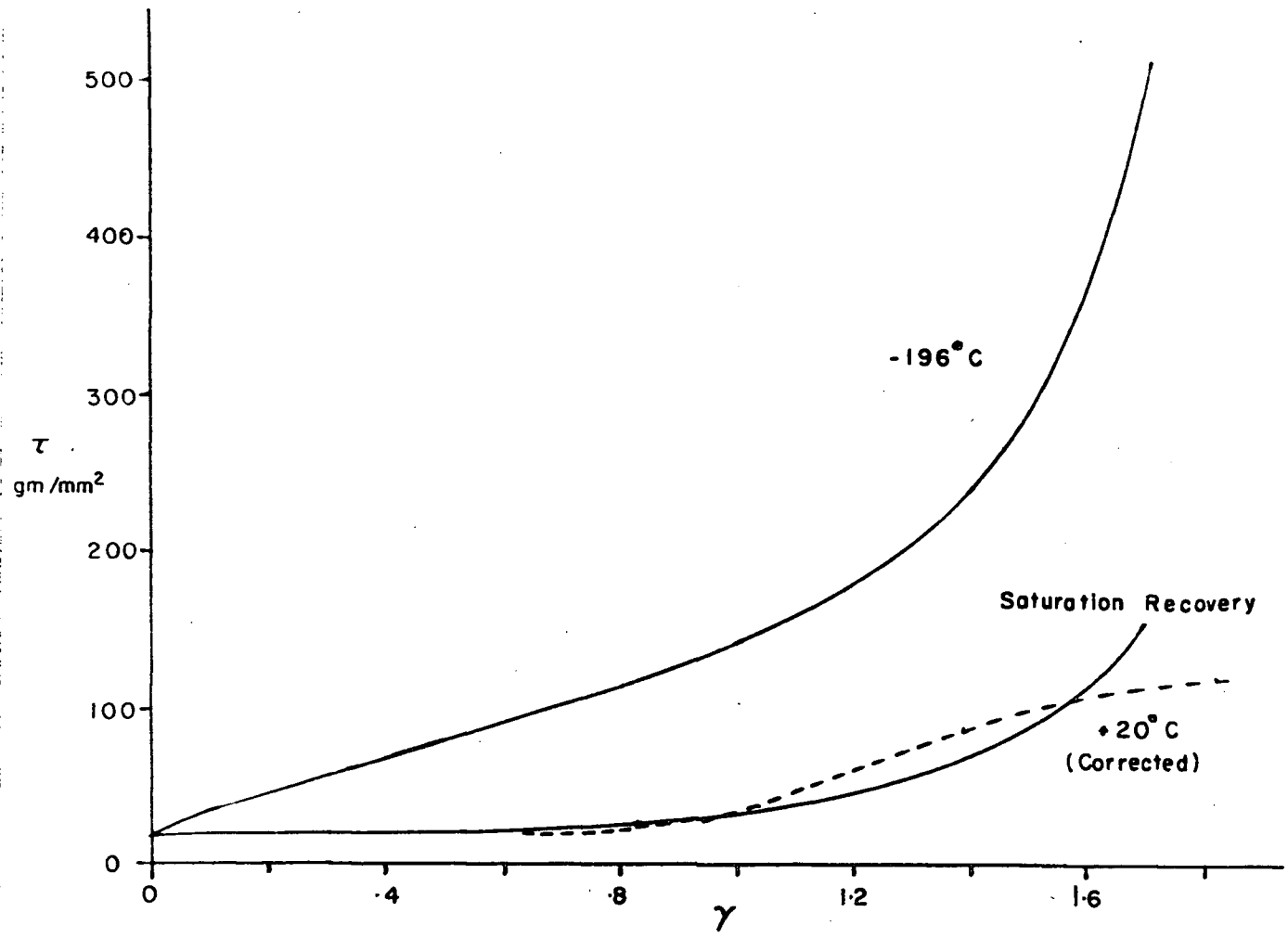


Fig 36. Comparison of saturation recovery with deformation at -196°C and 20°C .

the flow stress which is not recoverable. The dashed line in Fig. 36, labelled "+20°C corrected", is the stress-strain curve for a crystal deformed at 20°C, and as such represents high temperature deformation ($20^\circ\text{C} = .5T_M$). In this case dynamic recovery should proceed at such a rate that the crystal is essentially recovered at all times. For comparison between this and the previously calculated curve, the flow stress values in this case have been corrected to their equivalent at -196°C by a ratio of the shear moduli at -196°C and 20°C.

It is evident from comparison between this and the previously calculated curve that they are equivalent up to ~ 50% - 70% shear strain. This is the point at which saturation recovery starts to decrease from 100% (Fig. 11). This observation is also verified by the results of a single test at 70% shear strain as shown in Fig. 16.

Thus, it is concluded that initial easy glide deformation at low temperature is identical to deformation at high temperature with the addition of work hardening which is completely recoverable by the conditions employed.

At strains in excess of 70%, up to the end of easy glide, the two curves in Fig. 36 deviate slightly, and it is thought that this deviation may be due to activity on slip systems other than the basal system. This will be discussed later, with respect to the orientation results.

The deviation between the two curves is small, but it appears to be the opposite of what would be expected if a secondary slip system operated at low temperature. If this were the case, the recovered curve at -196°C should have a higher flow stress than the equivalent curve at +20°C since the stress at 20°C is so low that it is unlikely that a second system would operate. The only possible explanation for the discrepancy

as shown in Fig. 36 other than structural differences between the two crystals would be that the flow stress at 20°C was not completely recovered at high strains. This was not verified experimentally. This discrepancy should not, however, influence the conclusion that initial easy glide at low temperature is equivalent to that at high temperature with the addition of completely recoverable work hardening.

It should be possible to compare the results obtained from recovery methods (2) and (3), where deformation was at intermediate to high temperatures to those of method (1) where deformation was at low temperature.

Figures 12-15 showed the results of method (2) in which the crystals were deformed and then recovered with the load removed at the same temperature. As was seen with respect to Figs. 6-9 the primary difference between this type of test and that in which deformation was at low temperature was in the magnitude of recovery. One reason for this discrepancy lies in the definition of recovery as given in equation (3). In this definition, recovery is the fraction of the work hardening recovered, and since at temperatures greater than -120°C recovery takes place during deformation, there is a lower total work hardening measured than would be at temperatures less than -120°C. The schematic diagram in Fig. 37 shows the same flow stress is achieved by a recovery of .5 at elevated temperature, while a recovery of .75 is required at low temperature. This will explain the results at high recovery temperatures, where saturation is approached, but at lower temperatures (-100° to 0°C) this is not the case.

In the lower range of test temperatures (0°C) where saturation recovery, either by static or dynamic means, is not a factor, the above argument is not valid. In this range, the recovered flow stress at one

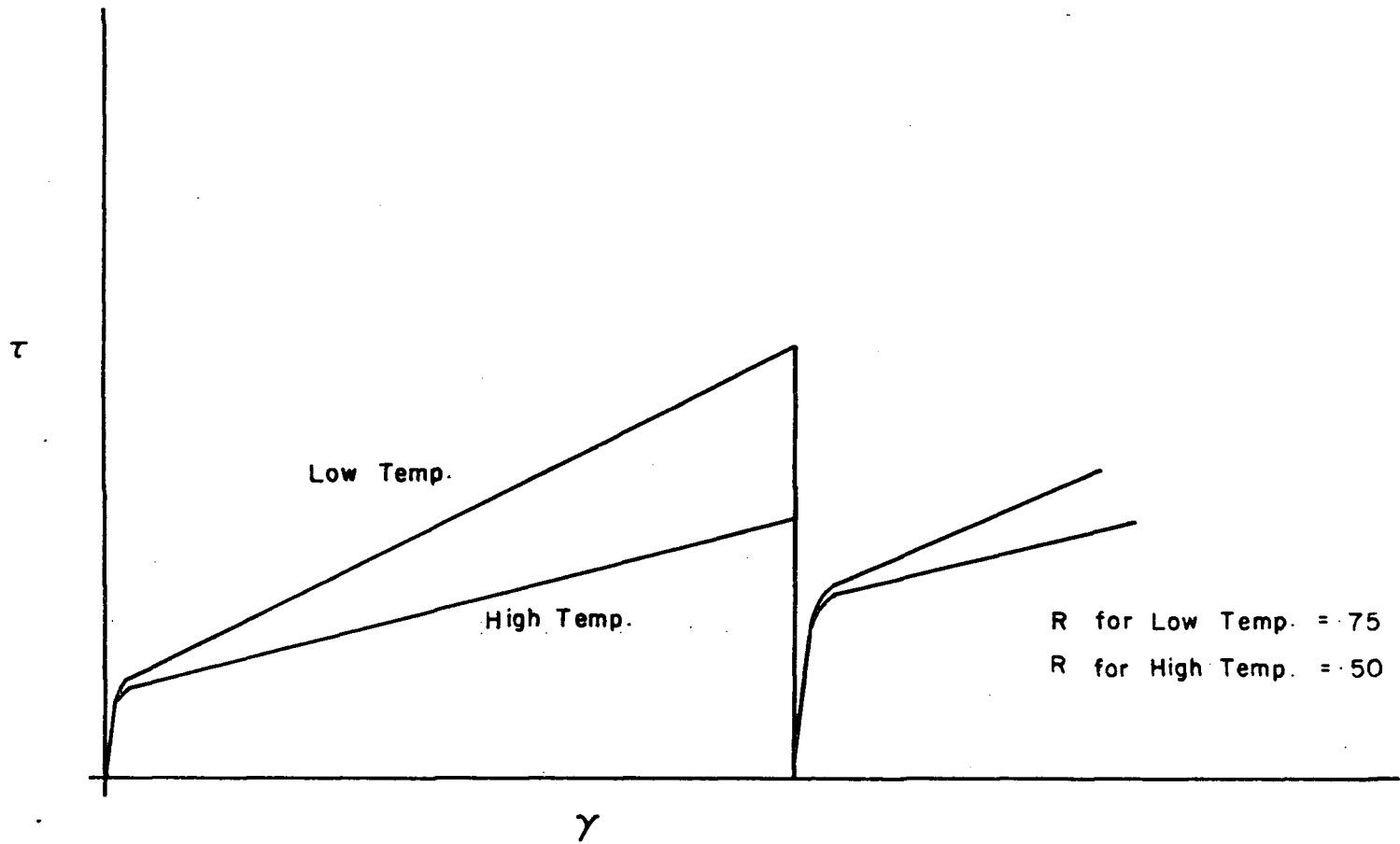


Fig 37. Schematic diagram of recovery to a similar stress level with deformation at different temperatures.

temperature is always significantly different from the flow stress at another temperature. This is illustrated in Fig. 38, at test temperatures of -70°C and -30°C . The difference in flow stress between these two curves is due primarily to the difference in the amount of dynamic recovery taking place in each case. Thus, to compare directly such curves along with the measured recovery values to data obtained from method (1) with deformation at -196°C , the comparison should be made of flow stress following recovery at each value of strain, as suggested with respect to the definition of recovery at the beginning of this thesis. However, this would require a knowledge of the absolute amount of dynamic recovery which has taken place up to any given strain. This has not been determined. Consequently no direct comparison of the results of method (2) with those of method (1) could be drawn.

Comparison of the results of method (3), in which the load was not removed from the sample, to either method (1) or method (2) was not made because of the negligible differences between this method and method (2).

Since recovery rates were found to increase with temperature, it is reasonable to assume that the recovery processes are thermally activated. Consequently, it was expected that there would be some increase in recovery due to the applied load acting in conjunction with the available thermal energy. The effects observed, however, were negligible.

In conclusion, the results of the three types of recovery test have indicated that recovery is thermally activated, and is the result of two or more processes which change with temperature. It remains for other types of test to show what these processes might be. Saturation recovery has shown that deformation at low temperature is related directly to deformation at high temperature in the initial easy glide region, but that this is not the case at strains in excess of 70%.

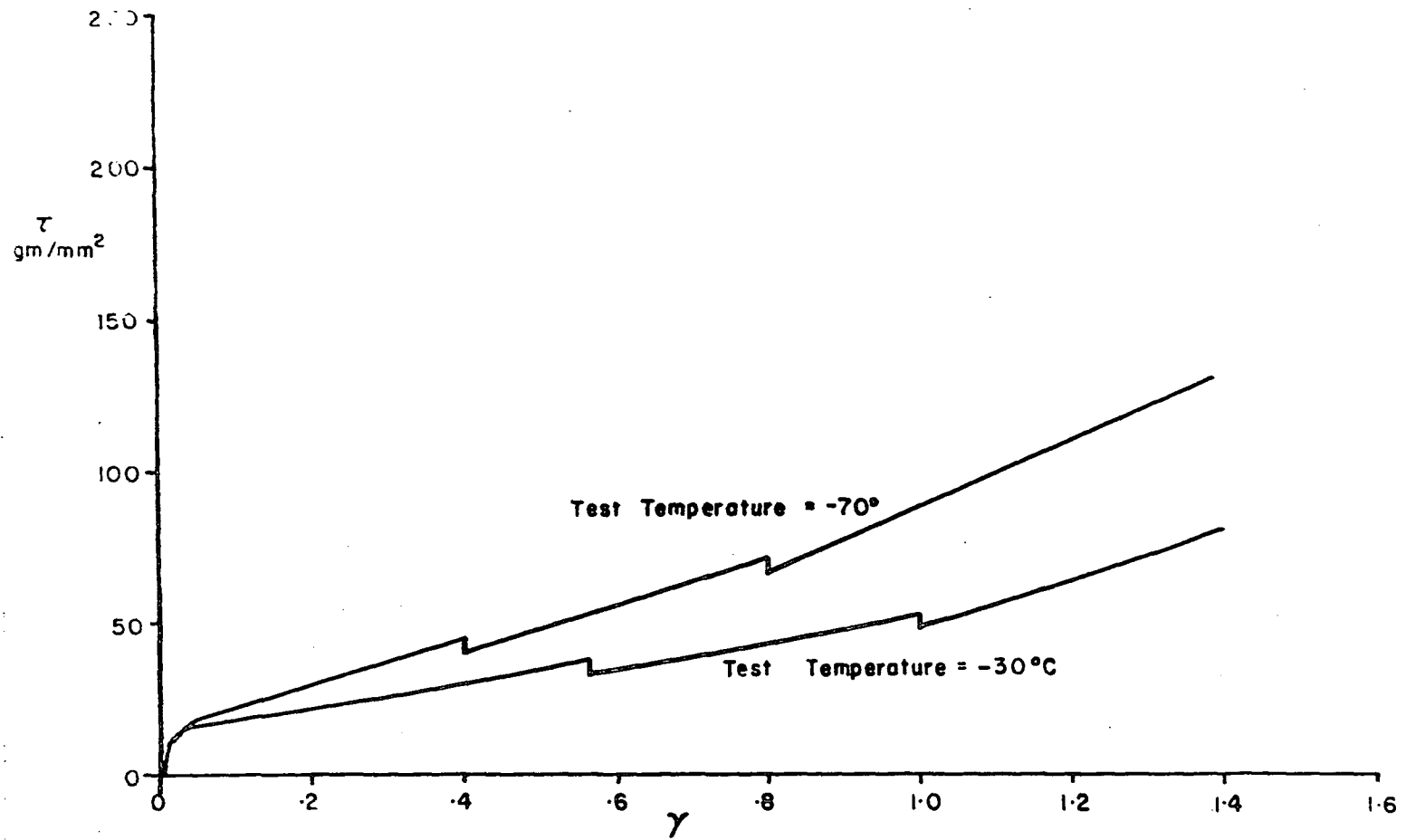


Fig 38. Typical method (2) recovery at -30°C and -70°C .

4.2 Work hardening parameters

It was observed that recovery, and in particular saturation recovery, is a function of strain. Since strain is directly related to orientation, it was thought that perhaps the above observation could be explained on the basis of crystal orientation. It was with this in mind that the effect of orientation upon various work hardening parameters, both by themselves and in conjunction with recovery, was studied.

4.2.1 Easy glide parameters

One of the most common parameters measured in any single crystal study is the critical resolved shear stress. Comparison of this factor between this work and others should give an idea of the comparability of the quality of the crystals used. This knowledge should then facilitate the comparison of other parameters.

Schmid and Boas¹¹ in some of the earliest work on cadmium found that 99.996% Cd at room temperature exhibited a critical resolved shear stress of 25 gm/mm^2 . Gibbons⁴² found critical stresses of 9.8 and 17.1 gm/mm^2 for 99.9994% Cd at 20°C . Boček et al¹⁵ tested the temperature dependence of various work hardening parameters in 99.99% Cd. Their results for crss vs. temperature along with those of the present work are shown in Fig. 39. It is seen that there is a large discrepancy between the two sets of data which might be thought to be due to impurity content since the present work used 99.999% Cd. However, the graphs presented by Davis¹⁶ for 99.9% and 99.9999% Cd show very little difference of crss for such a large difference in purity, with the crss being about $20\text{--}30 \text{ gm/mm}^2$. A more probable explanation for the discrepancy would be the presence of more substructure in Boček's crystals. In comparison to the present work,

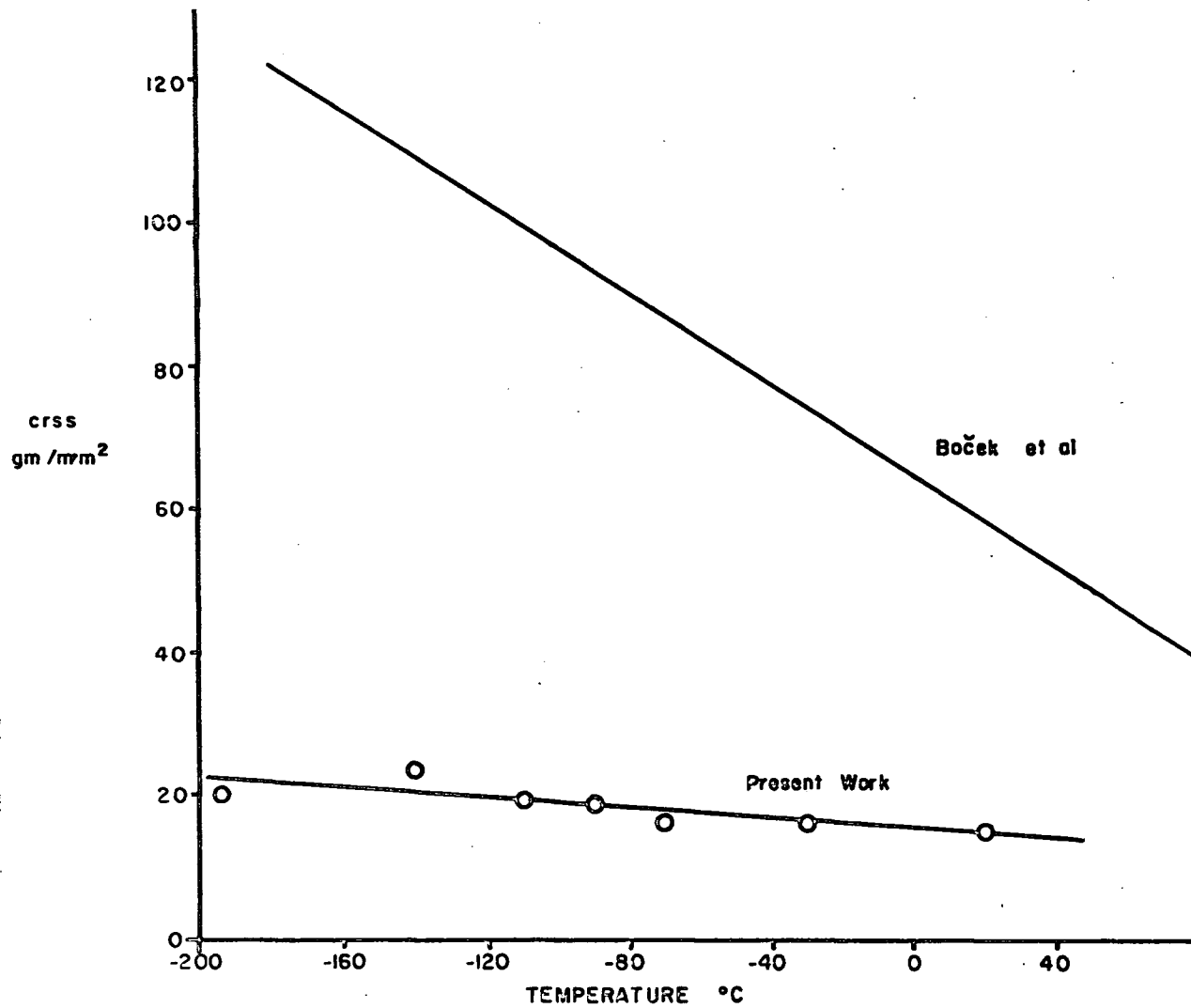


Fig 39. Comparison of present work to that of Boček and Kaska²⁰ regarding the temperature dependence of the critical resolved shear stress.

they showed significantly shorter easy glide, and Hirsch and Lally⁴ found that easy glide in Mg single crystals was reduced from 250% to 50% for crystals with substructure. The presence of substructure would also explain the higher work hardening rate found by Boček. Since the work by Boček is one of the most comprehensive studies of cadmium in the literature, the favourable comparison of the present work shows that the crystals used in this work must have been of high purity and have contained relatively little substructure.

Early work of Jillson¹⁷ and Deruyttere¹⁸ detected no systematic dependence on orientation of either work hardening rate or length of easy glide. Lücke et al⁷ observed that zinc single crystals at 20°C exhibited 130% shear strain in easy glide, independent of the initial orientation. Diehl¹⁹ observed no variation of the work hardening rate with orientation in hexagonal metals.

The results of the present study are contradictory to those of the above workers. It was found that there is a definite dependence on orientation of the length of easy glide, since easy glide terminates at a specific orientation (see Fig. 30; Table I). To a lesser degree, the work hardening rate also depends on orientation (see Fig. 27). These observations are more in accord with those of Boček and Kaska²⁰, who noted an increasing work hardening rate and decreasing length of stage I with decreasing χ_0 in zinc in the temperature range 50° to 100°C. Boček, Höttsch and Simmin²¹ also quote the results of Wolf⁴⁵ on Cd at 20°K and 90°K which show similar trends for the work hardening rate.

Lücke et al⁷ found that recovery has a distinct effect on the length of stage I. Their results showed that a zinc single crystal, which had been deformed 70% at room temperature showed a stress-strain curve identical to that of a virgin crystal after a recovery of 24 hrs. at 25°C.

Thus, the total length of easy glide increased by 70%. For cadmium crystals deformed at -196°C and recovered this was not the case. As shown in Fig. 28 and Table I, recovery had no effect at all on the length of easy glide. A possible reason for this discrepancy would be that the operation of second order pyramidal slip is not related to orientation in the same way in zinc at 20°C as it is in cadmium at -196°C .

4.2.2 Theories of stage II

While the topic of this study is the recovery of mechanical properties of cadmium, it is necessary to know something of the dislocation arrangements present during deformation to understand what might happen during recovery. As a consequence of this, the following section is concerned with the hardening characteristics of single crystals, and the possible dislocation mechanisms which may occur during deformation.

Perhaps one of the most critical points during the deformation of a single crystal is the transition from the first linear stage of hardening to the second linear stage. Various theories have been proposed to explain this transition in hexagonal metals. The principal alternatives are:

- 1) the formation of a critical density of obstacles as a result of the condensation of vacancies
- 2) the initiation of activity of the two previously non-active Burger's vectors in the basal plane
- 3) the onset of twinning
- 4) the initiation of activity on the second-order pyramidal system.

The last alternative is thought to be most important to this study; however all theories will be briefly discussed.

4.2.2.1 Condensation of vacancies

Seeger and Träuble²² ascribe the transition from easy glide to stage II to a critical density of obstacles. These obstacles have formed by the condensation of vacancies into immobile dislocation rings. Present experimental results are inconsistent with this theory. Firstly, it is difficult to imagine vacancies having adequate mobility at -196°C to form sessile loops. If such loops did manage to form, then saturation recovery should be sufficient to allow them to anneal out. Price²³ found that sessile dislocation loops formed by non basal glide in Cd annealed out by volume diffusion at temperatures above -40°C . No effect of annealing on the transition strain was observed in the present work.

4.2.2.2 Non-active basal dislocations

Kratochvíl and Koutnick²⁴, from shape change measurements during the deformation of cadmium single crystals, concluded that secondary dislocations in the basal plane must operate. By comparison with other work, principally that of Hirsch and Lally⁴ on magnesium, they conclude that the interaction of primary and secondary basal dislocations is responsible for strain hardening and the transition to stage II. It appears that such comparison is unjustifiable. Hirsch and Lally emphasize that their model is specifically designed for Mg and that hardening mechanisms in other hexagonal close-packed metals may be different. It is possible that secondary basal dislocations operate, but it is doubtful that they are responsible for the transition to stage II.

4.2.2.3 Twinning

Hirsch and Lally⁴, in a transmission electron microscope study of magnesium, found that stage II is accompanied by slip of the two previously

non-active Burger's vectors in the basal plane, the formation of sub-boundaries and twinning. They observed that at the onset of stage II, the stress on the prismatic plane was close to the experimentally determined value for prism slip. However in comparison of their work on Mg with face-centered cubic materials, they think that twins act as barriers to slip lines in Mg, whereas secondary dislocations provide the barriers in f.c.c.²⁵ It is stress concentrations arising from the twins which may now produce prism slip.

Hirsch and Lally state that the above argument may not be applicable to hexagonal metals other than magnesium and the results of Bell and Cahn²⁶, Risebrough⁵, and the present work agree with this. Bell and Cahn noted the presence of $\{11\bar{2}2\} \langle 11\bar{2}3 \rangle$ slip traces in zinc crystals prior to twinning, and associated the intersection of dislocations on this system with basal dislocations to produce stress concentrations which in turn would cause twinning. This is opposite to magnesium in which Hirsch and Lally thought that twins produced stress concentrations which in turn caused secondary (prism) slip. In cadmium, the present work and that of Risebrough have noted that twinning is always present in stage II. However, Risebrough has explained that since a considerable portion of the crystal remains untwinned in the transition region from stage I to stage II, and that the stress associated with the end of easy glide is relatively temperature independent, that twinning must be an "after the fact" consideration. On this basis, it must be some dislocation configuration which is responsible for the end of stage I.

4.2.2.4 Second order pyramidal slip

Boček, Švábová and Höttsch²⁷, in a study of single crystal cadmium at 20°K, assume that the onset of linearity in stage II is a result

of flow on the second order pyramidal system $\{11\bar{2}2\} \langle 11\bar{2}3 \rangle$. Their results show, however, that at this point there is a considerable variation in the shear stress on this system with respect to orientation. This is in disagreement with Schmid's law that the critical shear stress be independent of orientation. To compensate for this discrepancy, Boček et al have calculated an internal stress which may be present on the secondary system as a result of pile-ups of dislocations on the basal system. The results of this calculation show this internal stress to be of the order of the flow stress on the basal system. When this stress is added to the applied stress on the secondary system, the result is that the total stress is now essentially orientation independent. Also, this total stress is comparable to the stress found by Stoloff and Gensamer²⁸ for the appearance of second order pyramidal slip traces on cadmium single crystals oriented to suppress basal slip. Thus Boček et al conclude that the start of the linear stage II is associated with the onset of flow on the second order pyramidal system. Interaction of these dislocations with basal dislocations will produce sessiles which contribute to work hardening, and so explain the relatively high work hardening rate in stage II.

A number of problems with respect to the work of Boček et al²⁷ arise when it is compared to the results of the present study. The first problem is with respect to the variation of the stress at the beginning of stage II with orientation. The present results, which encompass considerably more tests than appear to have been done by Boček, show that the angle at which stage II begins is constant at $\chi = 20.2^\circ \pm 1.2^\circ$ (see Fig. 28). The flow stress at this point was also essentially constant at 750 gm/mm^2 . Another problem is that as yet no experiments have been able to show how many dislocations are contained in the supposed pile-ups, and this number

should significantly affect the magnitude of the internal stress on the secondary system. The major problem arises from the strain at which Boček considers flow on the secondary system to be effective. Results from the present orientation study, and from strain rate change tests have shown that it is not the onset of stage II but rather the start of deviation from stage I which is the critical point in the transition. Also, the present study as well as that of Risebrough⁵ has shown that the material is extensively twinned at the start of stage II, and Boček has not considered this point.

4.2.3 Present model

The basis for the present model is similar to that of Boček in that second order pyramidal slip is thought to be responsible for the transition from stage I to stage II. However, it is believed that there is some activity on this system in the latter part of stage I and that this is responsible for the non-recoverable work hardening as shown by the drop in saturation recovery with strain in Fig. 11. The end of stage I linearity is believed to be caused by macroscopic flow on this secondary system and this is then responsible for the increasing work hardening rate in the transition region. The onset of stage II linearity probably results from the development of a dynamic equilibrium between basal and pyramidal dislocations. This will be discussed in following sections. At this point, it is sufficient to note that stage II linearity is not as significant a factor as discussed by Boček et al²⁷.

The results of the present work show that it is possible that second order pyramidal slip could be responsible for various work hardening and recovery phenomena. Fig. 40 shows the shear stress on the second order pyramidal system compared to the flow stress on the basal plane for a crystal

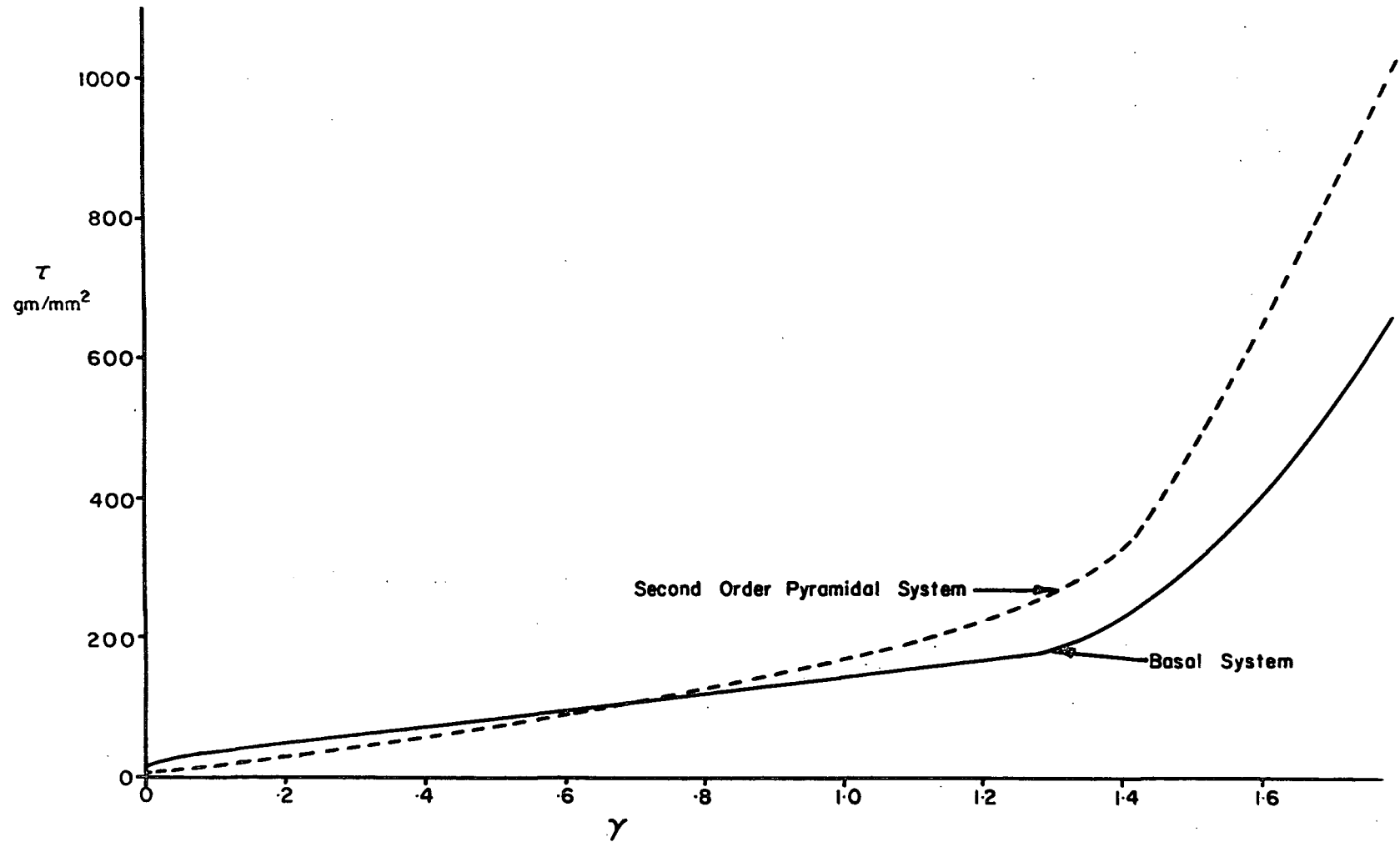


Fig 40. Comparison of shear stress on second order pyramidal plane with that on basal plane.

with initial orientation $\chi_0 = 45^\circ$. Fig. 41 is a replot of the data on Fig. 11, with strain transformed to orientation. It is seen from this plot that non-recoverable work hardening starts in the range $30^\circ < \chi < 35^\circ$. This range corresponds to $.5 < \gamma < .7$ on Fig. 40, and in this range, the stress on the second order pyramidal system is 75 to 100 gm/mm^2 . It is probably only coincidental that this is the range in which the stress on the secondary system becomes greater than the stress on the basal system. At the end of easy glide, at which $\chi \approx 23^\circ$ (see Fig. 28), the stress on the pyramidal system is $\sim 260 \text{ gm/mm}^2$.

Stoloff and Gensamer²⁸ found that the first appearance of pyramidal slip traces occurred at 500 gm/mm^2 in Cd crystals not oriented for basal slip. Their material, however, had a critical resolved shear stress for basal slip of 85 gm/mm^2 , while the material used in this work had a comparable stress of 20 gm/mm^2 . Consequently the critical stress for flow on the pyramidal system is probably less than 500 gm/mm^2 in this material, but since the effect of impurities and substructure on pyramidal glide is not known, it is impossible to assign a definite value. However, this value of 500 gm/mm^2 was given for the appearance of slip traces which would imply massive slip on this system, but to end easy glide relatively few dislocations would be required, so it would be reasonable to assume that these would be generated at a significantly lower stress.

Assuming that second order pyramidal dislocations are active at orientations $< 30^\circ$, it is possible to explain non-recoverable work hardening as shown in Fig. 41. Boček, Lukáč and Švábová²⁹ have shown that energetically favourable reactions between different second order pyramidal systems and between second order pyramidal and basal dislocations can occur. The resultant dislocations are sessile and will produce work hardening. These reactions are:

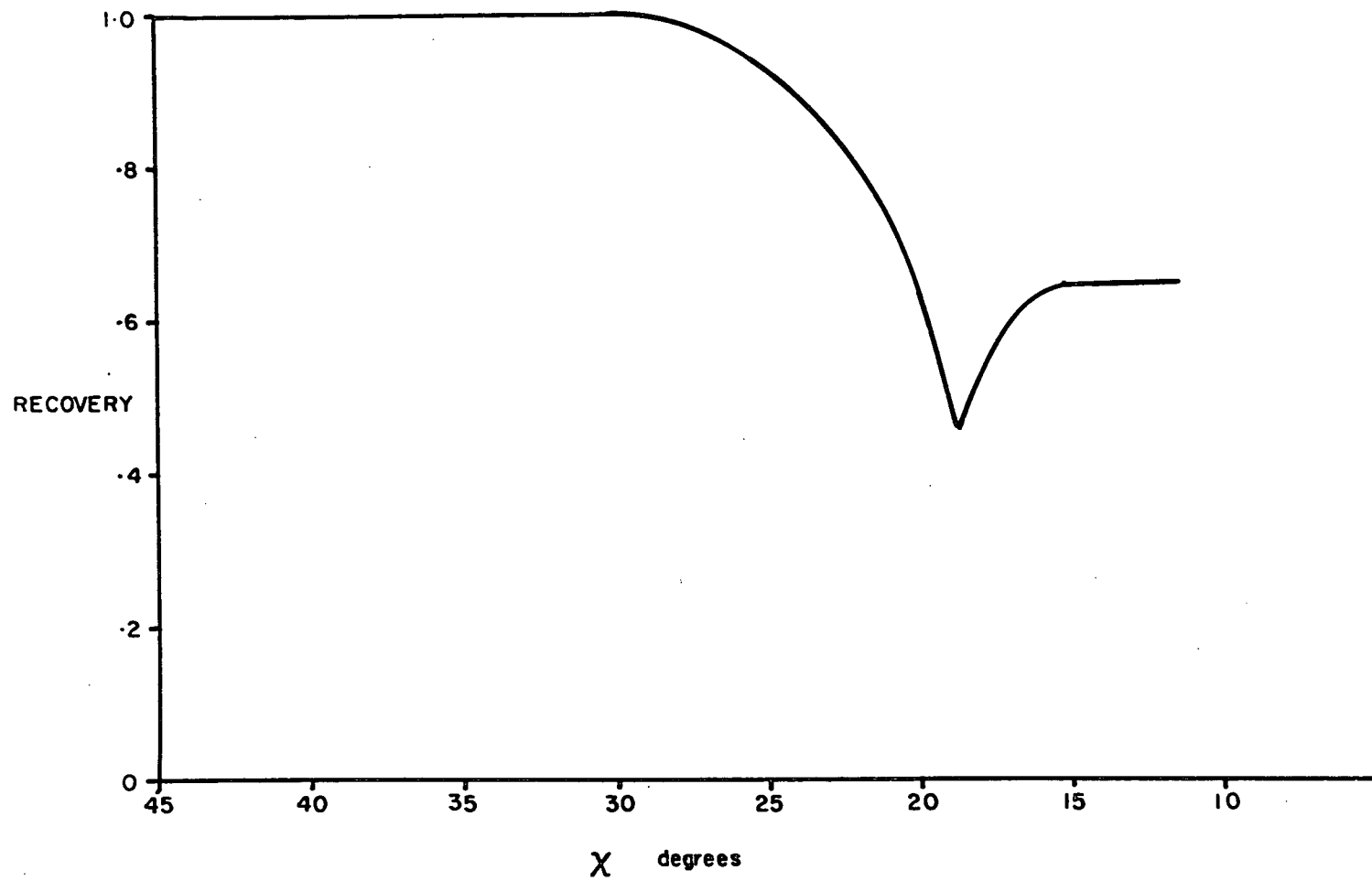
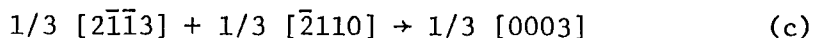
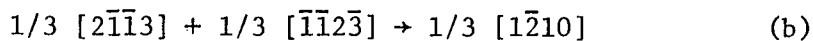
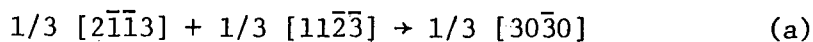


Fig 41. The variation of saturation recovery with orientation.



Reaction (c) between second order pyramidal and basal dislocations is probably the most important. Once these sessiles form, they would probably not be amenable to annealing, and so cause non-recoverable work hardening. Substantiating evidence for this was found in tests which combined recovery with strain rate changes. Laurent'ev et al³⁹ have found that the critical resolved shear stress in zinc at 20°C is a critical function of the pyramidal dislocation density. In zinc it appears that second order pyramidal dislocations may also cause non-recoverable work hardening.

It was also seen in Fig. 36 that there is a small deviation from a room temperature stress-strain curve of a stress-strain curve completely recovered at infinitesimal strain increments. The errors involved in the flow stress measurement, and in the reproducibility between two different specimens are too large to permit the calculation of the work hardening produced by pyramidal dislocations and their interaction with basal dislocations from $\chi = 30^\circ$ to $\chi \approx 23^\circ$ if this secondary system operates at -196°C and not at 20°C. When χ reaches 23°, the difference in Schmid factors on the two systems is such that there would be substantially more activity on the second system. At this point the stress on the pyramidal plane is 260 gm/mm² which may be very near the macroscopic critical stress. The present results show that this stress, at the end of easy glide, is independent of initial orientation. If this is the yield stress for second order pyramidal, then the massive activity on this system would explain the termination of linear easy glide.

Thus it may be concluded, that while a crystal with $\chi_0 = 45^\circ$ deforms entirely in basal glide in the initial stages of deformation, when the strain is such that χ is of the order of 30° to 35° , second order pyramidal dislocation activity becomes significant. This is not to say that macroscopic strain is achieved on this system, but merely that dislocations are generated which will subsequently interact with basal dislocations to cause poor recoverable work hardening. When χ reaches 23° macroscopic flow may occur on the pyramidal system thus terminating linear easy glide.

Since the end of the easy glide is determined by the angle between the basal (or second order pyramidal) plane and the tensile axis, it is reasonable to use this angle as a normalizing factor for all tensile results. However, since χ varies quite slowly with strain at low χ values, stress curves have been plotted versus strain, with the intercept of extrapolated easy glide and stage II slopes taken at $\chi = 20.2^\circ$ ($\gamma = 1.8$ for $\chi_0 = 45^\circ$).

4.3 Strain rate change tests

Activation volume measurements, which are derived from strain rate change tests, may indicate the nature of the rate controlling mechanism during deformation. The principal assumption made regarding interpretation of activation volume data is that the density of mobile dislocations remains constant during a strain rate change. If this is the case, then it is assumed that the change in flow stress resulting from a change in strain rate is due only to the deformation rate controlling process or processes.

It is known that the deformation made during easy glide in cadmium single crystals is slip on the basal system. Consequently, it is assumed that the flow stress in this region is determined only by the

density of basal dislocations and by the way in which they move through the lattice.

In stage II deformation, it is assumed that the flow stress is still controlled only by the density of basal dislocations which are assumed to be the mobile dislocations. For face-centered cubic materials, it has been shown by X-ray diffraction measurements of Ahlers and Haasen³⁰ and Mitchell and Thornton³¹ and by shape change measurements of Kocks³² that most of the deformation in stage II takes place by slip on the primary system. For the present system, Fig. 33 shows that while deformation is not homogeneous during stage II, the width of the crystal does not decrease significantly. (Fig. 33 compares a crystal deformed well into stage II at -196°C to a crystal deformed at 20°C where essentially all deformation was on the basal plane). Since the width did not decrease significantly, it is not unreasonable to assume that during stage II in cadmium, as well as for face-centered cubic materials, the majority of the deformation occurs on the primary system. Therefore, since flow still occurs on the basal system, it is assumed that the flow stress is still a measure of the basal dislocation density in stage II as it is in stage I.

From the results of the present work on orientation, and from the results of Risebrough⁵, it is expected that any secondary activity which takes place will be on the second order pyramidal system. Consequently it is assumed in the following discussion that the dislocation forest is composed entirely of second order pyramidal dislocations. It may be that other types are present as grown-in dislocations, but these should not change during deformation. It has also been assumed that the contribution to strain of the pyramidal dislocations is negligible.

4.3.1 Stage I

4.3.1.1 Activation volume behaviour

Fig. 19 shows that activation volume during easy glide is a steadily decreasing function of strain. At yield, the activation volume is $40 \times 10^{-20} \text{ cm}^3$, which is equivalent to $15,000 b^3$. This value drops to about $5500 b^3$ at the end of easy glide.

Activation volume values in this range are indicative of a rate controlling mechanism of either forest intersection by the basal dislocations or the non-conservative motion of jogs in the basal dislocations. It is not possible on the basis of rate parameter measurements alone to distinguish between these two mechanisms.

Risebrough⁵ has claimed that the mechanism controlling yield and flow in cadmium single crystals is one of forest intersection. He found no major inconsistencies in this argument whereas his experimental data did not agree with the limitations on the jog mechanism. He believed that the jog mechanism was unacceptable primarily because the flow stress in zinc and cadmium was temperature dependent below $T_H = 0.25$. This phenomenon would require that the nucleation of a vacancy in conjunction with the non-conservative motion of jogs be thermally activated. Mott³³ has stated that this vacancy nucleation is completely athermal, and secondly that single vacancies will not migrate at appreciable rates below $T_H = 0.5$.

The present results find inconsistencies in the forest intersection mechanism. In the initial stages of strain (up to 70%), it was found that the activation volume decreased significantly. If the forest intersection mechanism were rate controlling, this decrease would imply an increase in the forest density. However, when the crystals were recovered in this range,

it was found that the activation volume recovered back to the value found at yield (see Fig. 20). Since it is very unlikely that both primary and forest dislocations would recover in exactly the same manner, as the forest intersection mechanism would require, it has been assumed that the forest dislocations do not recover at all. It has been shown that second order pyramidal dislocations will combine with basal dislocations to form energetically stable obstacles, so it should be reasonable to assume that these will not anneal out in the same manner as mobile basal dislocations. This is made more apparent when compared to the behaviour of pyramidal dislocations at higher strains as discussed in a later section. Thus, it appears that the forest intersection mechanism is not applicable to the present system.

The other possible rate controlling mechanism is the non-conservative motion of jogs. In the present system it is believed that this is the rate controlling mechanism, while Risebrough⁵ has rejected this mechanism on the basis of the arguments of Mott³³, but some of these arguments are questionable as to their validity. First, Mott states that single vacancy migration is not appreciable below $.5 T_M$ in Cu. However, Sharp, Mitchell and Christian¹ have shown that in Cd vacancy migration occurs at about $.25 T_M$. Secondly, Mott does not adequately explain why the process of vacancy nucleation at a jog should be completely athermal. If such nucleation were thermally activated, then the combination of this plus vacancy migration could explain the temperature dependence of the flow stress in cadmium. This would then remove any objection to the assumption that the non-conservative motion of jogs is the rate controlling mechanism. Thus, since doubt does exist with respect to the Mott theory, and since experimental results preclude the acceptance of the forest intersection mechanism, it will be assumed that the non-conservative motion of jogs

controls flow in easy glide in cadmium.

Having made the above assumption, it is now possible to explain the behaviour of activation volume with strain in easy glide. During the initial stages of strain, there remains a constant density of forest dislocations. Activation volume decreases in this range due to the decreased inter-jog spacing along the mobile basal dislocations. On recovery, the jogs in these basal dislocations anneal out, probably by diffusion along the dislocation line. When a jog of one sign meets one of the opposite sign, the two annihilate and so decrease the jog density. Under conditions of saturation recovery, some equilibrium concentration of jogs is attained which would be the same concentration as existed at yield. Therefore, the activation volume following recovery will be the same as it was at yield.

If this equilibrium concentration of jogs in basal dislocations is such that the inter-jog spacing along the dislocations is larger than the spacing between forest dislocations, then the activation volume measured under such conditions should be indicative of the forest density. This should be true both at yield and following recovery. However, once the basal dislocation has moved through the first set of forest dislocations that it encounters, the inter-jog spacing will be less than the forest spacing, and so it will be the jog mechanism which is measured. If it is assumed that the inter-jog spacing is larger than the average forest spacing, then on the basis of the previous argument it is possible to calculate the forest density from activation volume data following recovery. Activation volume is defined as:

$$v = b\ell d$$

where b = Burger's vector

ℓ = activated length of dislocation

d = distance over which dislocation is moved.

If it is assumed that the activation distance is equal to the Burger's vector, then

$$\ell = \frac{v}{b^2}$$

If forest intersection is the rate controlling mechanism as has been assumed at yield and following recovery, then ℓ is the average spacing between the forest dislocations.

The forest density is then:

$$\rho = \frac{1}{\ell^2} = \frac{b^4}{v^2}$$

On the basis of the above assumption, the forest density at yield has been calculated as 4.7×10^6 lines/cm². Close to the end of easy glide, the pyramidal density has increased by about one order of magnitude to 4×10^7 cm⁻². Recovery in the middle of the transition region between stage I and stage II shows that the pyramidal density is about 2×10^9 cm⁻².

These above values are consistent with the results from the orientation analysis. Activation volume data show that the forest does not change up to about 70% strain. From this point to the end of easy glide, it is found that the forest density increases from 4×10^6 to 4×10^7 cm⁻² and it is this increase which is associated with microactivity on the second order pyramidal system. For a small strain increment from the end of easy glide to the middle of the transition region an increment from the end of easy glide to the middle of the transition region an increase in pyramidal dislocations of two orders of magnitude was found. This is consistent with the idea of macroactivity on the second order pyramidal at the end of easy glide. Thus, it is concluded from an unrelated type of test that the conclusions regarding work hardening parameters are valid in that there is microactivity on a secondary system

in the latter part of easy glide followed by macroactivity in the transition region.

4.3.1.2 Cottrell-Stokes behaviour

The Cottrell-Stokes behaviour of a metal is the variation in flow stress resulting from a change in strain rate (or temperature) as a function of the total stress on the system. If this variation is linear, passes through the origin, then the Cottrell-Stokes law is considered to be obeyed. The interpretation of the results and the significance of obedience or non-obedience is not clearly understood, and is usually only applied to face-centred cubic materials. Many tests, however, have been performed on many different materials to test this law. Most materials which obey the law are face-centered cubic, but obedience has been reported on some hexagonal metals. Basinski³⁴ has found obedience in magnesium single crystals below 47°K; Davis¹⁶ and Risebrough⁵ found obedience during stage II deformation of cadmium at -196°C and Boček and Lukáč³⁵ claim zinc in stage II at 20°C also obeys.

The present results show that nowhere during the deformation of single crystal cadmium at -196°C is the Cottrell-Stokes law obeyed.

The plotting of $\Delta\tau$ vs. τ as in a Cottrell-Stokes test gives useful information besides checking the obedience of the Cottrell-Stokes law. Since activation volume is representative of the rate controlling mechanism, and is determined directly from the measurement of $\Delta\tau$, then $\Delta\tau$ itself must also be indicative of the rate controlling process. In the present case, $\Delta\tau$ at yield is a direct measure of the number of forest intersections taking place at the time of the strain rate change. At strains past yield, $\Delta\tau$ is a measure of the density of jogs present in

basal dislocations. As mentioned previously, it is believed that the flow stress τ is dependent on the density of basal dislocations. Therefore, a plot of $\Delta\tau$ vs. τ is, in stage I, essentially a plot of the density of jogs vs. the density of basal dislocations.

Fig. 23 shows that the plot of $\Delta\tau$ vs. τ is linear in the initial portion of stage I. Using the above argument, this signifies that the basal jog density increases proportionately to the density of basal dislocations. In this initial strain region, the behaviour of $\Delta\tau$ vs. τ is unaffected by recovery in that relation of $\Delta\tau$ to τ is the same as it was during strain prior to recovery. Thus, the increase in the density of jogs with respect to the increase in basal density is unchanged. Following the second recovery, which is the point at which secondary activity is expected to begin, it is seen that there is a slight increase in the slope of the plot. This is explained if it is assumed that the pyramidal dislocation density in this range is increasing slightly. With a higher pyramidal density, there will now be a larger number of jogs being formed for a given increase in the basal dislocation density (τ).

At the end of linear easy glide, Fig. 22 shows that there is a significant increase in the slope of the $\Delta\tau - \tau$ plot. It is expected that there is a macroactivity on the pyramidal system at this point, causing a substantially higher forest density. (As mentioned previously, the density of forest dislocations was found to increase by two orders of magnitude from the end of easy glide to the middle of the transition region.) Under these circumstances, a given increase in basal density will result in a substantially higher number of jogs formed, and so the slope of the $\Delta\tau - \tau$ plot will increase.

4.3.2 Stage II

In stage II deformation, there is no evidence to suggest that the rate controlling mechanism changes in any way. However, for the purpose of simplification of the following discussion, it will be assumed that this mechanism is now one of forest intersection rather than the non-conservative motion of jogs. This assumption is probably not true, but it should not introduce significant errors since the two mechanisms are so similar in their behaviour. Thus in the following discussion, $\Delta\tau$ is assumed to be representative of forest density rather than jog density.

During stage II deformation, where the forest density is large, probably of the same order as the basal density, the basal dislocations will become highly jogged very quickly. Consequently these basal dislocations will probably not move appreciable distances. New dislocations will be generated and become jogged initially at a rate determined by the forest density. Therefore, the measured values of $\Delta\tau$ and activation volume would not be significantly different if forest intersection were the rate controlling mechanism.

The plot of $\Delta\tau$ vs. τ for deformation in stage II (Fig. 22) is essentially linear. This indicates that the factors leading to both τ and $\Delta\tau$ increase proportionately.

Comparing cadmium to face-centered cubic metals, it is seen that the above conclusion is consistent with the results of Steeds³⁶ and Basinski and Basinski³⁷. These workers found that the density of secondary dislocations in copper single crystals is comparable to the density of primary dislocations throughout stage II, in spite of the fact that plastic strain on the secondary system is very small. This is further evidence for the statement that the linearity of $\Delta\tau$ vs. τ is due to a proportional increase in both pyramidal (forest) and basal (primary) dislocations rather than an increase in basal jogs with no significant increase in forest density.

The behaviour of $\Delta\tau$ vs. τ with respect to recovery (Fig. 24) is significantly different in stage II than it was in stage I. While in stage I, recovery brought about a substantial decrease in both $\Delta\tau$ and τ , the initial recovery anneal in stage II caused a large drop in τ and essentially no change in $\Delta\tau$. Strain following this recovery showed that the slope of $\Delta\tau$ vs. τ is still the same as it was for strain preceding recovery.

That τ changes markedly indicates that the basal dislocation density decreases significantly since as was explained earlier, the flow stress is dependent primarily on basal density. Because $\Delta\tau$ does not change during this anneal, the density of pyramidal dislocations must remain constant during recovery. The fact that the slope of $\Delta\tau$ vs. τ is the same following recovery as it was preceding recovery indicates that the densities of pyramidal and basal dislocations are still increasing in the same relative proportion. However, since the basal density decreased while the pyramidal density remained constant during recovery, there must be a net increase of pyramidal dislocations to the system when it is compared at the same stress level. There are more pyramidal dislocations at point B in Fig. 24 than at point A.

The second recovery anneal gives a further shift to the $\Delta\tau - \tau$ plot as shown in Fig. 24. In this case, however, $\Delta\tau$ as well as τ does decrease significantly. On the basis of the above argument, this indicates that some pyramidal dislocations must be lost at this time. Again, strain following recovery shows that the increase of both basal and pyramidal dislocations remains in the same proportion as that prior to any recovery since the slope of the plot is unchanged. In this strain increment between recovery anneals, there is a further increase to the system of pyramidal dislocations, as shown by comparison of similar stress levels A, B, and C in Fig. 24.

Following further recoveries, the $\Delta\tau - \tau$ plots are coincident with that plot obtained following the second recovery. Thus, a condition must have been reached in which both pyramidal and basal dislocations are recovered. The proportion of each type of dislocation recovered is the same as that in which it is generated during strain, therefore establishing some sort of equilibrium in the structure. This equilibrium condition prescribes the density of basal and pyramidal dislocations at any stress level. This condition was found to be maintained in the crystal from the second anneal in stage II to failure of the specimen.

It is probably coincidence that it took exactly two recovery anneals in stage II to reach this equilibrium condition. If experimental conditions were different (i.e. if the stress at which recovery was carried out were different), then the number of anneals required to reach equilibrium might change, although it is thought that the end result would be the same.

The recovery of pyramidal dislocations as found in the above results may occur by the mechanism as observed by Price²³. He found that second order pyramidal dislocations which had formed long loops by the cross-glide of screw segments first annealed by these loops splitting up into rows of circular loops. These circular loops then annealed out of the sample by means of volume diffusion.

As a result of the findings of this section on Cottrell-Stokes behaviour, it is concluded that for a hexagonal close-packed metal such as cadmium, the Cottrell-Stokes law has no real significance. If it is found to be obeyed in any hexagonal system, it is probably only coincidental.

4.4 Flow stress following recovery

The flow stress measured following recovery is probably determined primarily by basal dislocation density at this point.

In stage II, the basal density present following saturation recovery appears to be a function of the pyramidal dislocation density which is also present. Fig. 42 is a plot of the flow stress achieved after saturation recovery as a function of strain. In this plot, stage II linearity begins in all tests at a strain of about 1.75. It is seen that the basal density rises to a maximum value at approximately 60% strain following the onset of stage II linearity, and then remains constant. This is very similar to the behaviour deduced for pyramidal dislocations in the previous section.

Fig. 42 shows that there is an increase in the basal density (flow stress) by a factor of 3 from 250 gm/mm^2 to 800 gm/mm^2 . Fig. 21 showed that the pyramidal density ($\Delta\tau$) in this same stress range also increases by a factor of 3. Thus, it appears that there is a direct relationship between the density of basal dislocations and the density of pyramidal dislocations present following recovery.

This relationship is probably caused by the way in which the basal dislocations are trapped by the pyramidal dislocations, or perhaps by a stress field associated with the pyramidal dislocations. That the pyramidal density is the governing factor in this relationship is more apt to be the case than the converse, in which the basal density prescribes the pyramidal density, since it has been shown in the previous section that the pyramidal density is insensitive to recovery.

4.5 Work hardening in stage II

These activation volume and $\Delta\tau$ vs. τ data also give some insight into the work hardening behaviour of cadmium single crystals in stage II.

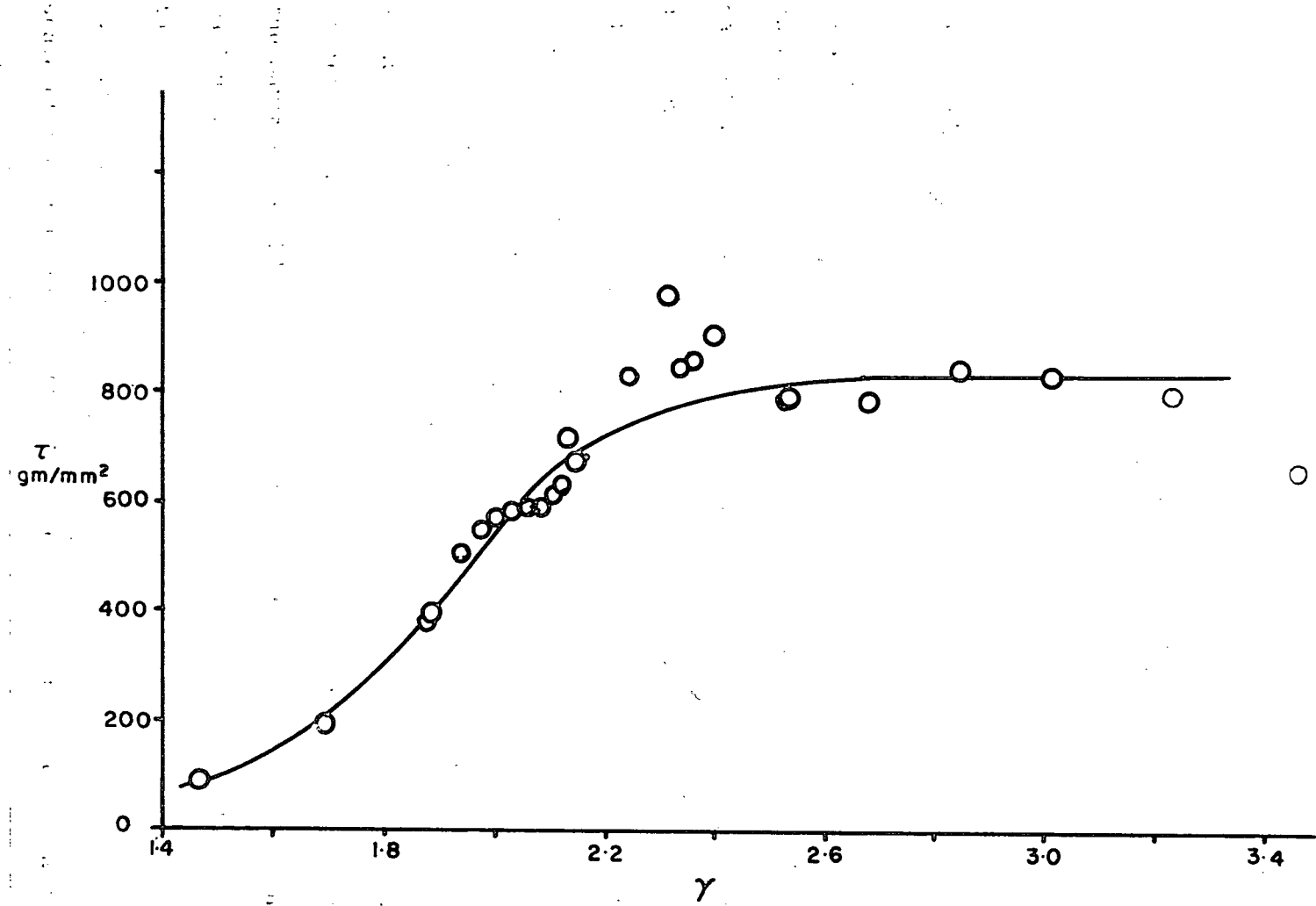


Fig. 42. The variation of flow stress following saturation recovery in stage II.

The data fit well with the arguments of Hirsch and Mitchell³⁸ based on face-centered cubic materials. The principal points in their theory, together with comparison to the present work are as follows:

- 1) At the end of stage I, there are long continuous obstacles which form barriers to newly formed slip lines. Dislocations are stopped by elastic interaction with both the primary and secondary dislocations in the obstacles. In cadmium, it is proposed that these barriers are the sessile dislocations formed by the interaction of basal and second order pyramidal dislocations.
- 2) Hardening is due to the hardening of potential primary sources by the increased density of primary and secondary dislocations. Since it is expected that there is significant secondary activity following linear easy glide, there should be sufficient density to harden primary sources in cadmium.
- 3) In the transition region between stage I and stage II, the ratio of new secondary dislocations to new basal dislocations generated increases rapidly, until the regions within which secondary sources operate extend throughout the crystal. At this point, the proportion of secondary dislocations depends on the internal stress pattern. For a given arrangement of primary dislocations, the density of secondary dislocations will be the maximum possible compatible with the internal stress, leading to the maximum possible hardening rate. Thus, Hirsch and Mitchell have assumed that a situation of similitude develops in which the ratio of secondary to primary dislocations remains constant throughout stage II, and only the scale of the structure decreases as the stress increases. The present results are compatible with this theory up to the point of recovery in stage II. At this point it was found that the secondary dislocation

density did not decrease whereas the primary density did. On further deformation, the secondary density was higher than the previously maximum possible density. Since recovery has permitted an increased secondary density with respect to primary density, it is possible to maintain this condition, and consequently give a higher work hardening rate. This was observed experimentally (see Fig. 32). This, too, is consistent with Hirsch and Mitchell's theory that the work hardening rate is dependent, among other factors, on the density of secondary dislocations in the region of the pile-ups.

4) The flow stress is determined partly by forest density, line tension, and long range stress in the softest region between pile-ups. The relative contributions have yet to be determined. In the present work, it appears that the flow stress is dependent primarily on the basal density, which would be equivalent to Hirsch and Mitchell's long range stress.

Thus the present results are consistent with the theory of Hirsch and Mitchell, and it is reasonable to assume that this theory could be extended to include hexagonal close-packed metals as well as face-centered cubic.

At very high strains, it was found that the work hardening rate decreased. This may be comparable to a stage III which is often associated with dynamic recovery. Since the $\Delta\tau$ vs. τ relationship does not change in this range, dynamic recovery should affect both basal and forest dislocations.

5. SUMMARY AND CONCLUSIONS

- 1) Deformation in easy glide at -196°C is by basal glide only when $\chi > 35^{\circ}$. In this range, the work hardening is completely recoverable by annealing at 75°C for 30 min.
- 2) Deformation in easy glide at -196°C from $\chi \approx 35^{\circ}$ to the end of easy glide is primarily by basal glide with some activity on the second order pyramidal slip system. Work hardening in this region is not completely recoverable. This is probably due to the formation of stable obstacles by the interaction of basal and pyramidal dislocations.
- 3) The end of easy glide occurs at $\chi = 20.1^{\circ} \pm 1.2^{\circ}$. This is probably a result of exceeding the yield stress on the second order pyramidal system, thus forming a much higher density of obstacles.
- 4) Deformation in stage II is primarily on the basal system, although the densities of basal and pyramidal dislocations are probably about the same. Recovery early in stage II causes a decrease in basal density with no corresponding decrease in pyramidal density. As a result of this, the work hardening rate following recovery is higher than that preceding recovery. At higher strains in stage II, both basal and pyramidal dislocations are recovered.
- 5) The strain attainable in stage II at -196°C is increased by recovery.

6) Deformation is probably controlled in stage I by the non-conservative motion of jogs. The data from stage II may also be interpreted in terms of this mechanism.

7) The Cottrell-Stokes law is not strictly obeyed through any portion of the deformation of cadmium single crystals. On the basis of the present results, it appears that obedience of this law in hexagonal metal would be coincidental.

8) It was found to be impossible to calculate a meaningful activation energy.

6. APPENDIX

6.1 Electron microscopy techniques

An attempt was made to thin sections of cadmium single crystals for observation in the electron microscope. In this way, it was hoped to observe the dislocation structure of the specimens, and to determine the effects of deformation and recovery upon this structure. Unfortunately, all attempts at thinning were unsuccessful, and no structures were observed.

The techniques employed in this study, and the problems encountered, are listed below.

6.1.1 Cutting a thin section

The first problem in this study was to obtain a thin, parallel-sided slice of a specified orientation from a bulk single crystal. It was also necessary to ensure that no extraneous dislocations were introduced into the slice during the cutting operation. There was no difficulty involved in determining the desired orientation since X-ray techniques are well established and sufficiently accurate. Problems were encountered in cutting a thin slice from the 5 mm. diameter bulk single crystal.

It was decided that cutting by any mechanical means such as a jeweller's saw would be unacceptable due to the amount of deformation introduced to the sample during the cutting operation.

Spark erosion was the first method tried to obtain the desired slice. It was hoped that by using a relatively low energy spark that there would be negligible deformation introduced into the sample. This method worked well for the first cut, but when a second cut was attempted to produce a thin slice, problems arose. During this second cut, the slice which was 1-2 mm. thick was bent by the forces developed during the cutting

procedure up towards the sparking tool. When this occurred, sparking took place between the side of the tool and the slice, and the originally parallel-sided slice was eroded into a wedge. Experiments in shielding the side of the tool to prevent this from happening were unsuccessful. Even if it could be assumed that the deformation involved in the bending was insignificant, it was impossible to thin the wedge-shaped slices for subsequent observation in the electron microscope.

As an alternative to spark erosion, acid cutting was tried to produce the desired slices. In this method, a counter-balanced specimen was held lightly against a reciprocating polyester thread. The thread was kept saturated with dilute nitric acid by a drip feed arrangement so that all cutting was produced by the dissolution of the cadmium by the nitric acid. The velocity of the thread was kept below 20 ft/min to reduce the possibility of damage from friction. One cut took approximately 8 hours.

The slices produced by this method varied in thickness throughout the section by as much as 1 mm. since the thread could not be prevented from moving slightly out of its intended plane during the cut. These slices were used in subsequent thinning experiments even though they were not of uniform thickness since they had sustained negligible deformation and were the best available.

6.1.2 Thinning

The slices produced by acid cutting were thinned by standard electro-polishing techniques. It was found that chromic-acetic electro-polishing solution used at the plateau voltage gave excellent polishing results, producing a clean, shiny surface. The major problem involved during thinning was to produce a regular, slightly concave surface on each side of the sample.

This was difficult since the original slices did not have perfectly smooth surfaces. To try to overcome this problem, a jet polishing technique was employed, in which a thin stream of polishing solution is directed towards the specimen surface during electro-polishing. This produced the desired concavity but it did not satisfactorily smooth out the irregularities in the surface. Consequently, when the specimen was subsequently thinned to perforation, the included angle of the specimen, leading up to the perforation was quite high. Chemical polishing in dilute nitric acid prior to electro-polishing was also found to be unsuccessful in removing surface irregularities.

6.1.3 Examination of thinned specimens

The samples thinned as described above were examined in the electron microscope. It was found that areas adjacent to perforations were always too thick for electron transmission. Consequently, it was impossible to determine any dislocation structures in these samples.

Since this work was attempted, two transmission electron micrographs of cadmium have appeared^{40,41}. However, due to the lack of clarity, and obvious difficulties involved in obtaining these photographs, the techniques used were not subsequently attempted for the present material.

REFERENCES

- 1 Sharp J.V., Mitchell A., and Christian J.W. *Acta Met.* 13, 965 (1965).
- 2 Peiffer H.R. and Stevenson F.R. *Phys. Stat. Soc.* 4, 411 (1964).
- 3 Kroupa F. and Price P.B. *Phil. Mag.* 6, 243 (1960).
- 4 Hirsch P.B. and Lally J.S. *Phil. Mag.* 12, 595 (1965).
- 5 Risebrough N.R. PhD Thesis, University of British Columbia (1965).
- 6 Rath B.B., Nakada Y., and Hu H. To be published.
- 7 Lücke K., Masing G., and Schröder K. *Z. Metallk.* 46, 792 (1955)
- 8 Oelschlägel D. *Z. Metallk.* 54, 354 (1963).
- 9 Lukáč P. *Phys. Status Solidi* 19, K47 (1967).
- 10 Feltham P. *Phys. Status Solidi* 3, 1340 (1963).
- 11 Schmid E. and Boas W. *Plasticity of Crystals*, Chapman and Hall, London (1968).
- 12 Dorn J.E. "Energetics in Dislocation Mechanics", National Research Council Seminar on Energetics in Metallurgical Phenomena, Denver (1962).
- 13 Cottrell A.H. and Stokes R.J. *Proc. Roy. Soc.* 233, 17 (1955).
- 14 Gerland C.W. and Silverman J. *Phys. Rev.* 119, 1218 (1960).
- 15 Boček M., Lukáč P., Smola B., and Švábová M. *Phys. Status Solidi* 7, 173 (1964).
- 16 Davis K.G. *Can. J. Phys.* 41, 1454 (1963).
- 17 Jillson D.C. *Trans. Met. Soc. AIME* 188, 1129 (1950).
- 18 Deruyttere A.E. *Trans. Met. Soc. AIME* 200, 667 (1954).
- 19 Diehl J. *Z. Metallk.* 47, 331 (1956).
- 20 Boček M. and Kaska V. *Phys. Status Solidi* 4, 325 (1964).
- 21 Boček M., Hötzsch G., and Simmin B. *Phys. Status Solidi* 7, 833 (1964)
- 22 Seeger A. and Träuble H. *Z. Metallk.* 51, 435 (1960).
- 23 Price P.B. *J. Appl. Phys.* 32, 1746 (1961).
- 24 Kratochvíl P. and Koutník M. *Czech. J. Phys.* B18, 1309 (1968).

- 25 Hirsch P.B. Disc. Faraday Soc. 38, 111 (1964).
- 26 Bell R.L. and Cahn R.W. Proc. Roy. Soc. A239, 494 (1957).
- 27 Boček M., Švábová M, and Hötzsch G. Rheol. Acta 6, 130 (1967).
- 28 Stoloff N.S. and Gensamer M. Trans. Met. Soc. AIME 224, 732 (1962).
- 29 Boček M., Lukáč P., and Švábová M. Phys. Status Solidi 4, 343 (1964).
- 30 Ahlers M. and Haasen P. Acta Met. 10, 977 (1962).
- 31 Mitchell T.E. and Thornton P.R. Phil. Mag. 10, 315 (1964).
- 32 Kocks U.F. Trans. Met. Soc. AIME 230, 1160 (1964).
- 33 Mott N.F. Trans. Met. Soc. AIME 218, 962 (1960).
- 34 Basinski Z.S. Aust. J. Phys. 13, 284 (1960).
- 35 Lukáč P. and Boček M. Ber. Internat. Symposium Reinstoffe in
Wissenschaft U. Technik, Dresden 1965,
Teil 3: Realstruktur U. Eigenschaften
von Reinstoffen p.539 (1967).
- 36 Steeds J.W. Relation Between Structure and Mechanical Properties
of Metals, H.M.S.O., London (1963).
- 37 Basinski Z.S. and Basinski S.J. Phil. Mag. 9, 51 (1964).
- 38 Hirsch P.B. and Mitchell T.E. Can. J. Phys. 45, 663 (1967).
- 39 Laurent'ev F.F., Vladimirova V.L., and Gaiduk A.L. Fizika Metallov
i Metallovedenie 27(4), 732 (1969).
- 40 Luke C.M. PhD Thesis, University of London (1968).
- 41 Kirchner H.O.K. J. Inst. Metals 97, 256 (1969).
- 42 Gibbons D.F. PhD Thesis, University of Birmingham (1949).
- 43 Schumacher D. [Commisariat à Energie Atomique] 10^e Colloque de
Métallurgie, Saclay 1966, p.49 (1967).
- 44 Baluffi R.W., Koehler J.S., and Simmons R.O. Recovery and
Recrystallization of Metals p.1 Interscience, New York
(1963).
- 45 Wolf, P. Diplomarbeit, Freiberg (1965).